Numerical analysis of electro-convection in dielectric liquids with residual conductivity

Junyu Huang[1](黄俊宇), Jian Wu[1*](吴健), Zhonglin Du[1](杜中林), Pedro A. Vázquez[2], Alberto T. Pérez[3]

[1] Key Laboratory of Aerospace Thermophysics, School of Energy Science and Engineering, Harbin Institute of Technology, Harbin 150001, PR China
[2]Departamento de Física Aplicada III, ETSII, Universidad de Sevilla, Camino de los Descubrimientos s/n, 41092 Sevilla, Spain
[3]Departamento de Electrónica y Electromagnetismo, Facultad de Física, Universidad de Sevilla, Avda. de Reina Mercedes s/n, 41013 Sevilla, Spain

Abstract

Injection-induced electro-convection (EC) of dielectric liquids is a fundamental problem in electrohydrodynamics (EHD). However, most previous studies with this type of EC assume that the liquid is perfectly insulating. By perfectly insulating, we mean an ideal liquid with zero conductivity, and in this situation, the free charges in the bulk liquid originate entirely from the injection of ions. In this study, we perform a numerical analysis with the EC of dielectric liquids with a certain residual conductivity based on a dissociation-injection model. The spatiotemporal distributions of the flow field, electric field, and positive/negative charge density in the parallel plate configuration are solved utilizing the finite volume method. It is found that the residual conductivity inhibits the onset of EC flow, as well as the strength of the flow field. The flow features and bifurcations are studied in various scenarios with three different injection strengths in the strong, medium, and weak regimes. Three distinct bifurcation sequences with abundant features are observed by continually increasing or decreasing the electric Reynolds number. The present study shows that the residual conductivity significantly affects the bifurcation process and the corresponding critical point of EC flows.

* Corresponding author. Tel.: +86 451 86402324; E-mail address: jian.wu@hit.edu.cn.

***Keywords**:* Electro-convection, dielectric liquids, dissociation-injection, residual conductivity, bifurcation, numerical analysis.

1. Introduction

Electrohydrodynamics (EHD), a multidisciplinary science that describes the interaction between the flow field and the electric field, has been employed in many practical applications, such as electrostatic precipitation and thrust [1, 2], EHD pumping[3, 4], heat transfer enhancement[5, 6], EHD mixing[7], electrophoretic display[8]. Electro-convection (EC) driven by Coulomb force in nonpolar dielectric fluids is a fundamental problem in EHD[9-11]. The behavior of poorly conducting nonpolar liquids has received a lot of attention because of its rich flow features and nonlinear characteristics[12-14]. There are two main mechanisms for the generation of free space charges in nonpolar isothermal dielectric liquids[9], namely: 1) injection and 2) conduction. The charges for injection cases are generated by ionic pairs that are adsorbed in the metal-liquid interface by electrostatic image forces. The electrochemical reaction at the liquid/electrode interface leads to free charges entering into the bulk from either single-side electrode (unipolar injection) or both electrodes (bipolar injection). Several injection laws have been proposed to describe the amount and rate of injected charges[9, 11]. For the conduction model, the charges originate from the un-equilibrium dissociation and recombination processes of liquid molecules under an electric field. When an external electric field is applied, the rate of dissociation increases. The electric field enhanced dissociation is usually named the Onsager effect[15, 16]. The dissociation and recombination process accounts for the origin of the residual conductivity of a dielectric liquid. Theoretically, the model based on the injection-conduction model can explain the current-voltage characteristics for various dielectric liquids in a wide range of applied voltage.

Electro-convection based on the unipolar injection model has been well studied in the past four decades[10, 17]. Various geometric configurations have been studied using different methods of theoretical analysis, experiments, and numerical simulations. In highly symmetrical configurations (such as parallel plates, concentric cylinders, and spherical electrodes) with homogenous injection, two typical features of the EC system, including the onset of the flow motion and subcritical bifurcation phenomenon are observed in extensive investigations[13, 18, 19]. The competition between two ionic transport mechanisms (drift due to the electric field and convection by the fluid field) explains the subcritical bifurcation and also the formation of the charge void region. The linear stability analysis performed with EC between parallel electrodes demonstrates that the onset of the flow motion is independent of the mobility parameter but is closely related to injection strength[20, 21]. Their results were also confirmed by experimental measurements[22] and numerical simulations[13, 19, 23]. Electrohydrodynamic flow caused by the field-enhanced dissociation has also received attention in recent years[24, 25]. Ryu *et al*.[26] reported the EHD flow generated due to the Onsager effect and a conductivity gradient caused by a non-uniform electric field. Particle image velocimetry (PIV) techniques were utilized to visualize such EHD flow. Meanwhile, both analytical and numerical solutions are performed to discuss the effect of the electric field strength, system geometry, and alternating current (AC) frequency on the velocity and pattern of the aforementioned EHD flow. Furthermore, the electrohydrodynamic flow based on the conduction model attracts the attention of researchers for the application of conduction pumping[3, 27-29]. This specific application is expected to be used in many engineering fields, including space thermal control and flexible microscale pumping, due to its advantages of having no mechanical components, no noise, easy miniaturization[30].

Direct Numerical Simulation (DNS) is an effective and direct method to investigate the phenomenon of EC. In recent decades, various numerical methods including the finite volume method[13], compact finite difference method[31], finite element[32], spectral element method[33], Discrete Unified Gas-Kinetic Scheme (DUGKS)[34], Particle-In-Cell method (PIC)[19], and the Lattice Boltzmann Method (LBM)[35, 36], have been developed for the analysis of EC problems. For these numerical works, the main task is to validate the algorithm's ability in solving space-charge coupled with the electric field, so the unipolar injection model is always adopted. Studies have also been extended to other configurations with more complex geometries and non-Newtonian fluids. Fernandes *et al.*[37, 38] investigated the critical value corresponding to the onset of flow motion and the complex flow characteristics of EC between concentric cylinders by performing linear stability analysis and numerical simulations. They reported that the number of charged plumes increases with the rise of the applied electric field before the system bifurcates to chaos. In our previous studies, we performed numerical simulations with the finite volume method with 2D concentric[39] and eccentric[40] cylinders. The characteristics of finite-amplitude bifurcation at the onset and routes to chaos were investigated. Very recently, Su *et al.*[41] has extended the numerical investigation to the instability in EC of viscoelastic fluids, while Chen *et al.*[42] has performed the first numerical simulation of EHD conduction pumping with viscoelastic fluids.

From the literature review described above, the difference between two typical mechanisms for charge generation in a dielectric liquid can be observed. Investigations on the EC flow of a dielectric liquid between parallel-placed electrodes observed rich flow characteristics corresponding to the linear and nonlinear phenomena in the EC system. When a strong electric field is applied between two parallel electrodes, charges are generated into the bulk by the injection mechanism and serve as the dominant origin for the free charges. However, the un-equilibrium of the dissociation-recombination process under the action of the electric field leads to the origin of residual conductivity in the dielectric liquid. Previous theoretical studies have shown that residual conductivity in a liquid significantly affects the linear and nonlinear stability of the EC and ETC systems[14, 43]. Therefore, in this study, an EC solver based on the dissociation-injection model is developed, and a series of numerical simulations are performed to investigate the rich flow features and bifurcation phenomena in dielectric liquids with different residual conductivities. The present model also considers the Onsager effect in EC flow. By this model, numerical simulations are believed to become closer to real situations as the dielectric liquids always possess weak conductivity. Three different injection strengths are adopted to systematically study such a bifurcation process. The remainder of this paper is organized as follows. In Sect. 2, the physical problem, governing equations, and boundary conditions are stated. Sect. 3. briefly explains the numerical methods and code validation. Results and discussion are presented in Sect. 4. Finally, a conclusion is drawn in Sect. 5.

2. Problem formulation

2.1 Physical Problem and Governing Equations

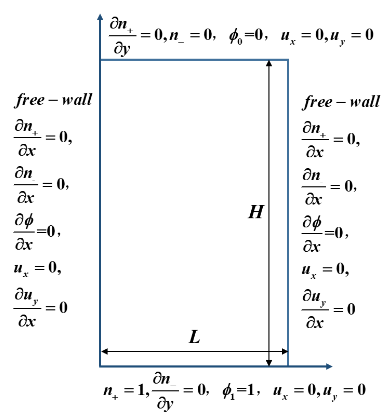

Fig. 1. Sketch of the physical domain and boundary conditions.

As shown in Fig. 1, the system under consideration is a nonpolar dielectric liquid layer enclosed between two parallel electrodes. Constant but different electrical potentials ϕ_1 and ϕ_0 ($\phi_1 > \phi_0$) are applied on the bottom and top electrodes, respectively. The injected ions are assumed to be positive ions that are released autonomously and homogeneously from the bottom electrode. The dielectric liquid between the parallel plates is assumed to be Newtonian, incompressible, isothermal, and with weak residual conductivity. Since both injected ions and electrolytic ions have a common origin in the ionic pairs, the injected positive ions are assumed to be the same as the positive ions generated due to dissociation[9, 11, 12].

The governing equations include the continuity equation, momentum equation, the additional equations describing the electric field (the Poisson equation, as well as the definition of the electric field), and positive/negative charge transport equations. Following the previous assumptions, the complete formulation of the governing equations can be expressed as follows[9, 11, 12]:

$$\nabla \cdot \mathbf{u} = 0 \tag{1}$$

$$\frac{\partial(\rho\mathbf{u})}{\partial t} + \nabla \cdot \left(\rho\mathbf{u}\mathbf{u}\right) = -\nabla p + \nabla \cdot (\mu\nabla\mathbf{u}) + e_0(n_+ - n_-)\mathbf{E} \tag{2}$$

$$\nabla \cdot (\varepsilon\mathbf{E}) = e_0(n_+ - n_-) \tag{3}$$

$$\mathbf{E} = -\nabla\phi \tag{4}$$

$$\frac{\partial n_+}{\partial t} + \nabla \cdot \left(n_+K_+\mathbf{E} - D_+\nabla n_+ + n_+\mathbf{u}\right) = \frac{e_0(K_+ + K_-)(n_0^{eq})^2}{\varepsilon}\left(F(w(|\mathbf{E}|)) - \frac{n_+n_-}{(n_0^{eq})^2}\right) \tag{5}$$

$$\frac{\partial n_-}{\partial t} + \nabla \cdot \left(-n_-K_-\mathbf{E} - D_-\nabla n_- + n_-\mathbf{u}\right) = \frac{e_0(K_+ + K_-)(n_0^{eq})^2}{\varepsilon}\left(F(w(|\mathbf{E}|)) - \frac{n_+n_-}{(n_0^{eq})^2}\right) \tag{6}$$

In these equations, $\mathbf{u}$ is the fluid velocity and $\mathbf{E}$ is the electric field, p represents the dynamic pressure. The scalars t, ρ, ϕ, n_+, n_- denote the time, fluid density, electric potential, positive and negative charge density, respectively. The symbols ε, μ, K_+, K_-, D_+, D_- represent the electrical permittivity, dynamic viscosity, ionic mobility, and the charge diffusivity of positive and negative accordingly. In this study, it is assumed that the ionic mobility and diffusion coefficients are equivalent for both positive and negative ions; thus, $K_+=K_-=K$, $D_+=D_-=D$. e_0 is the elementary charge, n_0^{eq} is the concentration of ionic species without external electric field applied. In equations (5) and (6), F is the Onsager function and $w(|\mathbf{E}|)$ is the enhanced dissociation rate coefficient[3, 12],

$$F(w(|\mathbf{E}|))=\frac{I_1(4w(|\mathbf{E}|))}{2w(|\mathbf{E}|)}, w(|\mathbf{E}|)=\frac{L_B}{L_O}=\left(\frac{e_0^3|\mathbf{E}|}{16\pi\varepsilon k_B^2\theta^2}\right)^{1/2} \tag{7}$$

Here, I_1 is the first-order modified Bessel function of the first kind. k_B is the Boltzmann constant, and θ is the absolute temperature. L_B is the distance where the electrostatic energy between two ions becomes the same order as the thermal energy, which is also named the Bjerrum distance. The Onsager distance L_O is the distance from a point charge where the magnitude of the external electric field $\mathbf{E}$ becomes of the same order as the electric field produced by the charge in the liquid. The expression of Bjerrum distance L_B and Onsager distance L_O is

$$L_B=\frac{e_0^2}{8\pi\varepsilon k_B\theta}, L_O=\sqrt{\frac{e_0}{4\pi\varepsilon|\mathbf{E}|}} \tag{8}$$

For universality in the description of the above physical problem, the following characteristic scales are chosen for non-dimensionalization,

$$\begin{array}{ccc} x_i=x_i^*H & t=t^*(\rho_0 H^2/\mu) & \mathbf{u}_i=\mathbf{u}_i^*(\mu/\rho_0 H) \\ p=p^*(\mu^2/\rho_0 H) & n_+=n_+^*(n_i+n_0) & n_-=n_-^*n_0 \\ \mathbf{E}=\mathbf{E}^*(\Delta\phi_0/H) & \phi=\phi^*\cdot\Delta\phi_0 & \rho=\rho^*\rho_0 \end{array}$$

The governing equations in the dimensionless form are derived,

$$\nabla\cdot\mathbf{u}=0 \tag{9}$$

$$\frac{\partial\mathbf{u}}{\partial t}+\nabla\cdot(\mathbf{uu})=-\nabla\hat{p}+\nabla\cdot(\nabla\mathbf{u})+M^2Re_E^2[(C+C_0)n_+-C_0n_-]\mathbf{E} \tag{10}$$

$$\nabla\cdot(\mathbf{E})=(C+C_0)n_+-C_0n_- \tag{11}$$

$$\mathbf{E}=-\nabla\phi \tag{12}$$

$$\frac{\partial n_+}{\partial t}+\nabla\cdot\left[\left(Re_E\mathbf{E}+\mathbf{u}\right)n_+-\alpha\nabla n_+\right]=\frac{2C_0^2}{(C+C_0)}Re_E\left(F(w(|\mathbf{E}|))-\frac{n_+n_-}{(n_0^{eq})^2}\right) \tag{13}$$

$$\frac{\partial n_-}{\partial t}+\nabla\cdot\left[\left(-Re_E\mathbf{E}+\mathbf{u}\right)n_--\alpha\nabla n_-\right]=2C_0Re_E\left(F(w(|\mathbf{E}|))-\frac{n_+n_-}{(n_0^{eq})^2}\right) \tag{14}$$

There are five dimensionless governing parameters of the system,

$$C = \frac{e_0 n_i d^2}{\varepsilon \Delta\phi_0} \qquad C_0 = \frac{e_0 n_0^{eq} d^2}{\varepsilon \Delta\phi_0} \qquad Re_E = \frac{\rho_0 K \Delta\phi_0}{\mu}$$

$$M = \frac{\sqrt{\varepsilon / \rho_0}}{K} \qquad \alpha = \frac{D}{K \Delta\phi_0}$$

The parameter C represents the injection strength and three regimes can be defined: strong ($5 < C$), medium ($0.2 < C < 5$), and weak ($C < 0.2$)[43]. C_0 is the conduction number, and it is utilized to differentiate between the two limit regimes in EHD conduction: ohmic regime ($C_0 >> 1$) and saturation regime ($C_0 << 1$)[3]. The ohmic regime is featured by the existence of two heterocharge layers next to the electrodes and an electroneutral bulk. While for the saturation regime, the heterocharge layers span all the volume between electrodes and overlapping without the existence of electroneutral bulk. The electric Reynolds number Re_E is a Reynolds number defined with the ionic drift velocity, and it plays the role of applied potential. The electric Rayleigh number T has also been widely used to represent the strength of the applied electric field in previous studies[13, 19]. Re_E is proportional to T with the relationship $Re_E = T/M^2$. The dimensionless mobility parameter M denotes the ratio of the hydrodynamic mobility and the true mobility of ions. The number α is the diffusion coefficient of the charges, which always takes a small value in dielectric liquids.

2.2 Boundary and initial conditions

The non-dimensional computational domain is a rectangular space defined by the length L and height H. For a better description of the computational domain, a geometric aspect ratio $A= L/H$ is defined. In this study, the aspect ratio under consideration is fixed at $A= \lambda/2$, where λ is a half wavelength predicted from the linear stability of an infinite fluid layer. The boundary conditions are depicted in Fig. 1. The fluid velocity is specified by the no-slip boundary condition at both the top and bottom electrodes. For the electric potential field, the Dirichlet conditions are applied along the two parallel electrodes. The charge density field is defined by applying Dirichlet and Neumann boundary conditions at the bottom (the emitter electrode) and top electrodes, respectively. For lateral walls, free-slip (symmetrical) boundary conditions are adopted to reduce computational cost. All the associated nondimensional boundary conditions are summarized as follows,

$$y = 0: \qquad n_+ = 1, \frac{\partial n_-}{\partial y} = 0, \ \ \phi_1 = 1, \ \ u_x = 0, u_y = 0$$

$$y = 1: \qquad \frac{\partial n_+}{\partial y} = 0, n_- = 0, \ \ \phi_0 = 0, \ \ u_x = 0, u_y = 0$$

$$x = 0,\ 0.5\lambda \qquad \frac{\partial n_+}{\partial x} = 0, \frac{\partial n_-}{\partial x} = 0, \frac{\partial \phi}{\partial x} = 0, \ \ u_x = 0, \frac{\partial u_y}{\partial x} = 0 \text{(Free wall)}$$

These boundary conditions are the same as in previous studies. For initial conditions, the simulations start either from a hydrostatic state or a state obtained from the previous simulation.

3. Numerical Methods and Validation

3.1 Numerical methods

The coupled set of governing equations includes the Navier-Stokes equations, the Poisson equation for the electric potential, and the charge conservation equations for positive and negative ions. There is a strong non-linear coupling between different fields. Additionally, the negligible diffusion terms in both positive and negative charge density equations mean that they are strongly convection-dominant. Therefore, specifically designed algorithms are required to accurately solve it. In our previous study, by utilizing the total variation diminishing (TVD) scheme to discretize the convective term in the charge transport equation, accurate and oscillation-free solutions are obtained in unipolar injection-induced EC problems[39, 44]. It is natural to extend such a method to the injection-conduction model and to solve injection-induced EC flow in a dielectric liquid with residual conductivity. The whole couple of equations are implemented and solved in the

OpenFOAM® FVM framework[45]. The governing equations are discretized using a sequential, iterative solution procedure based on the PIMPLE algorithm as described by Moukalled *et al.*[46] A collocated grid system is used, in which all variables are stored at the center of control volumes. The Laplacian terms present in the governing equations are discretized using a second-order accurate central differencing scheme. A third-order accurate cubic scheme is used to discretize the gradient terms. The convective terms in the momentum equations are discretized using a third-order accurate QUICK scheme.[47] For the convective terms in the positive/negative charge density equations, a second-order accurate Total Variation Diminishing (TVD) Van Leer scheme is used.[48] The time derivatives are discretized using the Crank-Nicolson scheme with a weighting factor of 0.9.

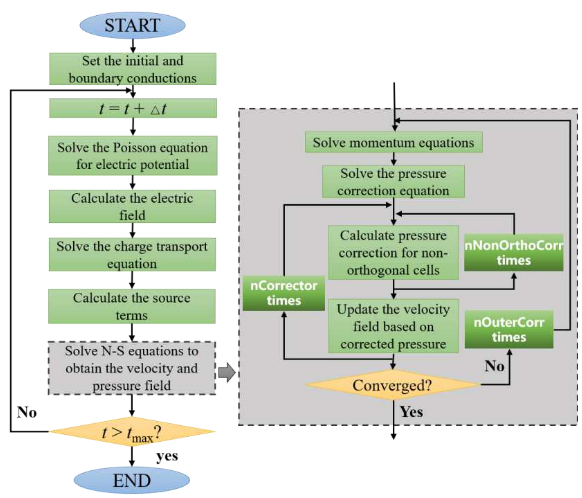

Fig. 2 Flow chart of the calculation procedure.

Note: nOuterCorr is the number of outer corrector loops; nNonOrthoCorr is the number of nonorthogonal pressure corrector loops, and nCorrector is the number of corrector loops).

The overall sequential solution procedure used to solve all equations is presented in Fig. 2. We briefly describe it as follows:

1. Initial conditions are set.
2. The computation begins with solving the Poisson equation to obtain the electric potential.
3. Then, the electric field is calculated.
4. After that, the positive and negative charge transport equations are solved successively with the electric field and the fluid velocity field.
5. The body force term included in the momentum equations is calculated.
6. An inner loop is performed to compute the fluid velocity field and pressure using the PIMPLE algorithm.
7. If you are not at the last time step, return to Step 2 for the next time step.

For the charge transport equations, an inner loop can be designed to couple Eq.(3) to (6) to enhance the convergence stability.

3.2 Code Validation

The FVM framework of OpenFOAM® utilized in this work has been successfully adopted in unipolar injection-induced EC, ETC (electro-thermo-convection) problems and even simulations of solid-liquid phase change process under the effect of an external electric field.[44, 49] In spite of this, two more cases are performed in this section to validate the solver in simulating the EC induced by injection coupled by the dissociation process of a dielectric liquid with residual conductivity. First, a 2D parallel plate case with no flow motion is performed, as depicted in Fig.3(a). The geometrical configuration, boundary conditions, and all other parameters are set the same as presented in the literature.[3, 50] A sufficiently fine uniform 200 × 200 Cartesian grid system is adopted. A constant electrical potential ϕ_1 (ϕ_1 = 1) is applied on the left electrode and the right electrode is grounded (ϕ_0 = 0). The injection process of the system is ignored, and the charges originate merely from dissociation; therefore, the system remains static, as the electrodes are symmetric and the ionic mobilities of the species are assumed to be identical. Fig.3(b) presents the comparison of the positive/negative charge density (n_+, n_-) and the magnitude of the electric field ($\boldsymbol{E}$) profiles along the x-direction for C_0 = 0.1 obtained by the present numerical simulations and the results of the literature. It can be seen that the present results match well with the numerical results provided in Ref. 3, which demonstrate the capacity of the present solver in simulating the electric field and charge distributions of a dissociation process.

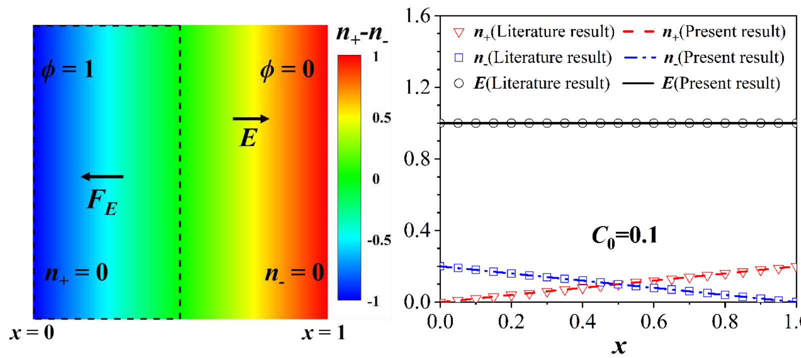

(a) (b)

Fig. 3. (a) Dimensionless configuration for the 2D parallel plate case, along with the net electric charge distribution at C_0 = 0.1, without flow motion. (b)Comparison of profiles of n_+, n_-, and $\boldsymbol{E}$ along the x-direction at C_0 = 0.1. The literature results are obtained by the commercial platform COMSOL Multiphysics.[3]

Table 1 Physical parameters used in the simulations.

Parameter	Value	Parameter	Value
Working fluid	Dodecane	Dynamic viscosity η	1.34×10^{-3} PaS
Diameter of the wire	1mm	Zero field conductivity σ_0	2.96×10^{-8} S/m
Height and width of the domain	5mm	Zero field concentration C_0	$3.28\times10^{19}/m^3$
Relative permittivity ε_r	2	Diffusivity D_i	7.16×10^{-11} m^2/s
Density ρ	749.50kg/m^3	Mobility μ_i	2.81×10^{-9} m^2/sV
Temperature θ	295K	Applied electric potentialϕ_0	1 and 1.5kV

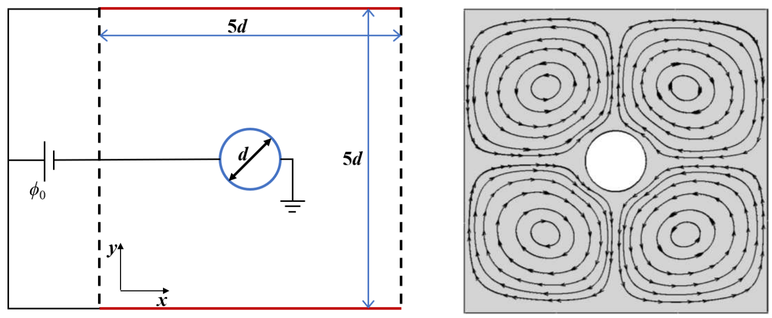

(a) (b)

Fig. 4. (a) Sketch of the EHD flow around a single cylindrical electrode bounded by a pair of flat plate electrodes, (b) overall flow pattern and direction at an applied voltage of 1.5KV.

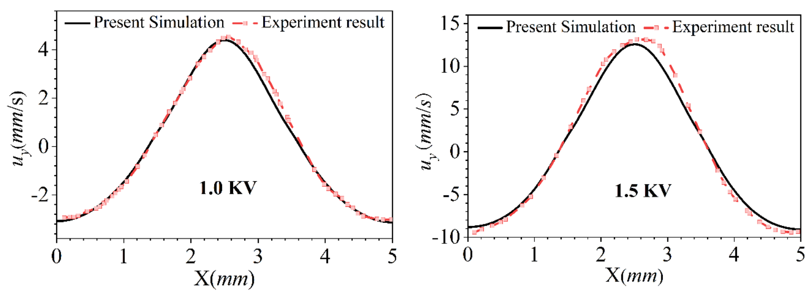

(a) (b)

Fig. 5. Comparison of the vertical velocity profile along y=3.75mm with two different voltages: (a) 1.0KV and (b) 1.5KV. Experimental results are taken from Ref. 51.

Secondly, the EHD flow around a single cylindrical electrode bounded by a pair of flat-plate electrodes is performed to further validate the solver. The schematic of the physical domain is shown in Fig. 4(a). The flat-plate electrodes are applied with a constant voltage (ϕ_0), and the central cylindrical electrode is grounded. In this case, the electric field enhanced dissociation effect (Onsager-Wien effect) is considered. Table 1 provides all the physical parameters used in the simulations, which are set the same as in the literature.[51] As presented in Fig. 4(b), the overall flow pattern and direction at an applied voltage of 1.5KV are the same as that in the literature. To further validate the solver, one more case with an applied voltage of 1.0KV is performed. Fig. 5 presents the comparison of the vertical velocity profile along y = 3.75mm at ϕ_0 = 1.0KV, and 1.5KV. It can be observed that the present numerical results match well with the experimental results reported by Fernandes et al.[51] The above validations demonstrate the ability of our solver to simulate the EC phenomena based on the dissociation injection model.

4. Results and Discussion

Numerical simulations are performed to study the flow features and the instability and bifurcations of the EC system in dielectric liquids with residual conductivities. The residual conductivity σ_0 ($\sigma_0 = 2e_0 K n_0^{eq}$) is proportional to the conduction number C_0. In the present study, the residual conductivity σ_0 is considered to vary in the range between 10^{-11} to 10^{-8} S/m, which are typical values in EHD experiments, and the corresponding conduction numbers C_0 are 0.001 to 1. Three different injection strengths are considered: weak, medium, and strong regimes with C = 0.1, 1, and 10. Considering that the amount of charges produced by the injection process is much higher than that produced by dissociation, C_0/C is set to be less than 0.1. The mobility parameter M is fixed at 10, a typical value widely used in previous studies. Based on a grid sensitivity analysis, a non-uniform grid with 200 × 175 cells is chosen for all the cases. We perform a detailed study about the effect of applied potential (Re_E) and residual conductivity (C_0) on the instability and bifurcation phenomena of the EC system.

4.1 Strong injection regime (C = 10)

We first consider a strong injection with C=10. The residual conductivity in a dielectric liquid generates additional charges other than the injected ones. As in the case of pure unipolar injection, the dielectric liquid with residual conductivity stays still when the applied electric field is weak, and the Coulomb force fails to overcome the viscosity effects. The static dielectric liquid loses its stability, and a steady EC flow arises through pitchfork bifurcation when the applied voltage measured by Re_E is over a critical value Re_{Ec1}. For pure injection, the critical value (Re_{Ec1}) of dielectric liquid without residual conductivity is found to be 1.636, which agrees well with the results of Wu *et al* [52]. While for the injection case of dielectric liquid with residual conductivity C_0=0.1, the value corresponding to the onset of motion is 1.656, which is a little higher than in the pure injection case.

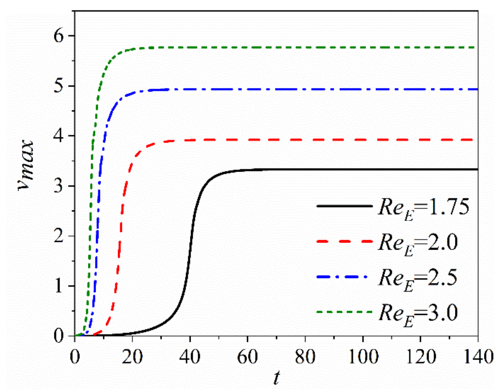

Fig. 6. Evolution of the maximum velocity with time for a dielectric liquid with residual conductivity at $C = 10$, $C_0 = 0.1$, $Re_E = 1.75$ to 3.0.

Fig.6 plots the evolution of maximum velocity $v_{\max} \equiv \mathrm{Max}\left(\sqrt{u_x^{\ 2} + u_y^{\ 2}}\right)$ in the bulk liquid with time for strong injection cases in dielectric liquid with residual conductivity at $C_0 = 0.1$ and $Re_E = 1.75$ to 3.0. The EC systems eventually develop into steady states for all the cases. The streamline and contours of the positive and negative charge density distributions for different time snapshots in the test case of $C = 10$, $C_0 = 0.1$, $Re_E = 1.75$ are presented in Fig.7. Under the simultaneous action of the electric field and flow field, the isolines of positive and negative charge density distributions gradually deform in time. The one-cell asymmetric counterclockwise rotating EC flow exhibits a charge void region in positive charge density distribution. This is a key feature in unipolar injection cases. The negative charges generated by the dissociation of the dielectric liquid are concentrated to the left of the domain center in a concentric egg shape. Fig.8 shows the positive and negative charge density and streamline distributions for $C_0 = 0.1$, $Re_E = 2.5$. The void region in the positive charge density distribution is greater than that in the case of $Re_E = 1.75$, and the negative charges are more concentrated in the egg-shaped area.

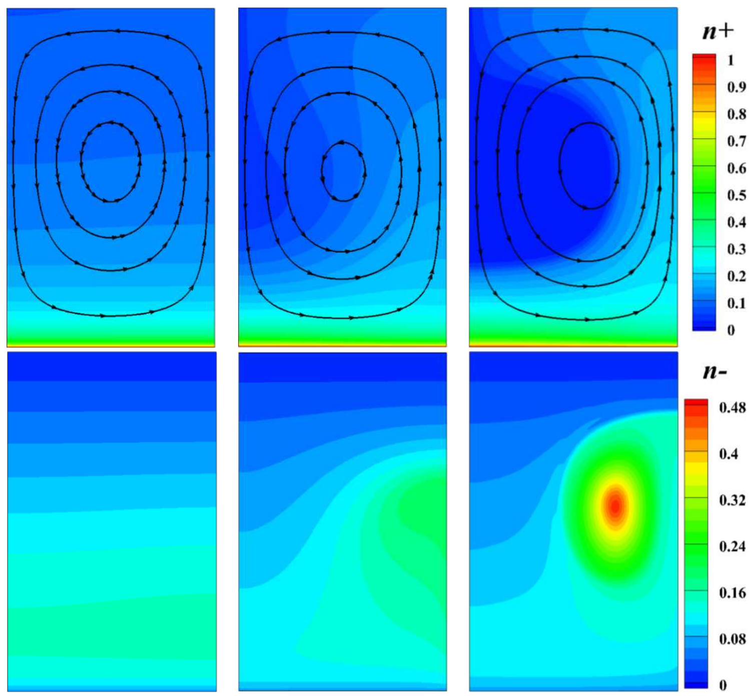

(a) $t = 20$ (b) $t = 40$ (c) $t = 100$

Fig. 7. Streamline and contours of the positive (upper) and negative (bottom) charge density distributions for different time snapshots in the case of $C = 10$, $C_0 = 0.1$, $Re_E = 1.75$ at: (a) $t = 20$, (b) $t = 40$, (c) $t = 100$.

To intuitively analyze the influence of residual conductivity on the flow field and charge density distribution, Fig.9 shows the velocity and charge density distribution along the vertical middle line for EC of dielectric liquids with and without residual conductivity ($C_0 = 0.1$ and $C_0 = 0$). The velocity and charge density distributions almost overlap with each other near the upper and lower walls but show some difference in the middle area.

Around the central area, the magnitudes of the horizontal and vertical velocity of EC flow in a dielectric liquid with no residual conductivity are larger than those with residual conductivity. However, the charge-density distribution presents an opposite trend. This means that the intensity of the EC flow in the dielectric liquid with residual conductivity is lower than that with no residual conductivity because of the distribution of the egg-shaped negative charges. This is also confirmed by the time evolution of the maximum velocity for dielectric liquids with different residual conductivities at C = 10 and Re_E = 2.5, as shown in Fig.10. The maximum velocity of EC decreases with increasing residual conductivity. Meanwhile, the growth rate of maximum velocity in the initial growth stage shows a similar trend. The Coulomb forces acting on positive and negative charges are in opposite directions at any specific point. The number of negative charges generated merely from the dissociation process is much smaller than the positive charges that originated from both the injection and dissociation processes. Therefore, electrical convection is mainly caused by the directional movement of the positive charges. At the same time, negative charges under the action of Coulomb force inhibit the intensity of the electro-convective flow.

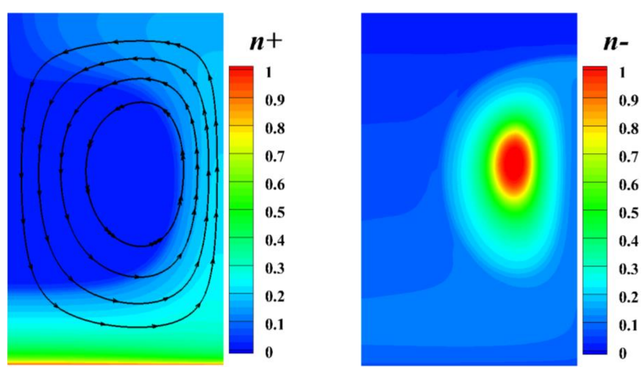

(a) (b)

Fig. 8. (a) Positive and (b) negative charge density and streamline distribution for case: C_0 = 0.1, Re_E = 2.5.

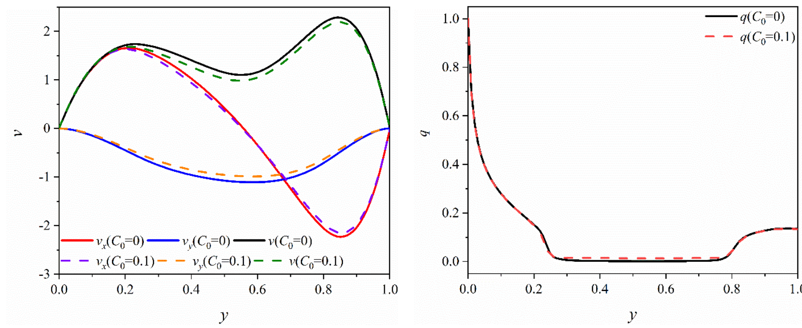

(a) (b)

Fig. 9. (a) Velocity and (b) charge density distribution for $C_0 = 0$ and 0.1 and $Re_E = 2.5$.

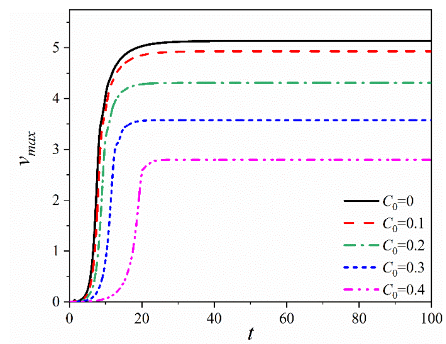

Fig. 10. Evolution of the maximum velocity with time for dielectric liquids with different residual conductivities at $C = 10$, $Re_E = 2.5$.

Fig.11 plots contours of both positive and negative charge density at a value of 0.1 for $Re_E = 2.5$ and different residual conductivities. The positive charge density contour lines for two weak residual conductivity ($C_0 = 0.01$ and 0.1) almost collapse with each other while the variation of corresponding negative charge density contour lines is evident. The regions of positive charge density less than 0.1 surrounded by the isolines plotted in Fig.11(a) can be viewed as a void region. The void region is not closed and allows for an open hole on the collecting electrode, which is consistent with previous observations of EC with zero residual conductivity[19, 52]. With a further increase in residual conductivity, the open hole on the collecting electrode expands and the void region shrinks inward. The void region of the negative charge shows a very different feature. For the dielectric liquid with relatively high residual conductivity (e.g. C_0 = 0.4), the isoline is distributed horizontally near the collecting electrode, while the void region of the negative charges is located above the isoline. As the residual conductivity gradually decreases, the negative charge void region expands, and the left side of the isolines noticeably bends downward. For relatively low residual conductivity (e.g. C_0 = 0.1), a negative charge void region also arises; see Fig.11(b). With the further decrease of residual conductivity, the negative charges cluster to a small egg-shaped area. Fig.12. present the streamlines of $Re_E\mathbf{E}+\mathbf{u}$ and $-Re_E\mathbf{E} + \mathbf{u}$ fields at C = 10, C_0=0.01, Re_E = 2.5. The origin of this egg-shaped area is the term $-Re_E\mathbf{E} + \mathbf{u}$ in equation (14). On the right side of the convective cell, the ion drift is acting downwards, while the liquid flow is going upwards. Since once the convection reaches the steady state the liquid velocity is greater than the ion drift velocity, there is a region from which the negative ions originated by dissociation can not get out. The origin of this negative charge is similar to the void of positive charge on the left side: the lines along with the charge are convected by the combined effect of ion drift and flow convection creates a disconnected region. In the case of positive charges, the injected charge cannot enter this region. For negative charges, the dissociation originates charges that can not get out from this region and discharge at the electrode.

Previous studies on dielectric liquids with no residual conductivity demonstrated that when the driving parameter Re_E is further increased over the critical value Re_{Ec2}, a second subcritical bifurcation takes place where the flow transits from one convective cell to two cells[13, 35, 52]. The same bifurcation phenomena can be observed in dielectric liquids with residual conductivity. We further increased the electric Reynolds number Re_E to explore the effect of residual conductivity on such a bifurcation process. Fig.13 shows the temporal evolution of the maximum velocity for dielectric liquids with different residual conductivities at C = 10 and Re_E = 5.0. After a period of evolution in the one-cell stage, the maximum velocity of the EC system drops suddenly and then gradually stabilizes at a lower value, which corresponds to the state with two convective cells. The dielectric liquid with higher residual conductivity experiences a longer evolution time in the one-cell state before it bifurcates to the two-cell state.

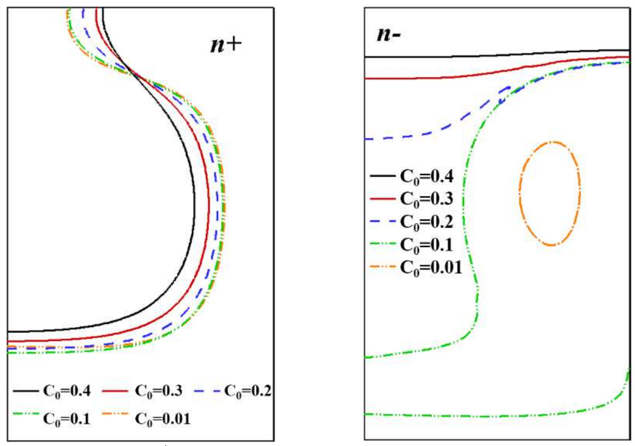

(a) n^+ (b) n^-

Fig. 11. (a) Positive and (b) negative charge density contour lines for strong injection at C = 10, Re_E = 2.5. Both positive and negative charge density contour lines are plotted at a value of 0.1.

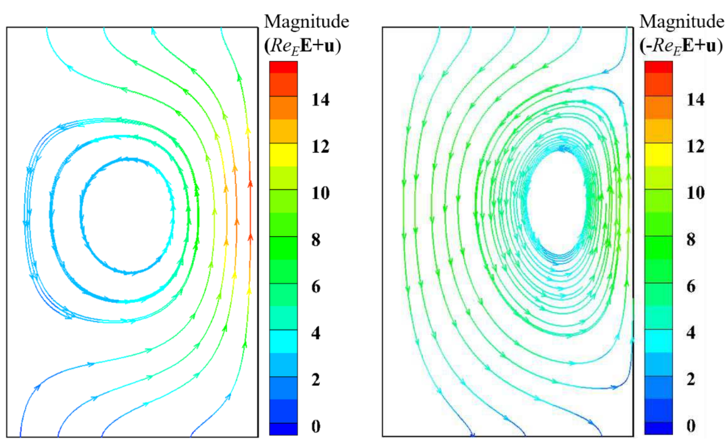

(a) (b)

Fig. 12. The streamlines of (a) Re_E**E**+**u** and (b) -Re_E**E**+**u** fields at C = 10, C_0=0.01, Re_E = 2.5.

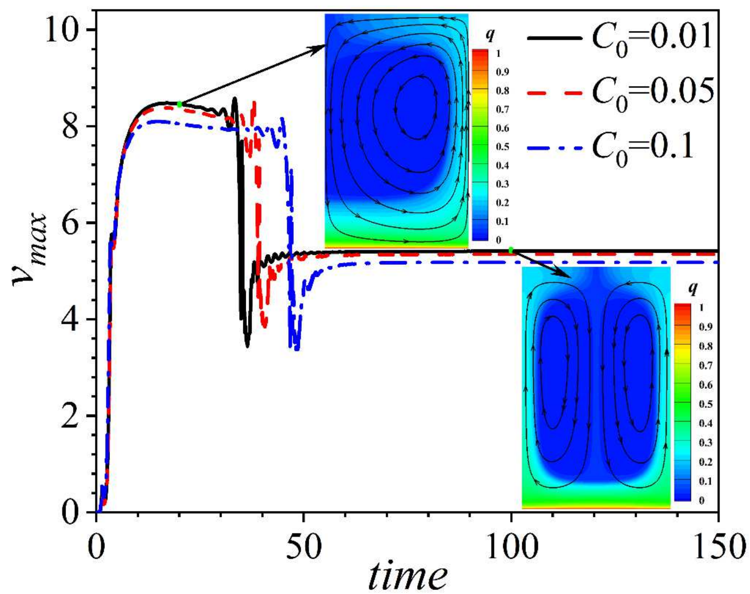

Fig. 13. Temporal evolution of the maximum velocity for dielectric liquids with different residual conductivities at C = 10 and Re_E = 5.0.

When we gradually decrease the applied electric field from the two-cell EC state at Re_E = 7 for dielectric liquids with residual conductivity, the EC systems experience similar subcritical bifurcation processes to the pure injection case. Such a subcritical bifurcation phenomenon is another key feature of the unipolar injection EC system. The EC in relatively high conductivity (C_0 = 0.5) cases first bifurcates from the two-cell structure to the one-cell structure. When the applied electric field is decreased, the EC system returns from a one-cell steady convective state to a hydrostatic state. The values of two critical points (Re_{Ef1} and Re_{Ef2}) are smaller than the values of the corresponding criteria (Re_{Ec2} and Re_{Ec1}). In addition, the influence of residual conductivity on such nonlinear criteria is clear. A dielectric liquid with lower residual conductivity has lower values of two non-linear criteria, while the corresponding maximum velocity increases.

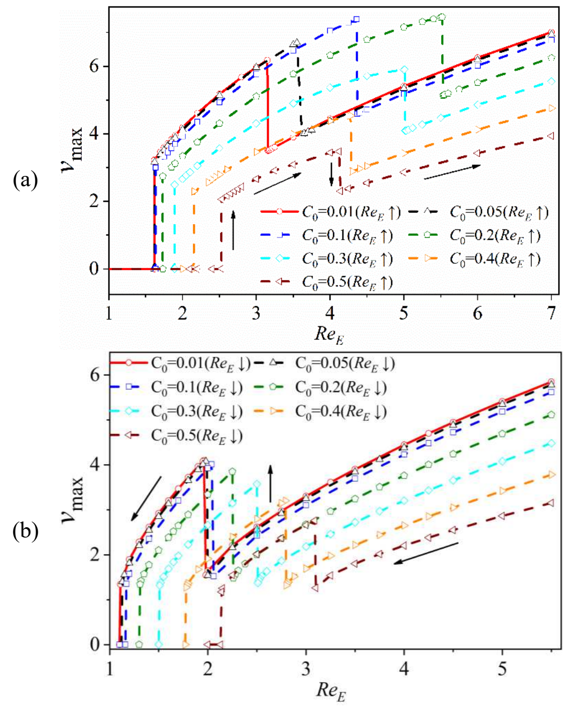

Fig. 14. Bifurcation diagrams of dielectric liquids with different residual conductivities at $C = 10$ with (a) increase and (b) decrease of the electric Reynolds number Re_E.

Table 2 The linear and nonlinear criteria (Re_{Ec1}, Re_{Ec2}, Re_{Ef1} and Re_{Ef2}) of dielectric liquids with different residual conductivities at strong injection strength ($C = 10$).

C_0	0	0.01	0.05	0.1	0.2	0.3	0.4	0.5
Re_{Ec1}	1.636	1.636	1.641	1.656	1.732	1.892	2.152	2.529
Re_{Ec2}	3.12-3.13	3.15-3.16	3.59-3.60	4.36-4.37	5.52-5.53	5.01-502	4.28-4.29	4.13-4.14
Re_{Ef1}	1.97-1.98	1.97-1.98	1.99-2.00	2.03-2.04	2.25-2.26	2.50-2.51	2.79-2.80	3.09-3.10
Re_{Ef2}	1.08-1.09	1.09-1.10	1.12-1.13	1.16-1.17	1.30-1.31	1.50-1.51	1.77-178	2.13-2.14

Here Re_{Ec1} corresponds to the critical point at which EC happens, Re_{Ec2} denotes the critical point at which EC bifurcates from a one-cell state to a two-cell state. Re_{Ef1} corresponds to the critical point that the two-cell EC system bifurcates to the one-cell state, and Re_{Ef2} represents the critical point that the one-cell EC system bifurcates to the hydrostatic state.

Complete bifurcation diagrams are drawn in Fig.14 to explain the influence of the residual conductivity parameters on the bifurcation process with increasing electric Reynolds number Re_E. The four corresponding criteria are summarized in Table 2. The critical values of the dielectric liquids in the saturation regime represented by weak conductivity ($C_0 = 0.01$ to 0.1) are slightly higher than those without residual conductivity. When the residual conductivity is further increased, the values of the linear (Re_{Ec1}) criteria increase significantly. The maximum velocity corresponding to the onset of one-cell EC decreases as the residual conductivity increases. This indicates that residual conductivity inhibits the occurrence of EC, especially when the dielectric liquid is at the transition regime between the saturation regime and the ohmic regime. The second criterion (Re_{Ec2}) and the bifurcation process to two-cell EC flow present a more complex pattern. When the residual conductivity parameter C_0 is less than 0.2, the value of Re_{Ec2} increases with increasing residual conductivity, while the range of electric Reynolds number Re_E in one-cell EC flow state expands. In addition, the maximum velocity corresponding to Re_{Ec2} also increases. However, such maximum velocities in the dielectric liquids with residual conductivity parameters $C_0 = 0.1$ and $C_0 = 0.2$ are very close to each other. As the conductivity parameter C_0 further increases, the range of Re_E at the one-cell EC state shrinks, and the corresponding maximum velocity reduces. There are two effects of the residual conductivity on the EC flow in a dielectric liquid. One is that residual conductivity inhibits the flow intensity of EC flow, the other is that it can stabilize the EC flow and expand the region of a steady EC system.

To explain the complex rule about the influence of residual conductivity on the above bifurcation criteria, the contour lines distribution of net charge density ($q = n_+ - n_-$) at $q = 0.05$ and the Coulomb force ($Fe = qE$) at $Fe = 150$ for the one-cell EC system at the critical point that bifurcating to the two-cell EC system are presented in Fig. 15. We define the region with $q < 0.05$ as the net charge void region and the region with $Fe < 150$ as the weak electric field force region. For the EC system, with the increase of electric Reynolds number Re_E, the overall intensity of the EC flow increase, and the electric torque required to maintain the convection increase correspondingly. As shown in Fig. 15, when $C_0 \leq 0.1$, the area of net charge void region and weak electric field force region expands with the increase of C_0. This means that with the increase of C_0, the net charge concentrates more at the right side of the region, and the intensity difference of the Coulomb force between inside and outside of the net charge void region increases with the increase of C_0, which results in stronger electric torque in the system. A stronger electric torque could maintain the stability of the one-cell EC under a larger driving parameter Re_E. When $C_0 \geq 0.2$, the area of the net charge void region, as well as the area of the weak electric field force region, decreases with the increase of residual conductivity. The intensity difference of the electric field force between inside and outside the charge void region decreases with the increase of C_0, and the electric torque in the domain decreases, making the EC system unable to maintain the one-cell state under larger driving parameters.

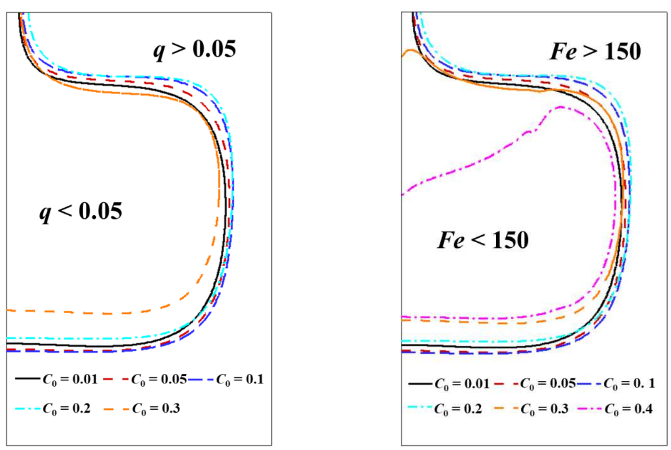

(a) (b)

Fig. 15. The contour lines distribution of (a) net charge density at q = 0.05 and (b) the Coulomb force at Fe = 150 for the EC systems with different residual conductivity at the critical point that bifurcates from the one-cell state to the two-cell state.

4.2. Medium and weak injection regime (C = 1 and 0.1)

In this section, the numerical analysis is extended to the medium and weak injection regime with C=1 and 0.1 correspondingly. In Fig. 16 the bifurcations of dielectric liquids with different residual conductivities at C = 1 with increasing and decreasing electric Reynolds number Re_E are depicted. When the electric field is increased, the bifurcation diagram shows characteristics similar to those in the strong injection cases. After the initial static state, the system loses its stability and generates one cell EC flow when Re_E is greater than the critical value of Re_{Ec1}. The flow strength increases with increasing electric field. When Re_E is greater than the second critical point (Re_{Ec2}), the flow evolves from a one-cell structure to one pair of cells.

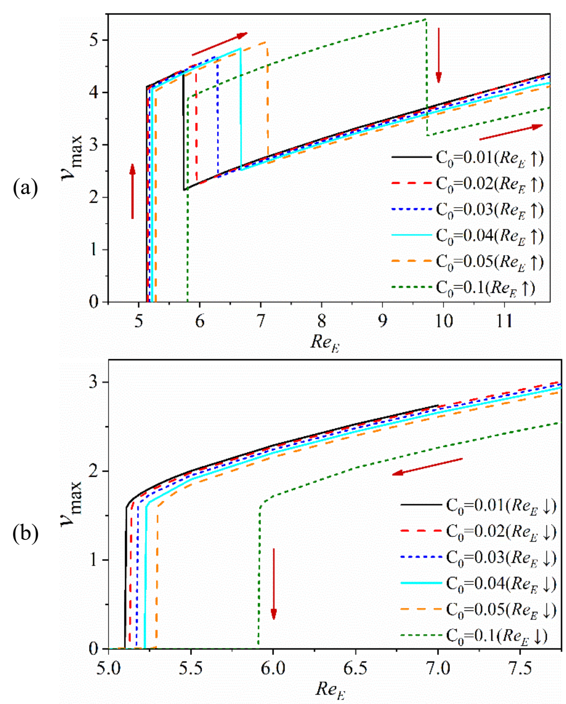

Fig. 16. Bifurcation diagrams of dielectric liquids with different residual conductivities at C = 1 with (a) increase and (b) decrease of the electric Reynolds number Re_E.

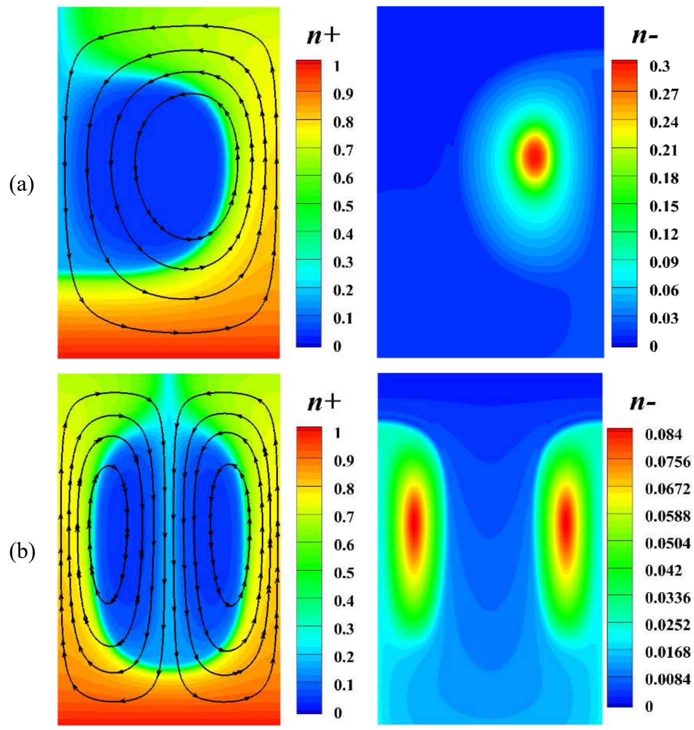

Fig. 17. Streamline and isocontours of the positive (left) and negative (right) charge density distributions in the case of $C = 1$, $C_0 = 0.01$ at (a) $Re_E = 5.4$ and (b) $Re_E = 7.5$.

The streamline and charge density of the EC flow with $C_0 = 0.01$ and $C = 1$ are depicted in Fig.17. For cases at $C_0 = 0.01$, the EC flow of one cell structure exists only within a relatively narrow range of Re_E before the system bifurcates to the two-cell structure. The range of Re_E at the one-cell state expands for dielectric liquids with larger residual conductivities. When the applied electric field is reduced from the one-cell EC states, the EC systems keep the one-cell state at the first linear critical point (Re_{Ec1}) until eventually bifurcate into the hydrostatic state at the first nonlinear critical point (Re_{Ef}^{1}) for dielectric liquids with residual conductivity parameter C_0 in the range of 0.001 to 0.1. However, when the applied electric field reduces from the two-cell EC states, the EC keeps the two-cell EC states without transforming into a one-cell structure, until eventually bifurcates into the hydrostatic state at the second nonlinear critical point (Re_{Ef}^{2}). As explained in the previous study, there are three different possible scenarios when restarting the computation from the previous two-cell EC state, but with lower Re_E values.[52] The flow would keep a two-cell structure but with weaker velocity amplitude and a smaller area of the charge void region if $Re_E > Re_{Ef2}$. If $Re_{Ec1} < Re_E < Re_{Ef2}$, the flow motion (two cells) will jump to rest at first, and then it will restart again but with one cell, which is due to the loss of the linear instability. If $Re_E < Re_{Ec1}$ the flow will return and keep still. In the present study, as shown in Table 2, the criteria (Re_{Ef1}) correspond to the critical point that the two-cell EC system bifurcates to the one-cell state obeys the rule of $Re_{Ec1} < Re_E$ for EC with residual conductivity in a strong injection regime. It is a little different for dielectric liquids with different residual conductivity in a medium injection regime. Table 3 summarizes the linear and nonlinear criteria (Re_{Ec1}, Re_{Ec2}, Re_{Ef}^{1} and Re_{Ef}^{2}) of dielectric liquids with different residual conductivities at medium injection strength (C = 1). Both linear and nonlinear criteria in medium injection cases increase as the residual conductivity is increased. The maximum velocity at the non-linear critical point also increases. The value of Re_{Ef}^{1} is much less than the value of Re_{Ec1}, while Re_{Ef}^{2} remaining close to the value of Re_{Ec1}. For $C_0 \leqslant 0.02$, the criteria (Re_{Ef}^{2}) correspond to the critical point that the two-cell EC system bifurcate to the rest state is slightly smaller than the onset (Re_{Ec1}) of one-cell EC, which is the same as the strong injection. For C_0 = 0.03, Re_{Ef}^{2} is almost equivalent with Re_{Ec1}; while for $C_0 \geqslant 0.04$, Re_{Ef}^{2} is a little greater than Re_{Ec1}. The explanation for this variation is that the greater residual conductivity inhibits more flow intensity of the EC system. This results in the electric torque becoming lower than the viscous one and leading to the stop of the EC motion from the steady two-cell state.

Table 3 The linear and non-linear criteria of dielectric liquids with different residual conductivities at medium injection ($C = 1$).

C_0	0.001	0.01	0.02	0.03	0.04	0.05	0.1
Re_{Ec1}	5.122	5.130	5.149	5.178	5.219	5.278	5.803
Re_{Ec2}	5.68-5.69	5.73-5.74	5.91-5.92	6.33-6.34	6.67-6.68	7.11-7.12	9.72-9.73
Re_{Ef}^{1}	2.36-2.37	2.37-2.38	2.39-2.4	2.41-2.42	2.43-2.44	2.47-2.48	2.76-2.77
Re_{Ef}^{2}	5.09-5.10	5.10-5.11	5.13-5.14	5.17-5.18	5.22-5.23	5.29-5.30	5.91-5.92

Here Re_{Ec1} corresponds to the critical point at which electroconvection happens, Re_{Ec2} denotes the critical point at which electroconvection bifurcates from a one-cell state to a two-cell state. Re_{Ef}^{1} represents the critical point that the one-cell EC system bifurcates to the hydrostatic state. Re_{Ef}^{2} represents the critical point that the two-cell EC system bifurcates to the hydrostatic state.

For weak injection ($C = 0.1$), the EC flow occurs when the applied electric field is much stronger than that in strong and medium injection cases. In addition, the EC flows in weak injection cases are always oscillating, which is different from the steady flow state observed in strong and medium injection cases. As explained in a previous study,[52] Fig.18 plots the temporal evolution of the maximum velocity for dielectric liquids with residual conductivities for $C = 0.1$ at $Re_E = 300$ and 500. There are always small oscillations even when finer meshes are adopted. The maximum velocity and amplitude of the oscillation increase with the increase in Re_E. Three snapshots of streamline and contours of the positive (upper) and negative (bottom) charge density distributions in cases of $C = 0.1$, $C_0 = 0.001$ for Re_E = 300, 500, and 1000 are depicted in Fig.19. The distribution of positive charge density is more concentrated near the boundary, while the feature of the charge void region is not as typical as that in the strong and medium cases. However, the non-zero positive electric charge along the left side is an artifact of the numerical method for weak injection; see Ref.53. This fact does not invalidate the computation of the critical threshold but may influence the details of amplitude oscillations. There exists a charge density decline region for weak injection cases with residual conductivity. At the same time, the negative charge density concentrates toward the center of the egg-shaped area and the egg-shaped negative charge density distributed region is larger. Additionally, different from the flow field of one cell in the strong and medium injection cases, there are two small angular vortices located on the diagonal of the larger global vortex cell for $Re_E = 300$ and 500. As Re_E increases, the strength of the flow field increases, and the distributions of positive and negative charges are more irregular. The positive charges are located more around the bulk, while the negative charges are concentrated in the center.

Fig. 20 presents four snapshots of the streamline and charge density (q) distributions in the case of $C = 0.1$, $C_0 = 0.001$. The two large symmetrical cells structured flow field as depicted in Fig.20(a) could only be observed at the initial period in the evolution process of the EC flow when a very strong electric field is applied. The system evolves into a state featuring a main cell together with a medium cell underneath, as shown in Fig.20(b). In addition, three extra small vortices in the top left corner of the bulk could be observed. Subsequently, the size of the main cell expands while the bottom and upper left vortices disappear, replaced by two new small vortices in the upper right and lower left corners. Eventually, the system evolves into the main cell, accompanied by several smaller cells located at the corner. Similar patterns exist for dielectric liquids with larger residual conductivities. The numerical study by Traoré *et al*.[54] confirms that in the range of $M \propto [5, 10]$, the convective structure of a cell is the dominant flow structure.

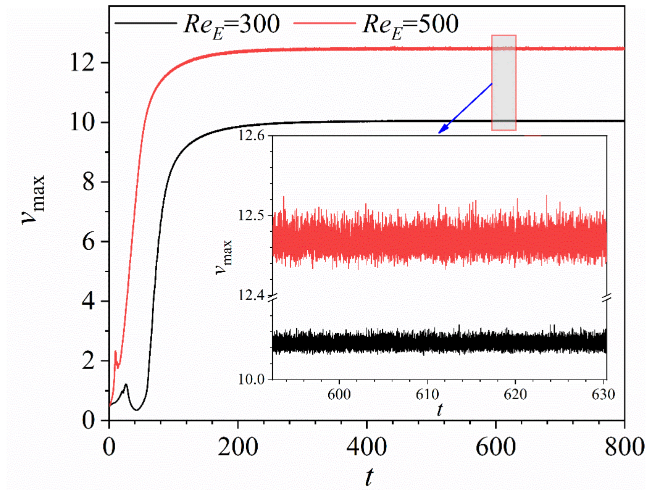

Fig. 18. Temporal evolution of the maximum velocity for cases of dielectric liquids at C = 0.1, C_0 = 0.001, Re_E = 300 and 500.

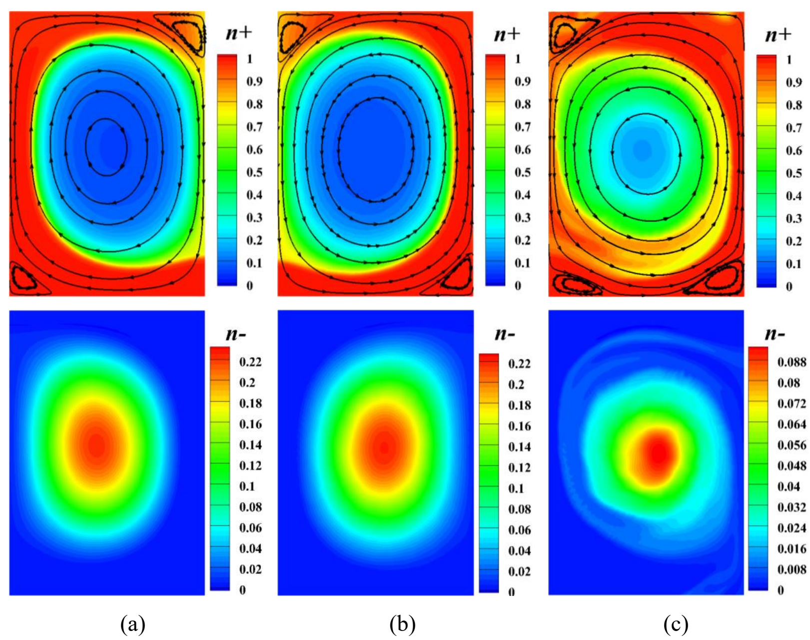

Fig. 19. Streamline and contours of the positive (upper) and negative (bottom) charge density distributions in the case of C = 0.1, C_0 = 0.001 for (a) Re_E = 300, (b) Re_E = 500 and (c) Re_E = 1000.

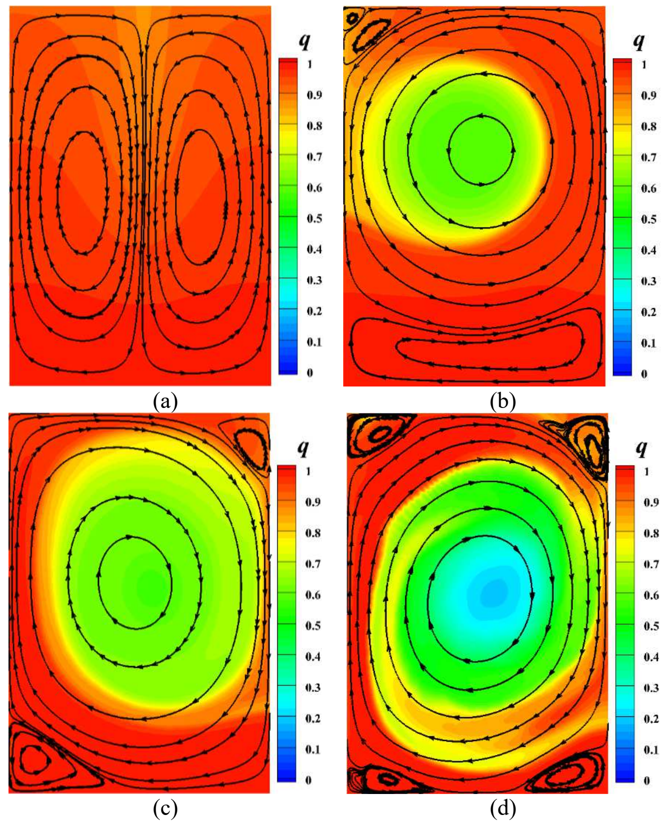

Fig. 20. Four snapshots of the streamline and charge density (q) distributions in the case of $C = 0.1$, $C_0 = 0.001$, $Re_E = 1200$ at (a) $t = 10$, (b) $t = 30$, (c) $t = 50$, and (d) $t = 160$.

Table 4 The linear criterion (Re_{Ec}) and the nonlinear criterion (Re_{Ef}) of dielectric liquids with different residual conductivities at weak injection ($C = 0.1$).

C_0	0.001	0.002	0.003	0.004	0.005	0.01
Re_{Ec}	218.62	224.16	234.52	248.96	263.54	283.97
Re_{Ef}	40-50	40-50	50-60	85-95	90-100	100-110

Here Re_{Ec} corresponds to the critical point at which electro-convection occurs, and Re_{Ef} corresponds to the critical point that the EC system bifurcates to the hydrostatic state.

Table 4 presents the summary of linear and nonlinear criteria (Re_{Ec} and Re_{Ef}) of dielectric liquids with different residual conductivities at weak injection strength (C =

0.1). The values of nonlinear criteria (Re_{Ef}) in weak injection cases are not as accurate as those in strong and medium injection cases. The strong oscillatory EC flow obtained in weak injection cases can affect the final flow state when reducing the applied electric field from the previous simulations with higher Re_E. For all this, many simulations have been performed, and the values of Re_{Ef} are always within the range given in Table 4. Therefore, some qualitative rules which are consistent with those in the cases of strong and medium injection can be obtained. The increase of residual conductivity will inhibit the occurrence of electroconvection and make the critical value of Re_{Ec} increase. At the same time, the residual conductivity also inhibits the flow intensity of the electroconvection. When the intensity of the applied electric field gradually reduces, the residual conductivity in a dielectric liquid accelerates the process of the electric convection returning to the static state. Therefore, the corresponding critical value Re_{Ef} decreases with the decrease of the residual conductivity.

5. Conclusions

In this study, we extended the numerical analysis of electro-convection (EC) of perfectly insulating liquids to dielectric liquids with residual conductivity. A finite-volume method in the framework of OpenFOAM® based on the dissociation-injection model is developed. Three different typical injection strengths of the strong, medium, and weak (C =10, 1, and 0.1) were considered. The influence of residual conductivity on flow characteristics and bifurcation processes was explored. The results showed that the residual conductivity significantly affects the critical points of the bifurcation. Two effects of the residual conductivity to the EC flow in a dielectric liquid could be identified. One is that the residual conductivity inhibits the onset of EC flow and reduces the strength of the flow field; the other is that it can stabilize the EC flow and expand the region of the steady EC system. Meanwhile, the existence of both positive and negative charges in dielectric liquids with residual conductivity resulted in abundant flow features and charge density distributions. In addition, three distinct bifurcation sequences for dielectric liquids with varied residual conductivities at different injection strengths are observed by gradually raising or reducing the electric Reynolds number. For the strong and medium injection, the bifurcation from a one-cell state to a two-cell state could be observed. However, one dominant convective cell accompanied by several small vortices at the corner is always the main flow structure for the weak injection, even for highly oscillating EC flow.

Acknowledgments

This work is supported by the National Natural Science Foundation of China (Grant No. 12172110, 11802079) and the Fundamental Research Funds for Central Universities (Grant No. AUGA9803500921). A. T. Pérez and P. A. Vázquez acknowledge Grant PGC2018-099217-B-I00 funded by MCIN/AEI/ 10.13039/501100011033 and by “ERDF A way of making Europe”, and Grant CTQ2017-83602-C2-2-R funded by MEC.

Data Availability

Data supporting the findings of this study are available from the corresponding author on a reasonable request.

References

1. E. D. Fylladitakis, M. P. Theodoridis, and A. X. Moronis, "Review on the History, Research, and Applications of Electrohydrodynamics," IEEE Transactions on Plasma Science **42**, 358 (2014).
2. H. Xu, Y. He, K. L. Strobel, C. K. Gilmore, S. P. Kelley, C. C. Hennick, T. Sebastian, M. R. Woolston, D. J. Perreault, and S. R. H. Barrett, "Flight of an aeroplane with solid-state propulsion," Nature **563**, 532 (2018).
3. P. A. Vázquez, M. Talmor, J. Seyed-Yagoobi, P. Traoré, and M. Yazdani, "In-depth description of electrohydrodynamic conduction pumping of dielectric liquids: Physical model and regime analysis," Physics of Fluids **31**, 113601 (2019).
4. V. Cacucciolo, J. Shintake, Y. Kuwajima, S. Maeda, D. Floreano, and H. Shea, "Stretchable pumps for soft machines," Nature **572**, 516 (2019).
5. D. Nakhla, and J. S. Cotton, "Effect of electrohydrodynamic (EHD) forces on charging of a vertical latent heat thermal storage module filled with octadecane," International Journal of Heat and Mass Transfer **167**, 120828 (2021).
6. Z. Lu, G. Liu, and B. Wang, "Flow structure and heat transfer of electro-thermo-convection in a dielectric liquid layer," Physics of Fluids **31**, 064103 (2019).
7. Y. Guan, T. Yang, and J. Wu, "Mixing and transport enhancement in microchannels by

electrokinetic flows with charged surface heterogeneity," Physics of Fluids **33**, 042006 (2021).

8. B. Comiskey, J. D. Albert, H. Yoshizawa, and J. Jacobson, "An electrophoretic ink for all-printed reflective electronic displays," Nature **394**, 253 (1998).

9. A. Castellanos, *Electrohydrodynamics* (Springer New York, 1998).

10. P. Atten, "Electrohydrodynamic instability and motion induced by injected space charge in insulating liquids," IEEE Transactions on Dielectrics and Electrical Insulation **3(1)**, 1 (1996).

11. Y. K. Suh, "Modeling and simulation of ion transport in dielectric liquids-Fundamentals and review," IEEE Transactions on Dielectrics and Electrical Insulation **19**, 831 (2012).

12. F. Pontiga, and A. Castellanos, "Physical mechanisms of instability in a liquid layer subjected to an electric field and a thermal gradient," **6**, 1684 (1994).

13. P. Traoré, and A. T. Pérez, "Two-dimensional numerical analysis of electroconvection in a dielectric liquid subjected to strong unipolar injection," Physics of Fluids **24**, 037102 (2012).

14. A. V. Taraut, and B. L. Smorodin, "Electroconvection in the presence of autonomous unipolar injection and residual conductivity," Journal of Experimental and Theoretical Physics **115**, 361 (2012).

15. S. A. Vasilkov, K. D. Poluektova, and Y. K. Stishkov, "Experimental and numerical study of an electrohydrodynamic pump operating due to the field-enhanced dissociation near a dielectric barrier," Physics of Fluids **32**, 107102 (2020).

16. L. Onsager, "Deviations from Ohm's Law in Weak Electrolytes," The Journal of Chemical Physics **2**, 599 (1934).

17. A. Castellanos, "Coulomb-driven convection in electrohydrodynamics," IEEE Transactions on Electrical Insulation **26**, 1201 (1991).

18. M. Zhang, "Weakly nonlinear stability analysis of subcritical electrohydrodynamic flow subject to strong unipolar injection," Journal of Fluid Mechanics **792**, 328 (2016).

19. R. Chicón, A. Castellanos, and E. Martin, "Numerical modelling of Coulomb-driven convection in insulating liquids," Journal of Fluid Mechanics **344**, 43 (1997).

20. P. Atten, and R. Moreau, "Stabilité électrohydrodynamique des liquides isolants soumis à une injection unipolaire," J. Mécanique **11**, 471 (1972).

21. M. Zhang, F. Martinelli, J. Wu, Peter J. Schmid, and M. Quadrio, "Modal and non-modal stability analysis of electrohydrodynamic flow with and without cross-flow," Journal of Fluid Mechanics **770**, 319 (2015).

22. J. C. Lacroix, P. Atten, and E. J. Hopfinger, "Electro-convection in a dielectric liquid layer subjected to unipolar injection," Journal of Fluid Mechanics **69**, 539 (1975).

23. K. Luo, J. Wu, H.-L. Yi, and H.-P. Tan, "Three-dimensional finite amplitude electroconvection in dielectric liquids," Physics of Fluids **30**, 023602 (2018).

24. S. A. Vasilkov, V. A. Chirkov, and Y. K. Stishkov, "Electrohydrodynamic flow caused by field-enhanced dissociation solely," Physics of Fluids **29**, 063601 (2017).

25. V. A. Chirkov, S. A. Vasilkov, and Y. K. Stishkov, "The role of field-enhanced dissociation in electrohydrodynamic flow formation in a highly non-uniform electric field," Journal of Electrostatics **93**, 104 (2018).

26. J. C. Ryu, H. J. Park, J. K. Park, and K. H. Kang, "New Electrohydrodynamic Flow Caused by the Onsager Effect," Physical Review Letters **104**, 104502 (2010).

27. Z. Du, J. Huang, Q. Liu, R. Deepak Selvakumar, and J. Wu, "Numerical investigation on electrohydrodynamic conduction pumping with an external flow," Physics of Fluids **33**, 123609 (2021).

28. L. Wang, Z. Wei, T. Li, Z. Chai, and B. Shi, "A lattice Boltzmann modelling of

electrohydrodynamic conduction phenomenon in dielectric liquids," Applied Mathematical Modelling **95**, 361 (2021).

29. N. J. O'Connor, A. J. Castaneda, P. N. Christidis, N. Vayas Tobar, M. Talmor, and J. Yagoobi, "Experimental Study of Flexible Electrohydrodynamic Conduction Pumping for Electronics Cooling," Journal of Electronic Packaging **142**, (2020).

30. M. R. Hossan, D. Dutta, N. Islam, and P. Dutta, "Review: Electric field driven pumping in microfluidic device," Electrophoresis **39**, 702 (2018).

31. B.-F. Wang, and T. Wen-Hann Sheu, "Numerical investigation of electrohydrodynamic instability and bifurcation in a dielectric liquid subjected to unipolar injection," Computers & Fluids **136**, 1 (2016).

32. P. A. Vázquez, and A. Castellanos, "Numerical simulation of EHD flows using Discontinuous Galerkin Finite Element methods," Computers & Fluids **84**, 270 (2013).

33. Y. Wang, G. Qin, W. He, and X. Ye, "Spectral element method for numerical simulation of ETHD enhanced heat transfer in an enclosure with uniform and sinusoidal temperature boundary conditions," International Journal of Heat and Mass Transfer **141**, 949 (2019).

34. Z.-G. Su, T.-F. Li, and H.-L. Yi, "Simulation of electroconvection in a dielectric liquid by DUGKS," Computers & Fluids **188**, 31 (2019).

35. K. Luo, J. Wu, H.-L. Yi, and H.-P. Tan, "Lattice Boltzmann model for Coulomb-driven flows in dielectric liquids," Physical Review E **93**, 023309 (2016).

36. Y. Guan, and I. Novosselov, "Two relaxation time lattice Boltzmann method coupled to fast Fourier transform Poisson solver: Application to electroconvective flow," Journal of Computational Physics **397**, 108830 (2019).

37. D. V. Fernandes, H.-D. Lee, S. Alapati, and Y. K. Suh, "Numerical simulation of the electro-convective onset and complex flows of dielectric liquid in an annulus," Journal of Mechanical Science and Technology **26**, 3785 (2012).

38. D. V. Fernandes, H.-D. Lee, S. Park, and Y. K. Suh, "Electrohydrodynamic instability of dielectric liquid between concentric circular cylinders subjected to unipolar charge injection," Journal of Mechanical Science and Technology **27**, 461 (2013).

39. J. Wu, P. A. Vazquez, P. Traore, and A. T. Perez, "Finite amplitude electroconvection induced by strong unipolar injection between two coaxial cylinders," Physics of Fluids **26**, (2014).

40. J. Huang, Q. Wang, Y. Guan, Z. Du, R. Deepak Selvakumar, and J. Wu, "Numerical investigation of instability and transition to chaos in electro-convection of dielectric liquids between concentric cylinders," Physics of Fluids **33**, 044112 (2021).

41. Z.-G. Su, T.-F. Li, K. Luo, and H.-L. Yi, "Nonlinear behavior of electrohydrodynamic flow in viscoelastic fluids," Physical Review Fluids **6**, 093701 (2021).

42. D.-L. Chen, K. Luo, J. Wu, and H.-L. Yi, "Electrohydrodynamic conduction pumping of a viscoelastic dielectric fluid with the Onsager–Wien effect," Physics of Fluids **33**, 113101 (2021).

43. R. Tobazeon, "Electrohydrodynamic instabilities and electroconvection in the transient and A.C. regime of unipolar injection in insulating liquids: A review," Journal of Electrostatics **15**, 359 (1984).

44. R. D. Selvakumar, J. Wu, J. Huang, and P. Traoré, "Electro-thermo-convection in a differentially heated square cavity under arbitrary unipolar injection of ions," International Journal of Heat and Fluid Flow **89**, 108787 (2021).

45. H. G. Weller, G. Tabor, H. Jasak, and C. Fureby, "A tensorial approach to computational continuum mechanics using object-oriented techniques," Computers in Physics **12**, 620 (1998).

46. F. Moukalled, L. Mangani, and M. Darwish, *The Finite Volume Method in*

Computational Fluid Dynamics (Erratum to The finite volume method in computational fluid dynamics [Fluid Mechanics and Its Applications, 113, DOI 10.1007/978-3-319-16874-6], 2016).

47. B. P. Leonard, "A stable and accurate convective modelling procedure based on quadratic upstream interpolation," Computer Methods in Applied Mechanics and Engineering **19**, 59 (1979).

48. B. van Leer, "Towards the Ultimate Conservative Difference Scheme," Journal of Computational Physics **135**, 229 (1997).

49. R. D. Selvakumar, L. Qiang, L. Kang, P. Traoré, and J. Wu, "Numerical modeling of solid-liquid phase change under the influence an external electric field," International Journal of Multiphase Flow **136**, 103550 (2021).

50. P. Atten, and J. Seyed-Yagoobi, "Electrohydrodynamically induced dielectric liquid flow through pure conduction in point/plane geometry," IEEE Transactions on Dielectrics and Electrical Insulation **10**, 27 (2003).

51. D. V. Fernandes, D. S. Cho, and Y. K. Suh, "Electrohydrodynamic flow of dielectric liquid around a wire electrode - effect of truncation of onsager function," IEEE Transactions on Dielectrics and Electrical Insulation **21**, 194 (2014).

52. J. Wu, P. Traoré, A. T. Pérez, and P. A. Vázquez, "On two-dimensional finite amplitude electro-convection in a dielectric liquid induced by a strong unipolar injection," Journal of Electrostatics **74**, 85 (2015).

53. P. A. Vázquez, G. E. Georghiou, and A. Castellanos, "Characterization of injection instabilities in electrohydrodynamics by numerical modelling: comparison of particle in cell and flux corrected transport methods for electroconvection between two plates," Journal of Physics D: Applied Physics **39**, 2754 (2006).

54. P. Traoré, and J. Wu, "On the limitation of imposed velocity field strategy for Coulomb-driven electroconvection flow simulations," Journal of Fluid Mechanics **727**, R3 (2013).

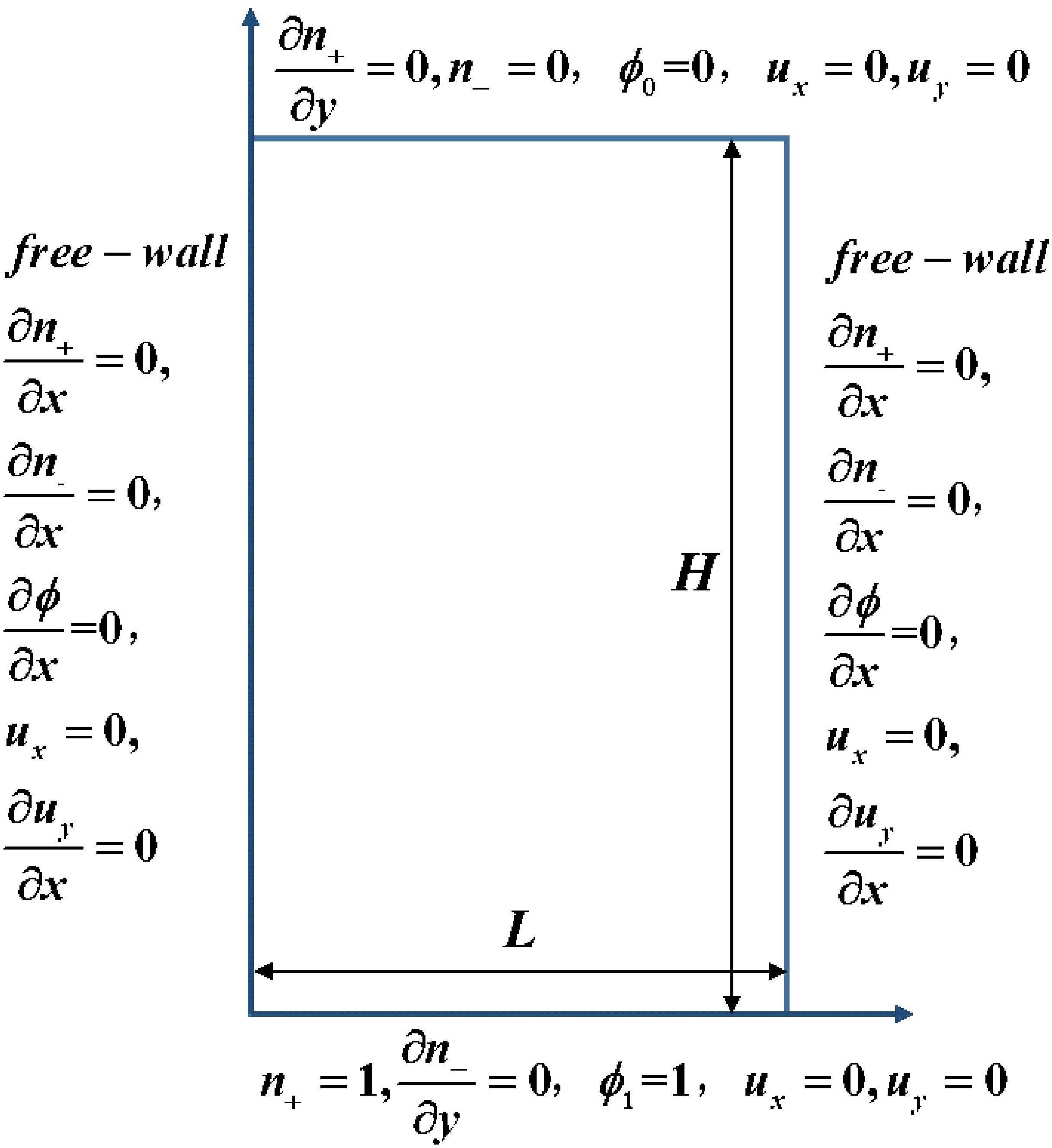
$\frac{\partial n_+}{\partial y} = 0, n_- = 0, \quad \phi_0 = 0, \quad u_x = 0, u_y = 0$
$free - wall$
$\frac{\partial n_+}{\partial x} = 0,$
$\frac{\partial n_-}{\partial x} = 0,$
$\frac{\partial \phi}{\partial x} = 0,$
$u_x = 0,$
$\frac{\partial u_y}{\partial x} = 0$
$free - wall$
$\frac{\partial n_+}{\partial x} = 0,$
$\frac{\partial n_-}{\partial x} = 0,$
$\frac{\partial \phi}{\partial x} = 0,$
$u_x = 0,$
$\frac{\partial u_y}{\partial x} = 0$
H
L
$n_+ = 1, \frac{\partial n_-}{\partial y} = 0, \quad \phi_1 = 1, \quad u_x = 0, u_y = 0$

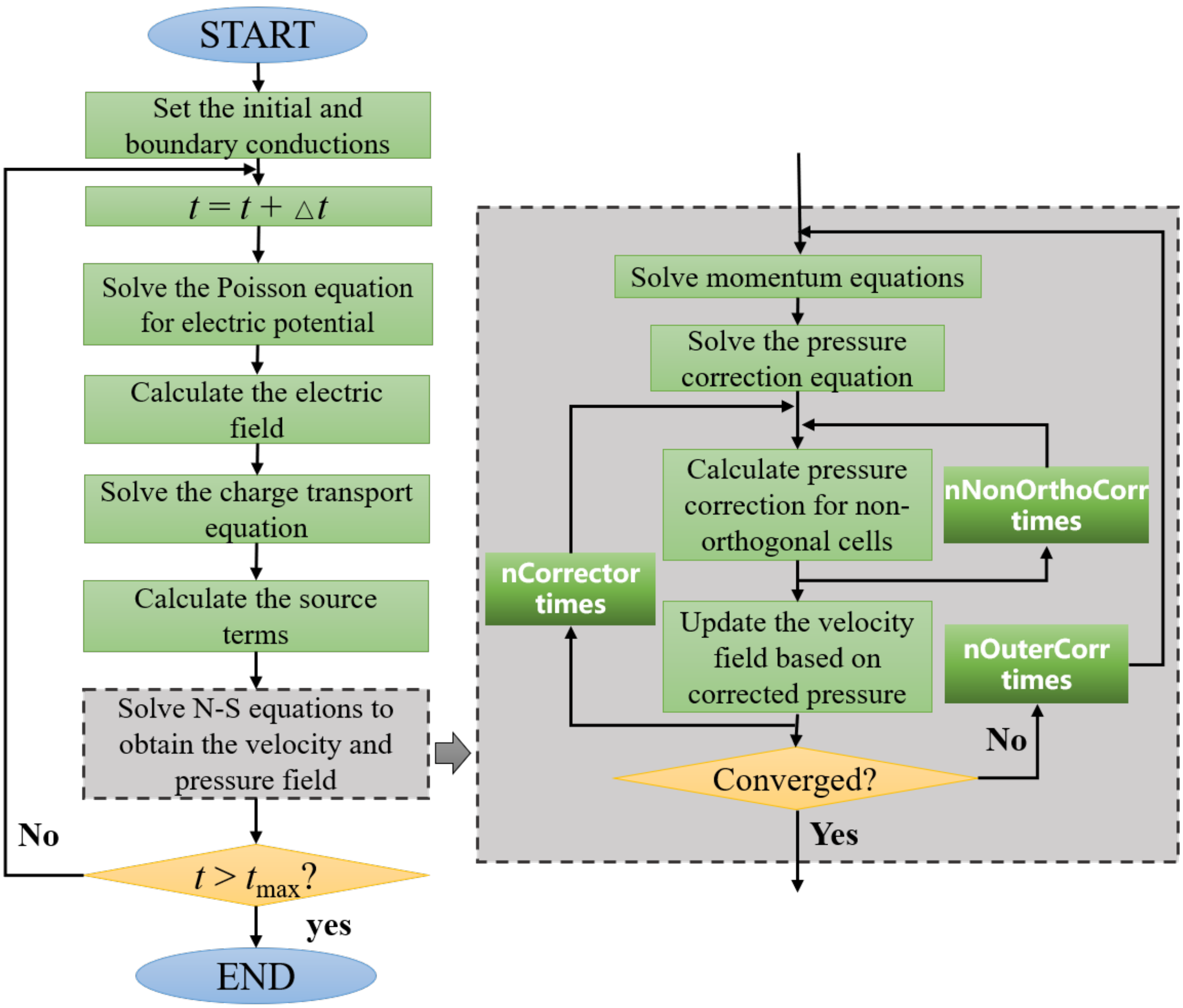
START
Set the initial and boundary conductions
t = t + △t
Solve the Poisson equation for electric potential
Calculate the electric field
Solve the charge transport equation
Calculate the source terms
Solve N-S equations to obtain the velocity and pressure field
t > tmax?
No
yes
END
Solve momentum equations
Solve the pressure correction equation
Calculate pressure correction for non-orthogonal cells
nNonOrthoCorr times
nCorrector times
Update the velocity field based on corrected pressure
nOuterCorr times
No
Converged?
Yes

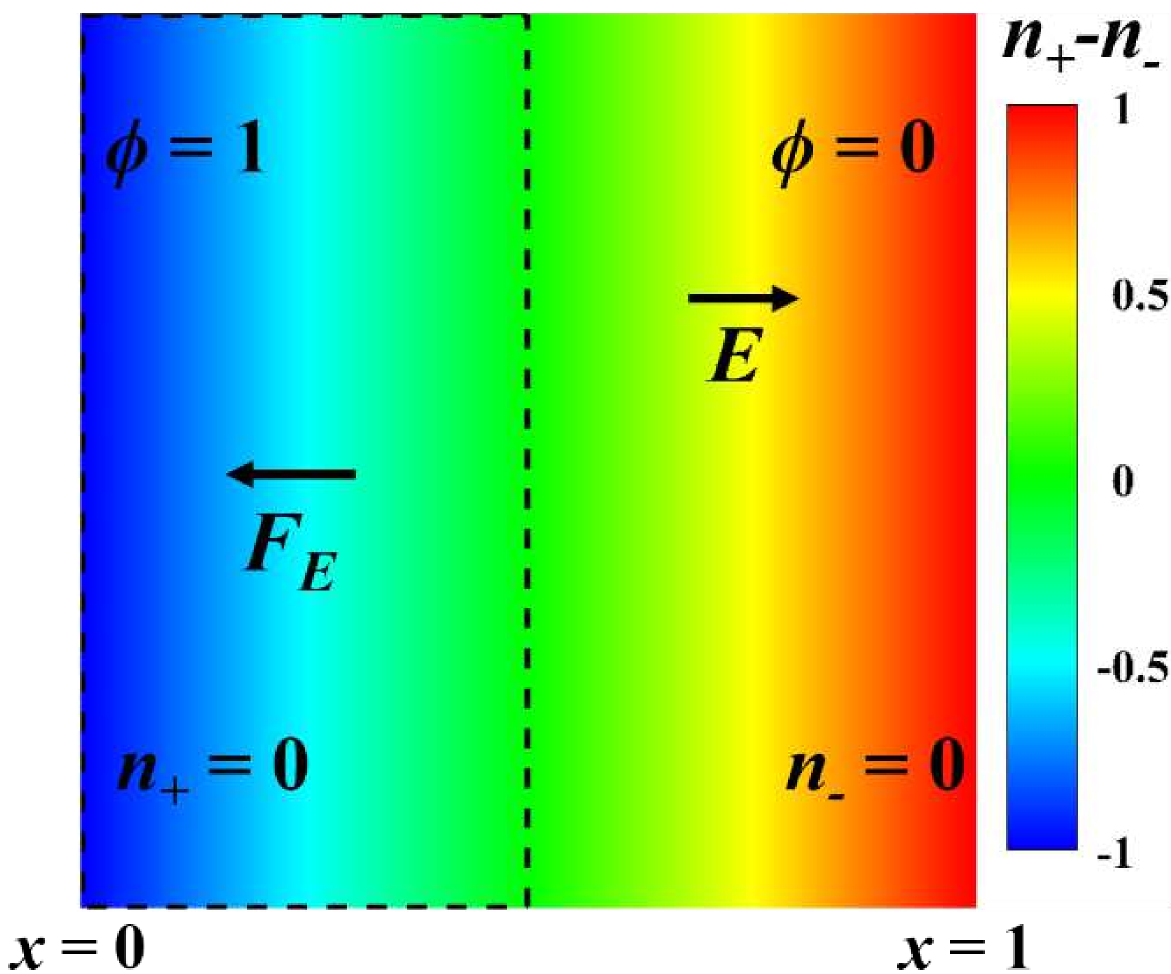
$\phi = 1$
$\phi = 0$
$\boldsymbol{E}$
$\boldsymbol{F_E}$
$n_+ = 0$
$n_- = 0$
$x = 0$
$x = 1$
$n_+ - n_-$
1
0.5
0
-0.5
-1

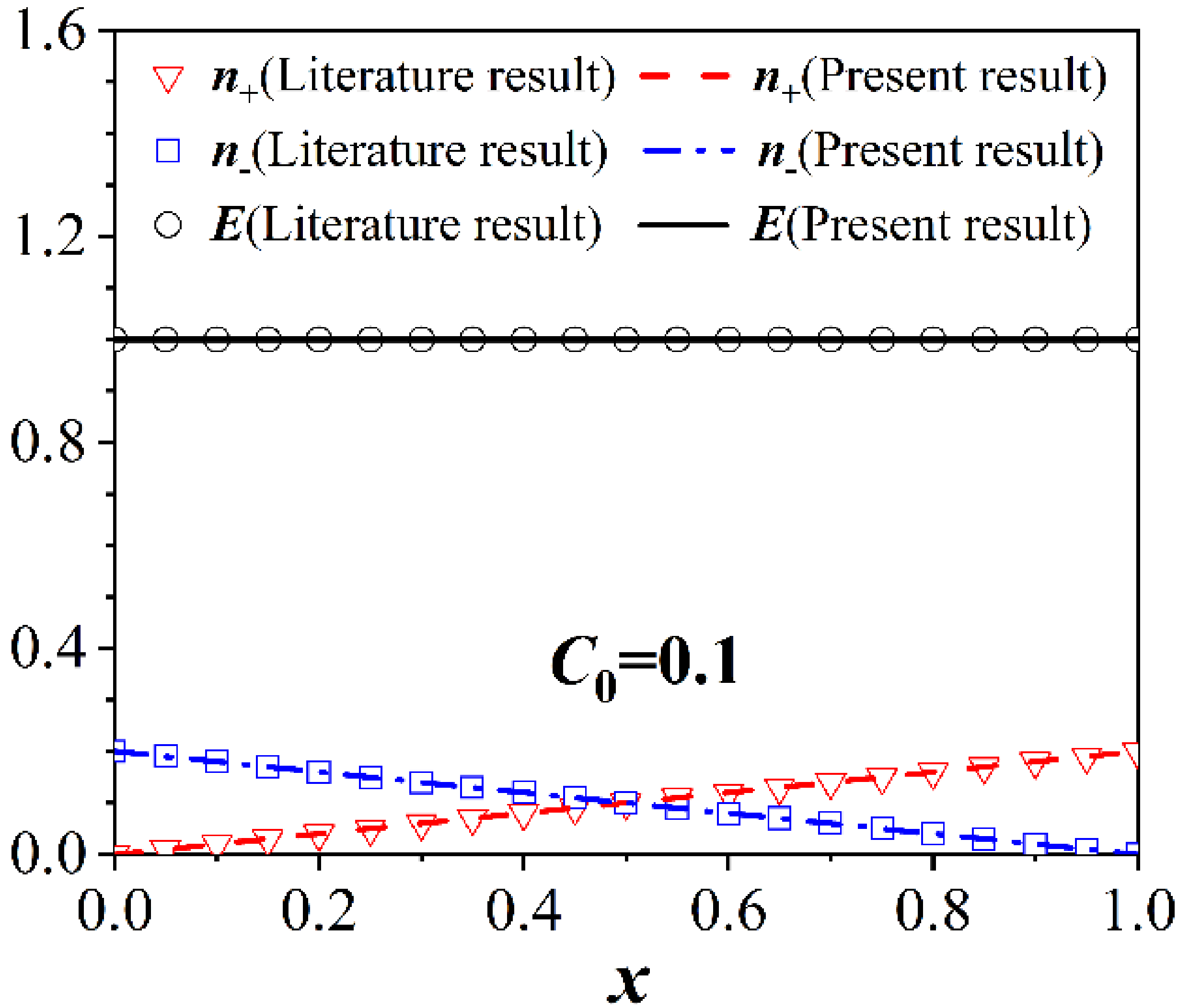
n_+(Literature result)
n_+(Present result)
n_-(Literature result)
n_-(Present result)
E(Literature result)
E(Present result)
C_0=0.1
1.6
1.2
0.8
0.4
0.0
0.0
0.2
0.4
0.6
0.8
1.0
x

PLEASE CITE THIS ARTICLE AS DOI: 10.1063/5.0086189

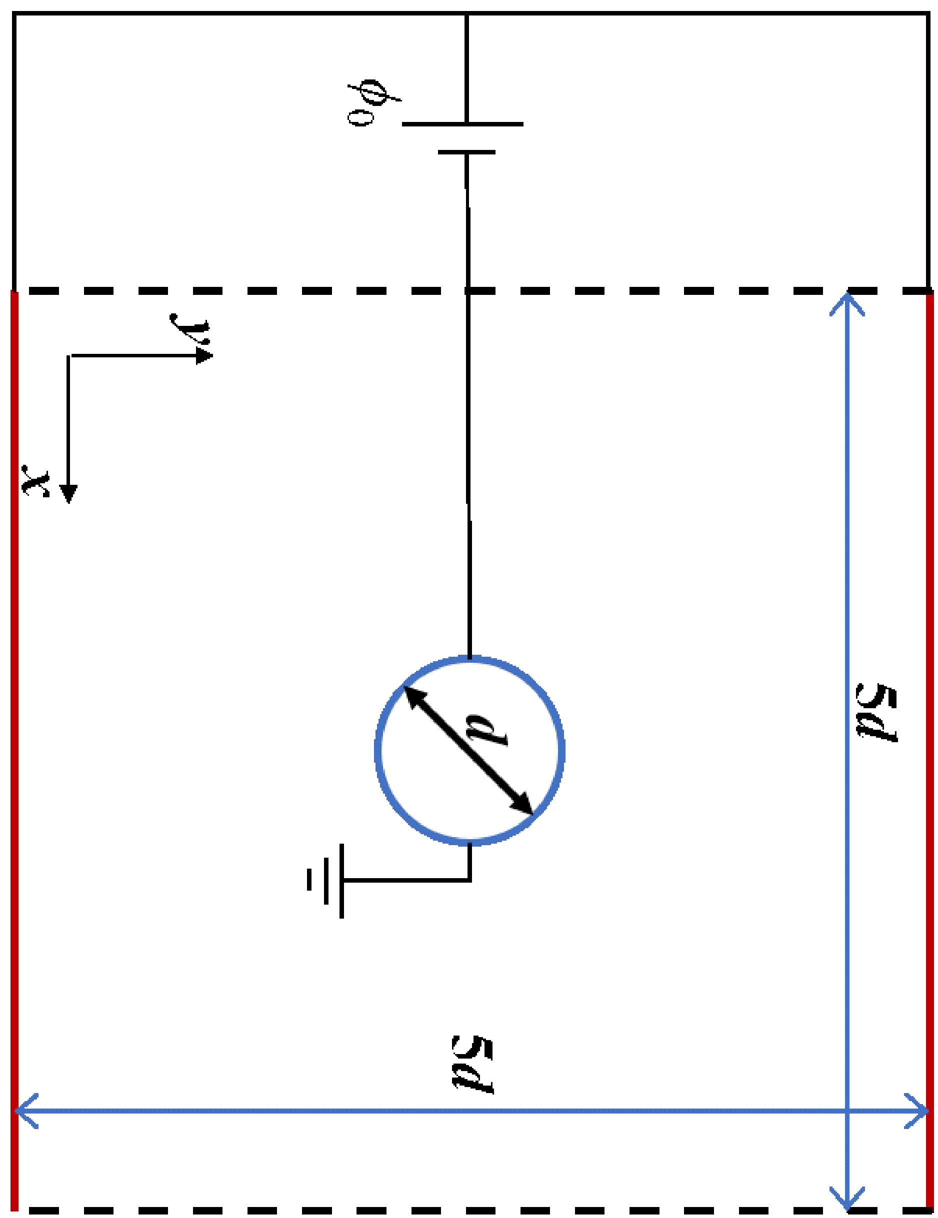

PLEASE CITE THIS ARTICLE AS DOI: 10.1063/5.0086189

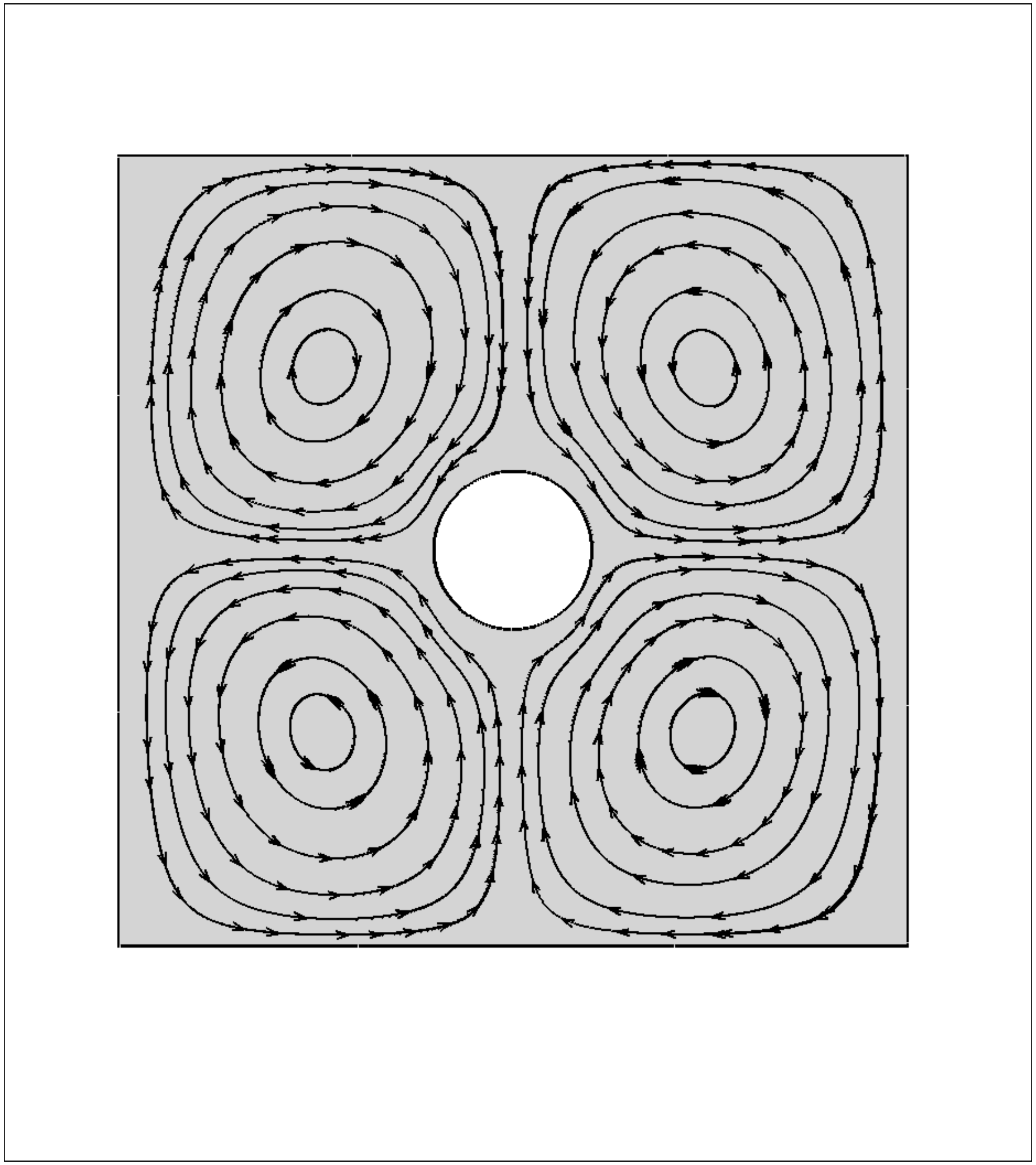

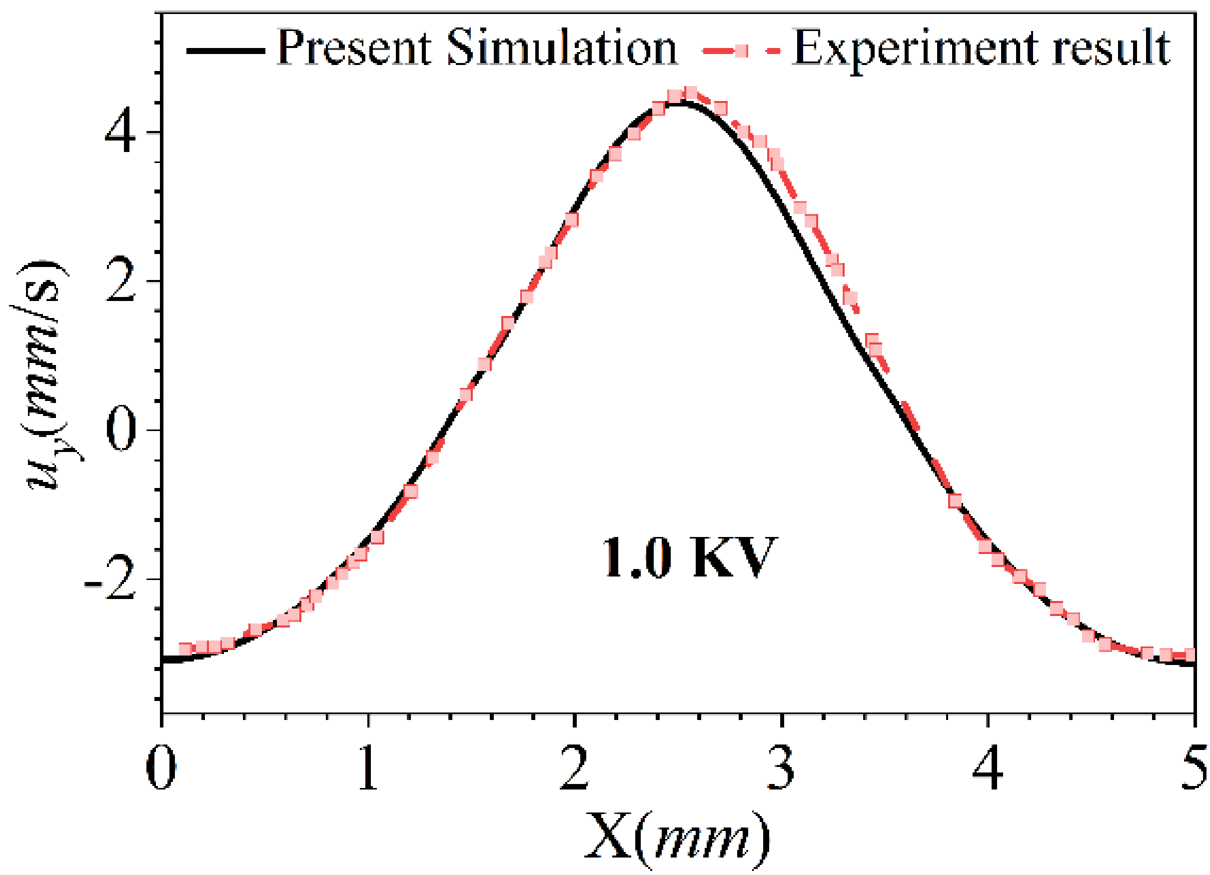
Present Simulation
Experiment result
1.0 KV
$u_y(mm/s)$
X(mm)
4
2
0
-2
0
1
2
3
4
5

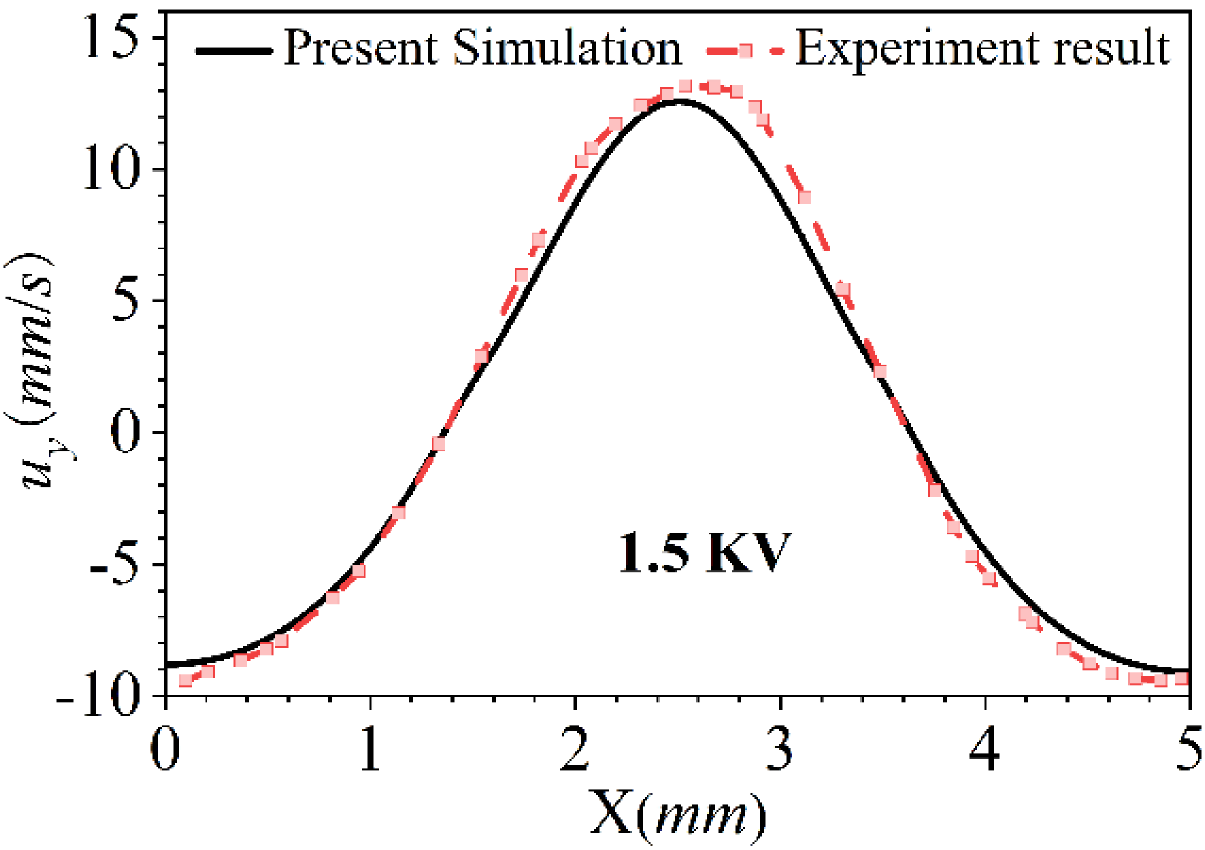
Present Simulation
Experiment result
1.5 KV
$u_y\,(mm/s)$
X(mm)
15
10
5
0
-5
-10
0
1
2
3
4
5

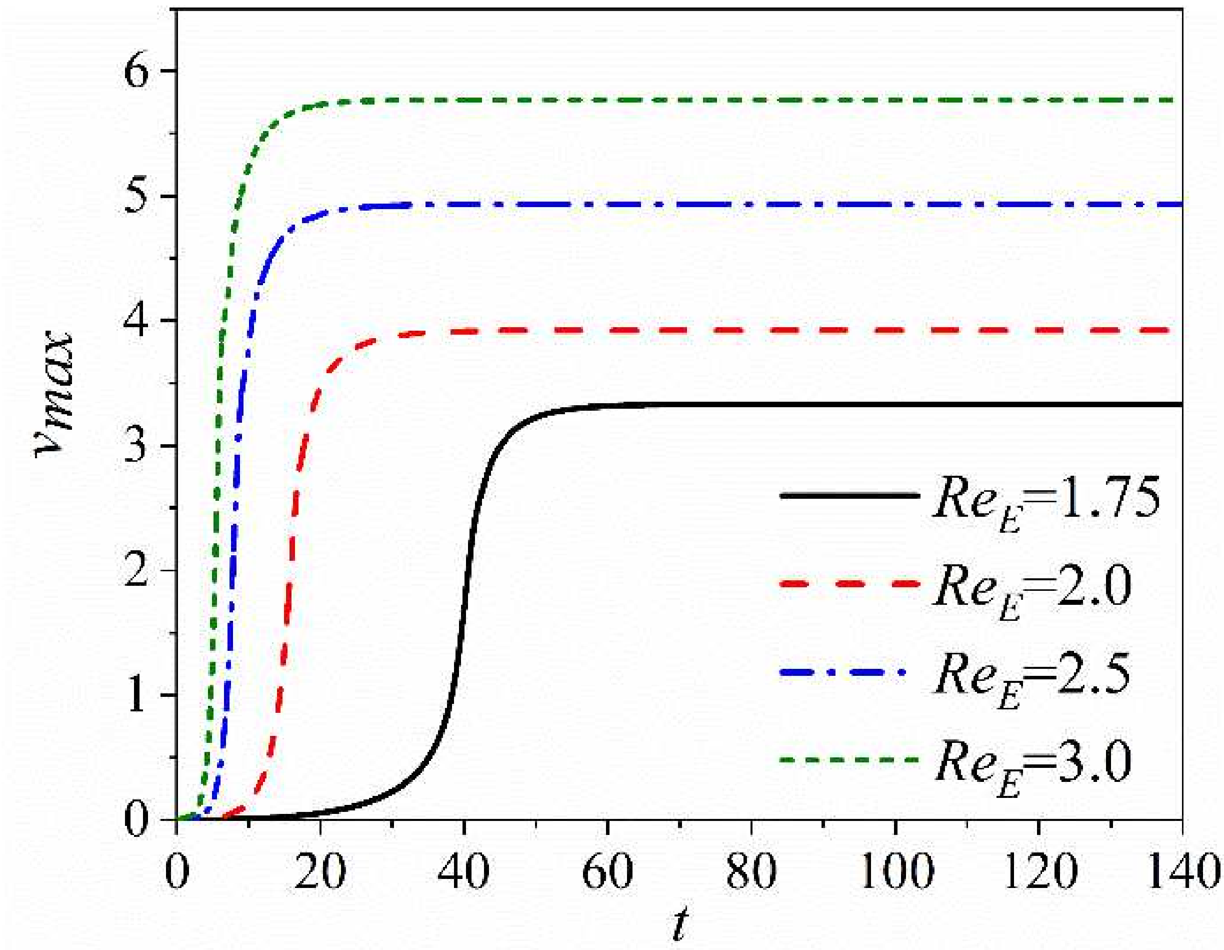
v_{max}
t
Re_E=1.75
Re_E=2.0
Re_E=2.5
Re_E=3.0

PLEASE CITE THIS ARTICLE AS DOI: 10.1063/5.0086189

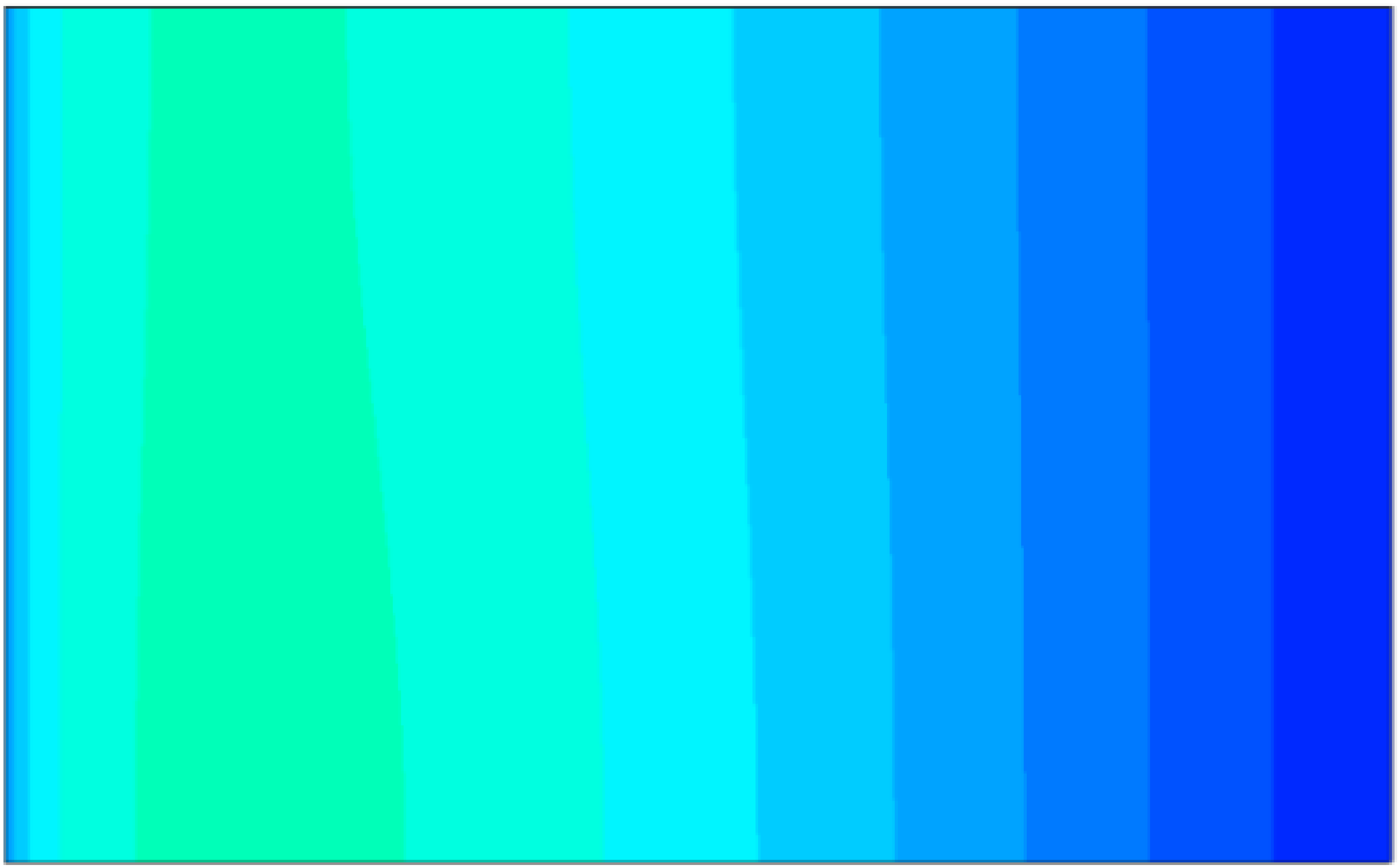

PLEASE CITE THIS ARTICLE AS DOI: 10.1063/5.0086189

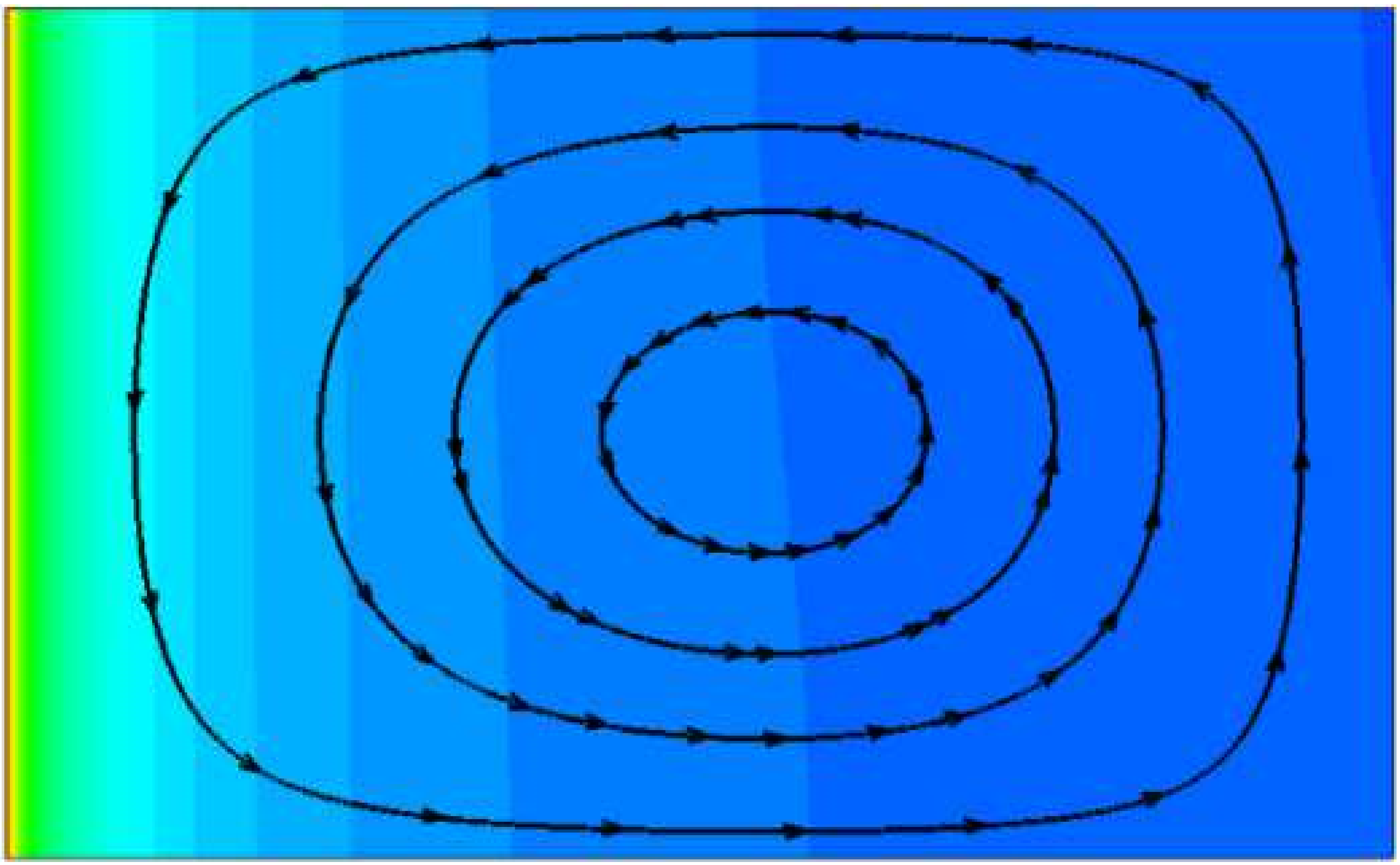

PLEASE CITE THIS ARTICLE AS DOI: 10.1063/5.0086189

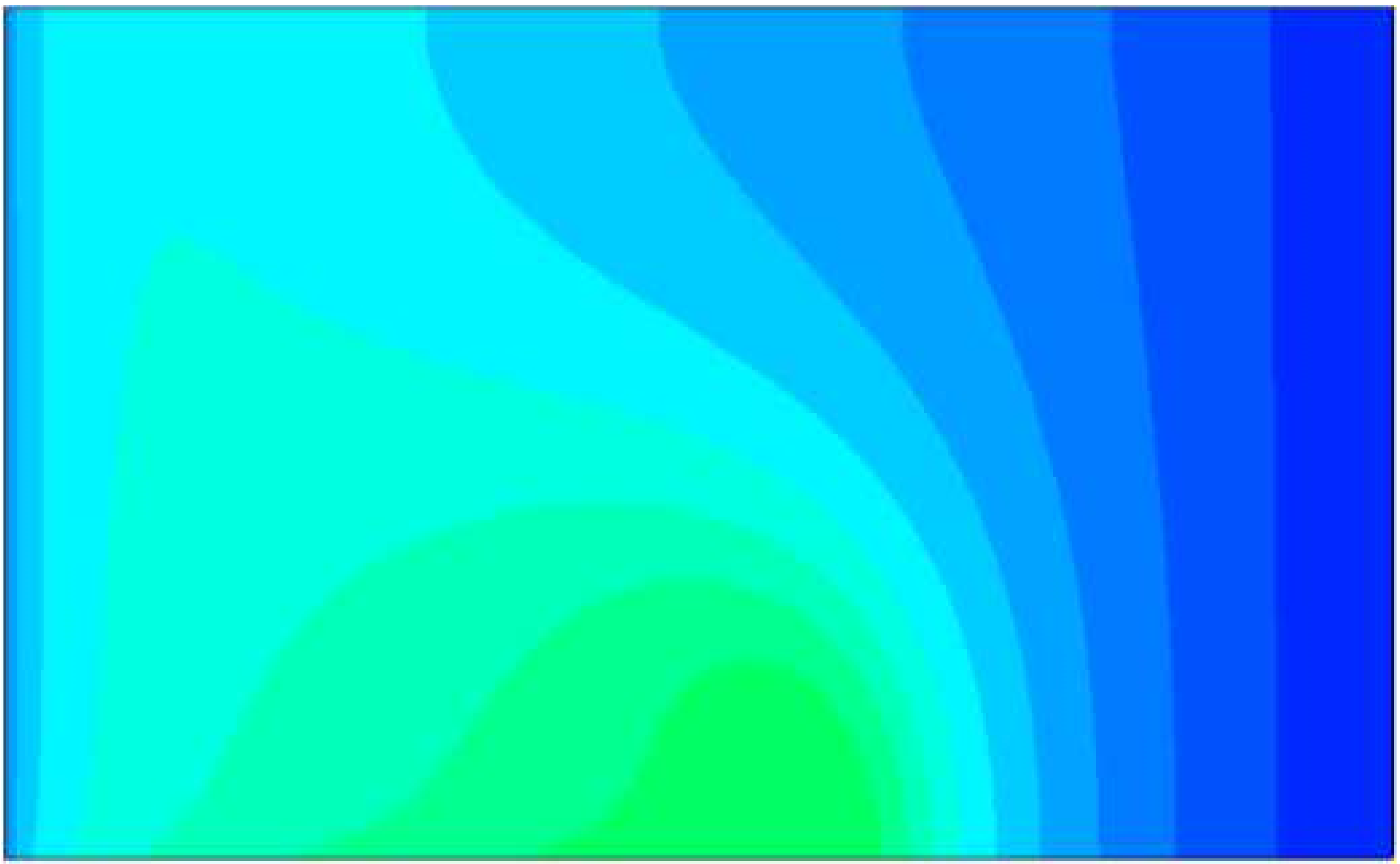

PLEASE CITE THIS ARTICLE AS DOI: 10.1063/5.0086189

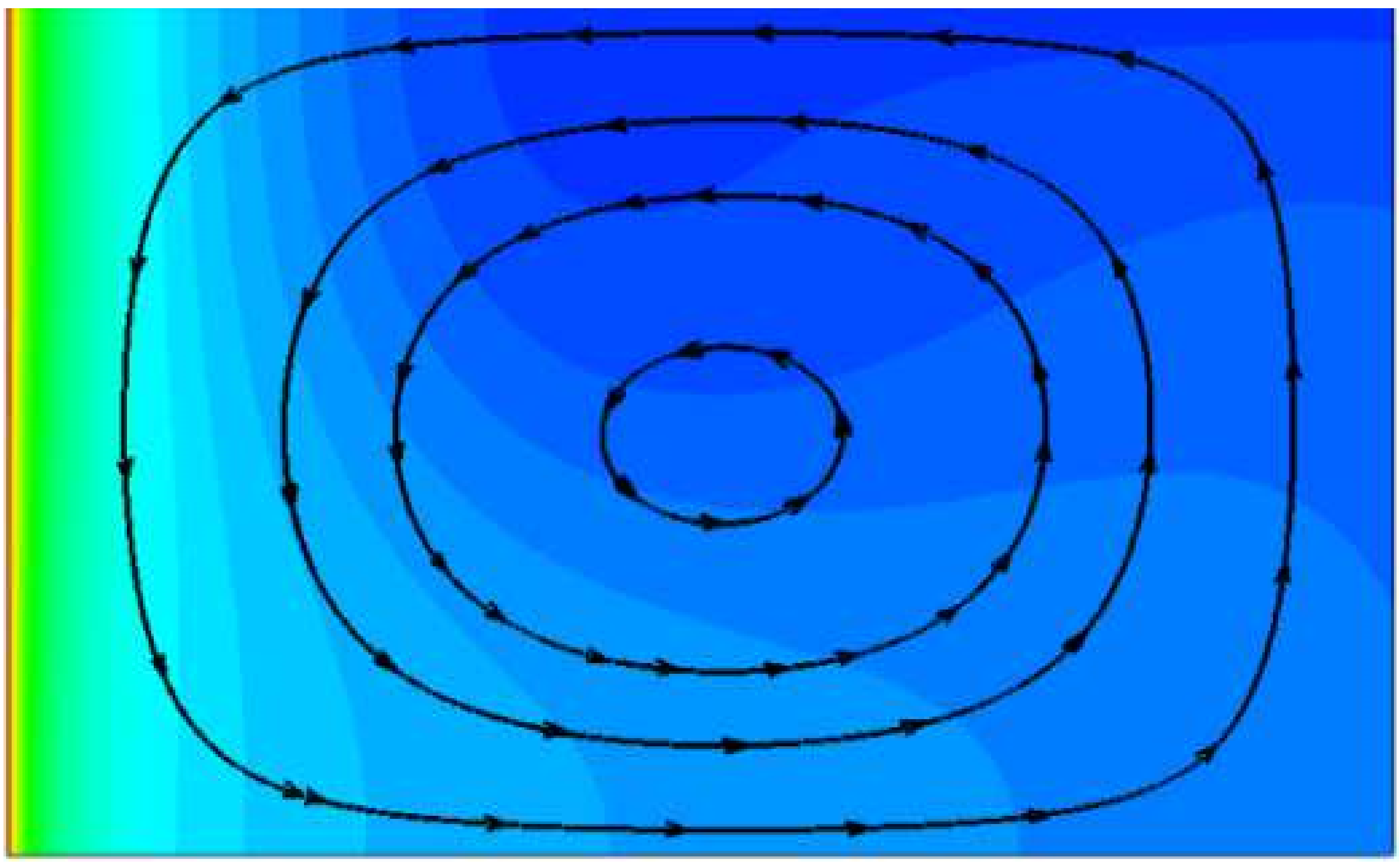

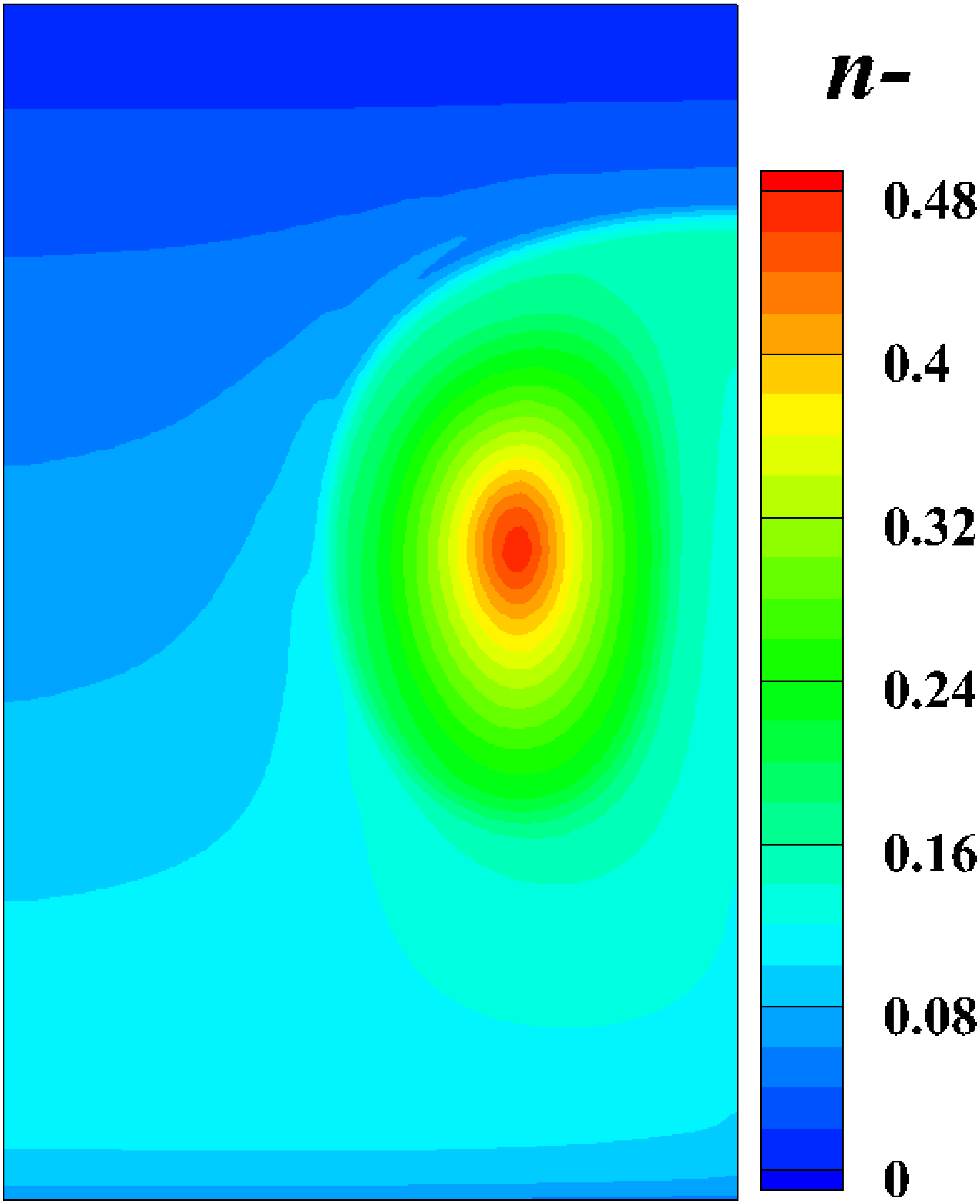
n-
0.48
0.4
0.32
0.24
0.16
0.08
0

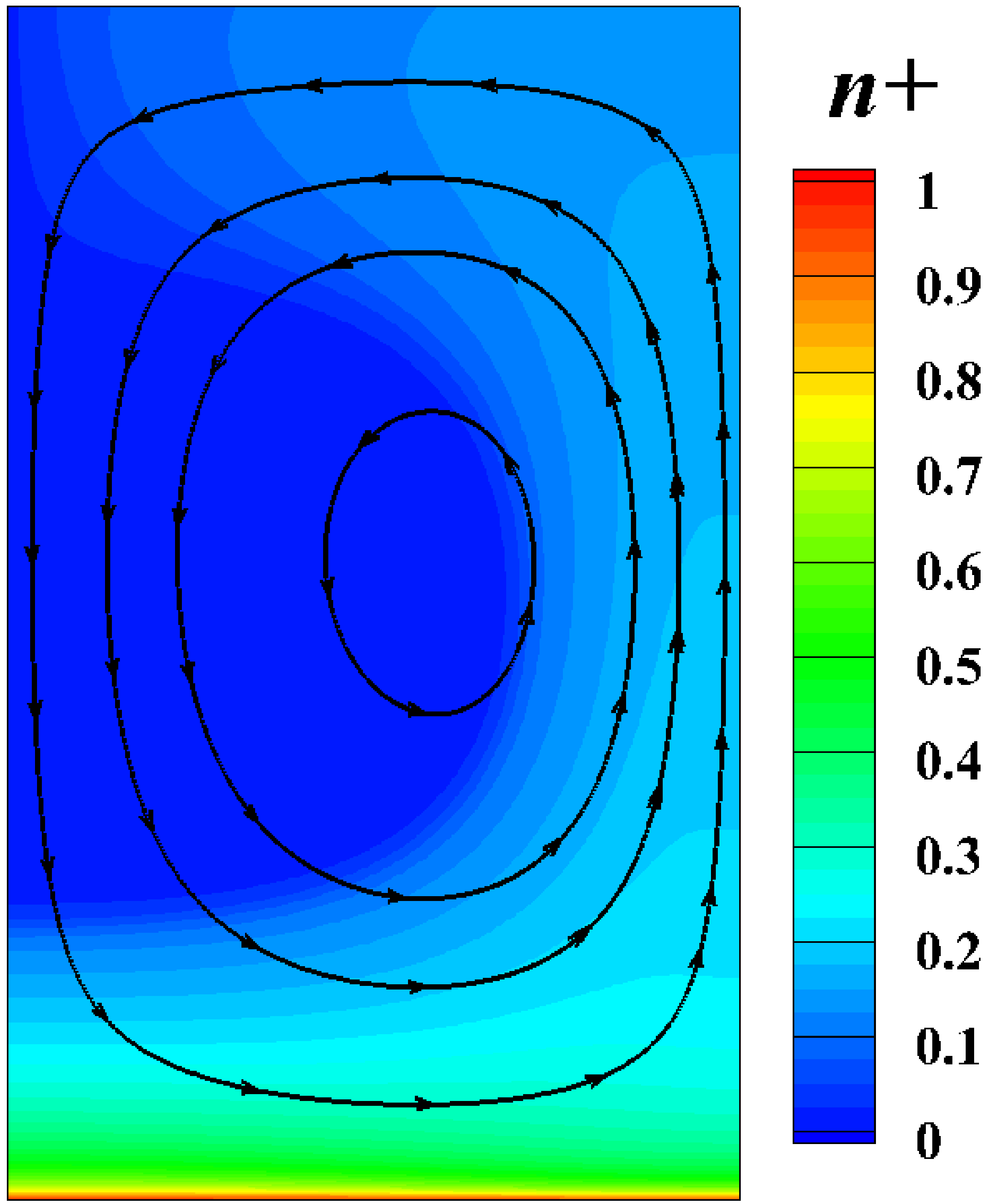
n+
1
0.9
0.8
0.7
0.6
0.5
0.4
0.3
0.2
0.1
0

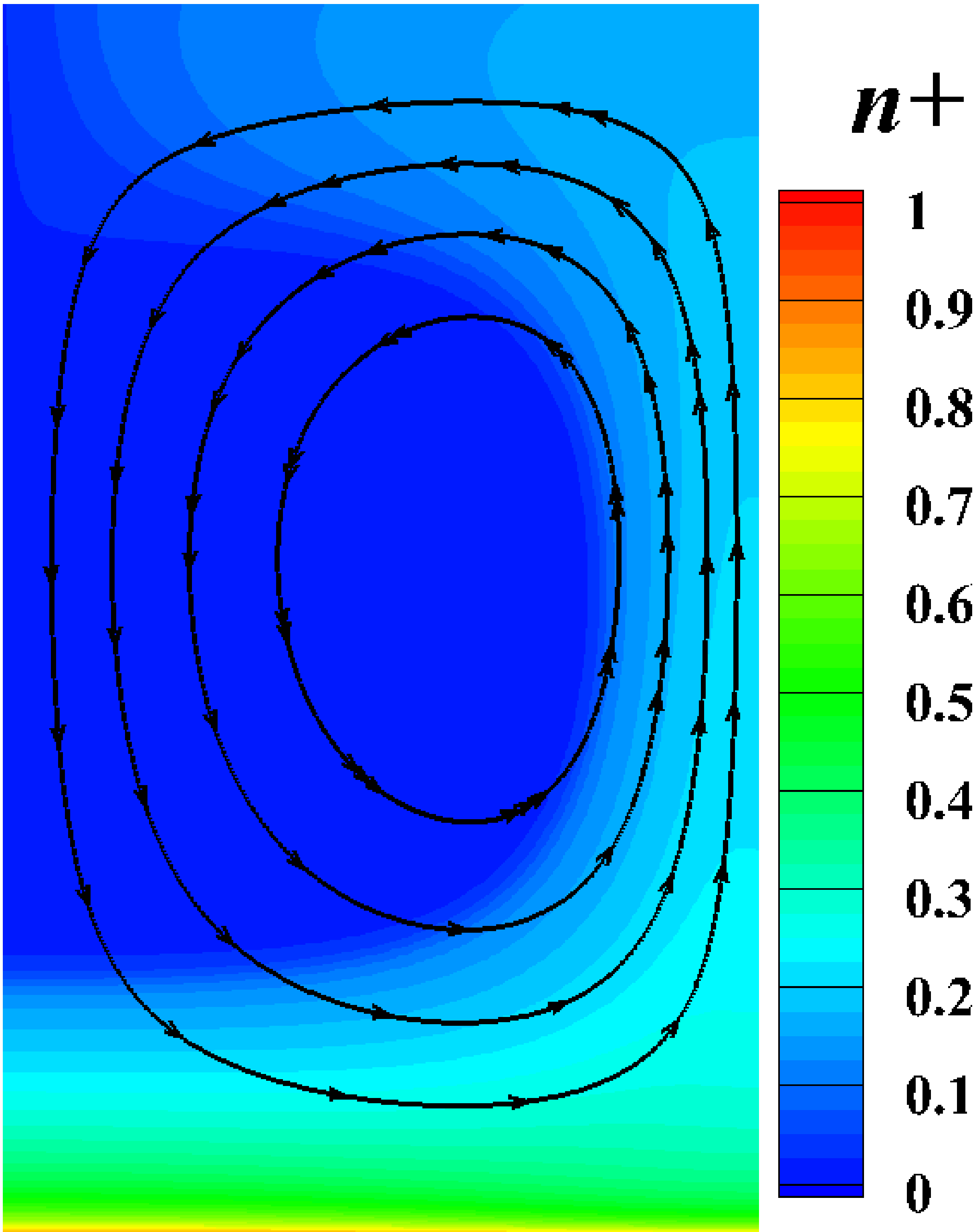
$n+$
1
0.9
0.8
0.7
0.6
0.5
0.4
0.3
0.2
0.1
0

PLEASE CITE THIS ARTICLE AS DOI: 10.1063/5.0086189

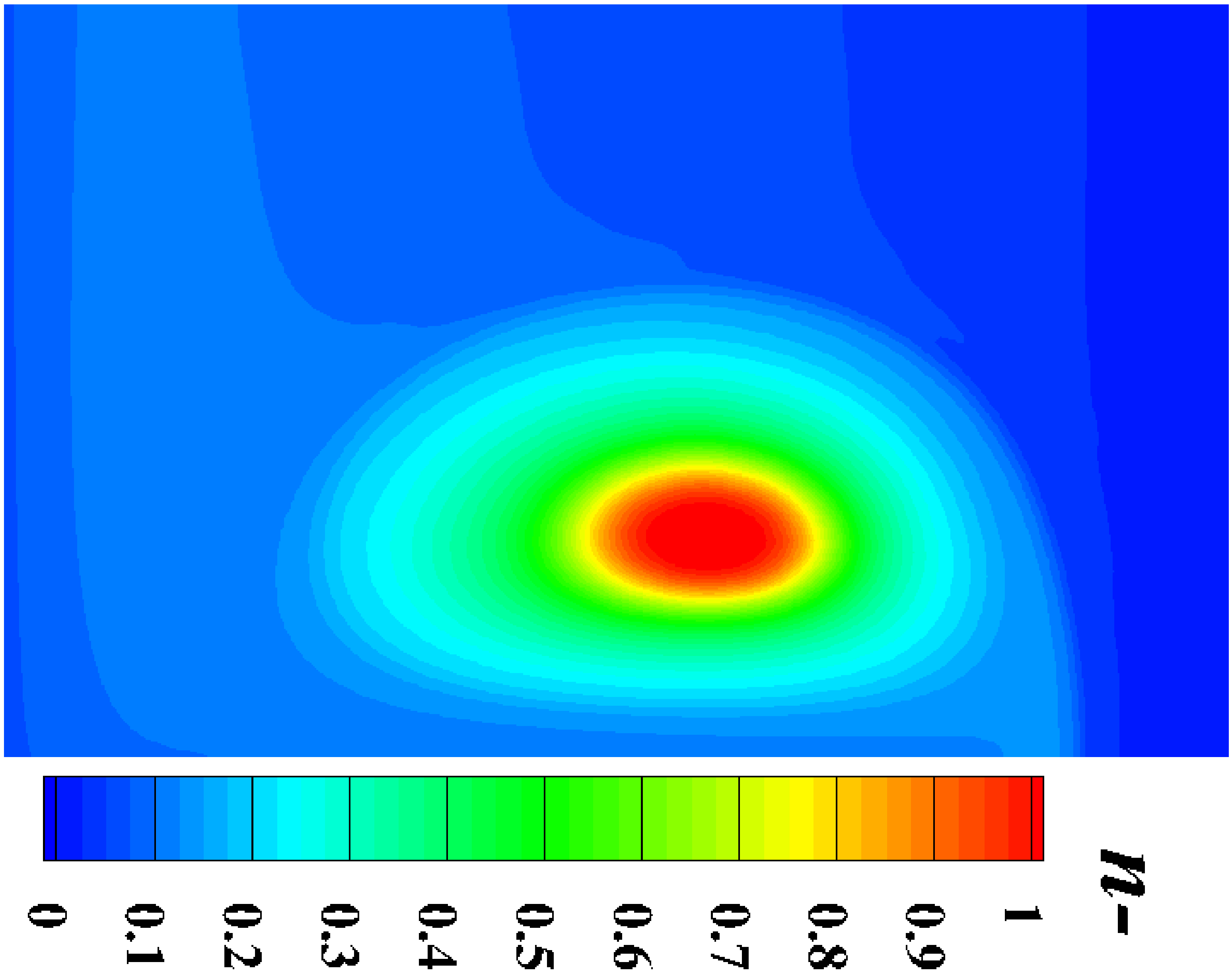

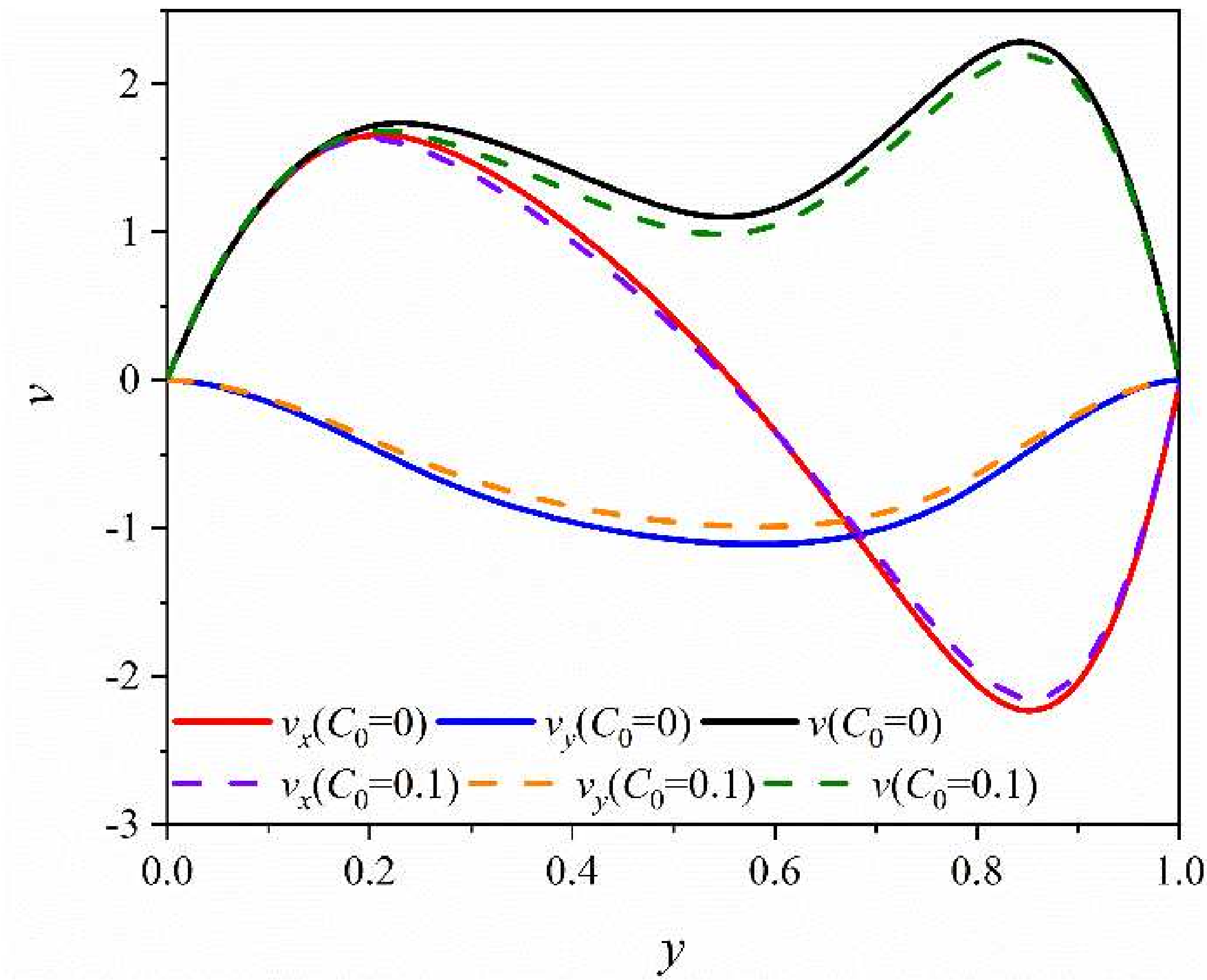
2
1
0
-1
-2
-3
v
0.0
0.2
0.4
0.6
0.8
1.0
y
$v_x(C_0=0)$
$v_y(C_0=0)$
$v(C_0=0)$
$v_x(C_0=0.1)$
$v_y(C_0=0.1)$
$v(C_0=0.1)$

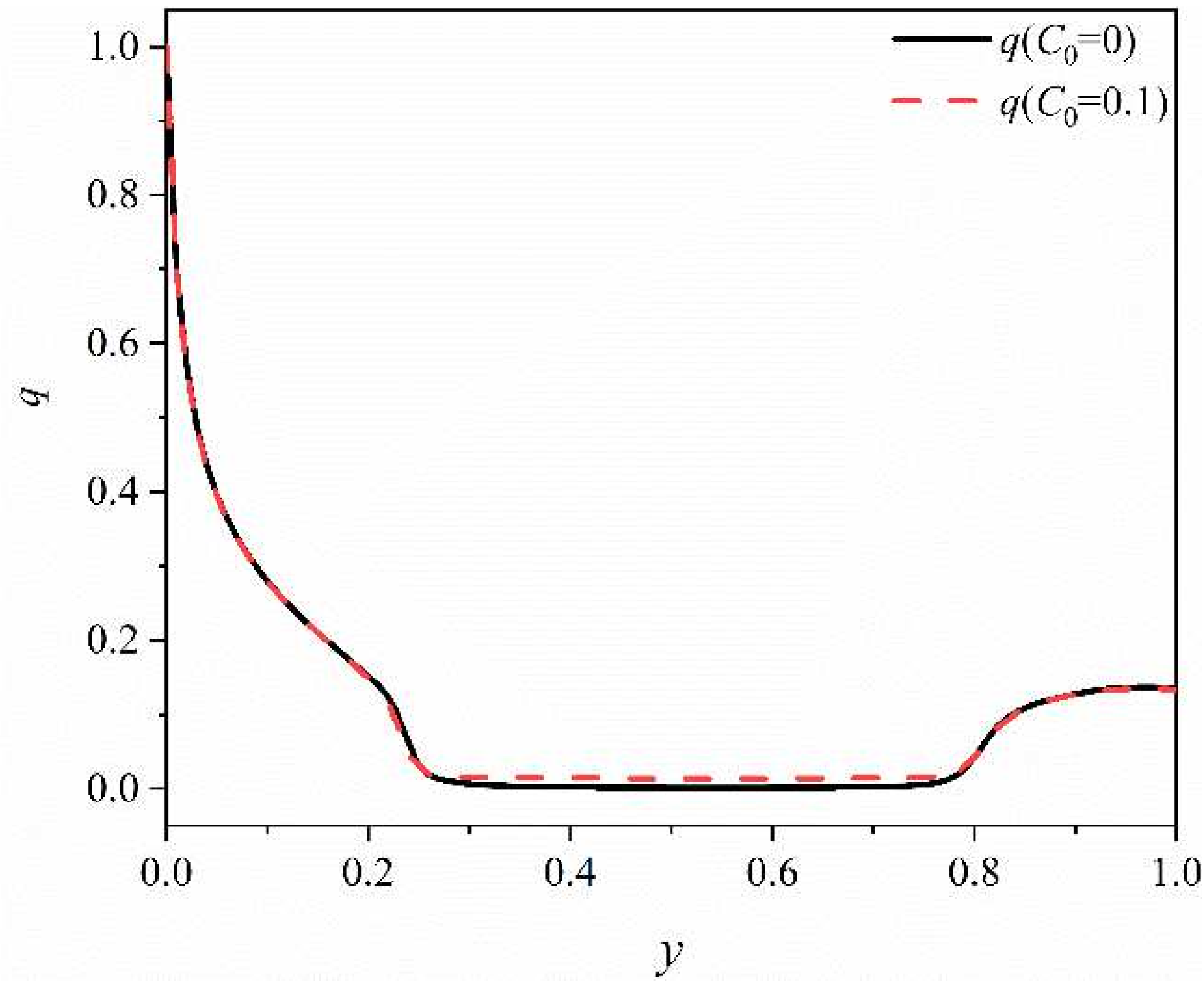
$q(C_0=0)$
$q(C_0=0.1)$
q
y
0.0
0.2
0.4
0.6
0.8
1.0

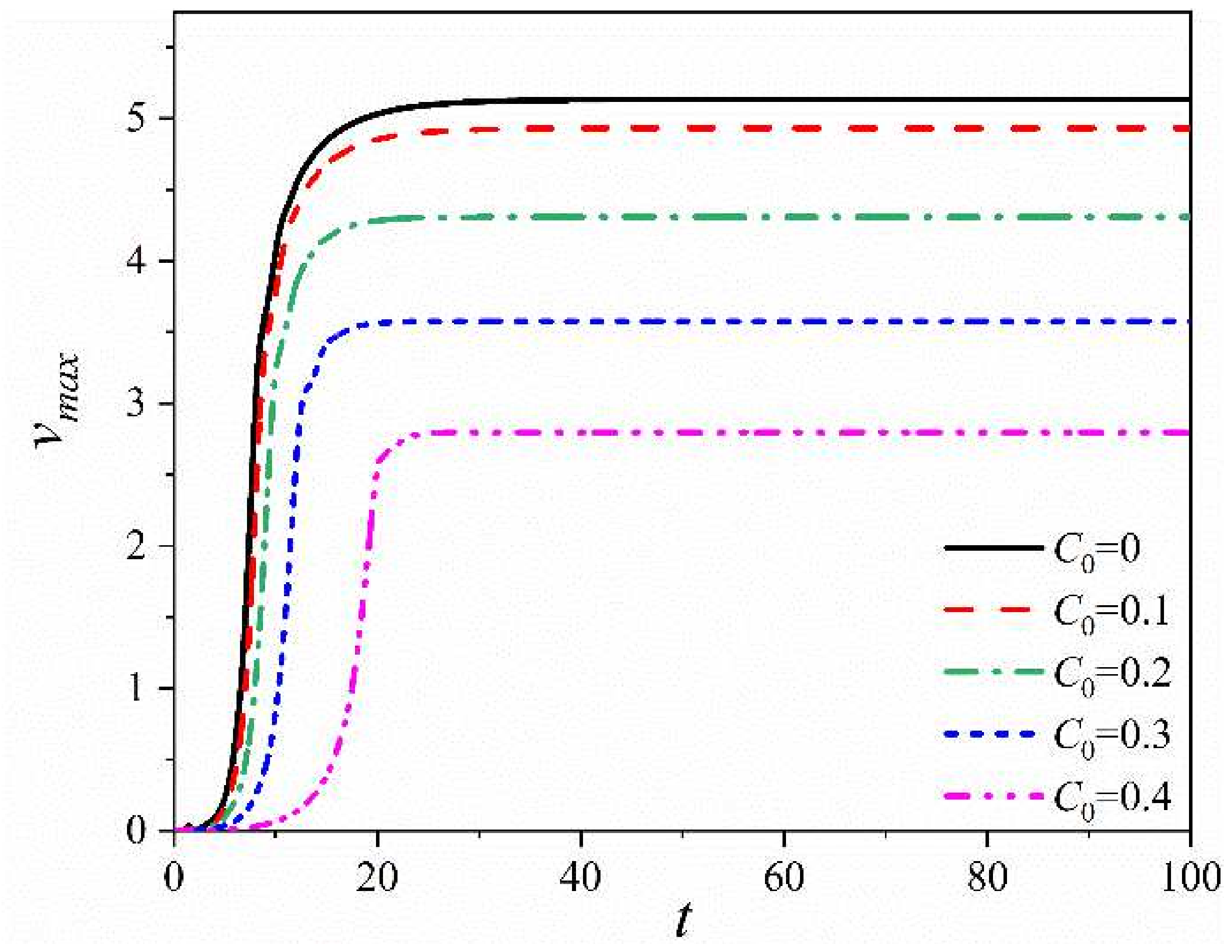
v_{max}
t
0
1
2
3
4
5
0
20
40
60
80
100
C_0=0
C_0=0.1
C_0=0.2
C_0=0.3
C_0=0.4

PLEASE CITE THIS ARTICLE AS DOI: 10.1063/5.0086189

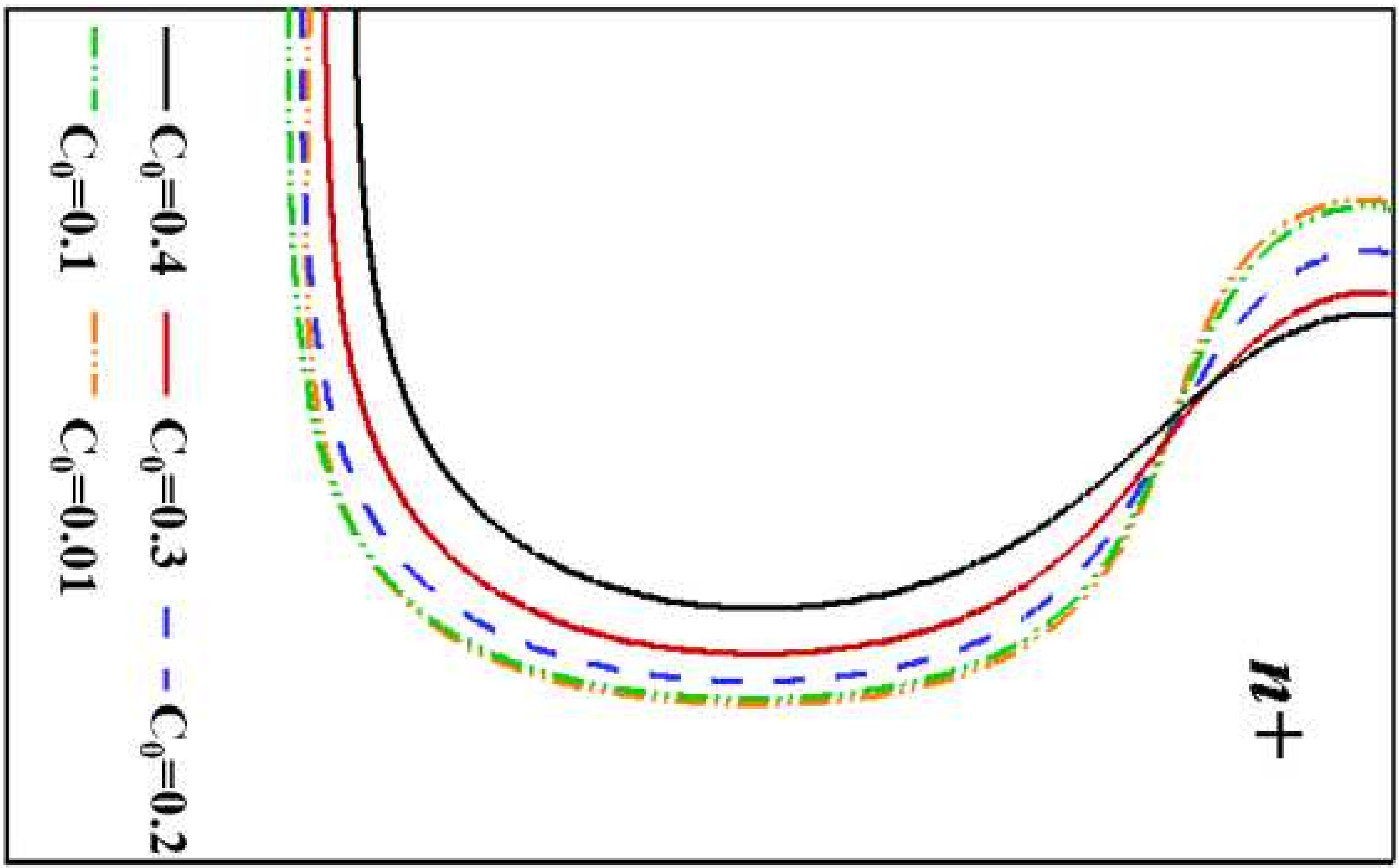

PLEASE CITE THIS ARTICLE AS DOI: 10.1063/5.0086189

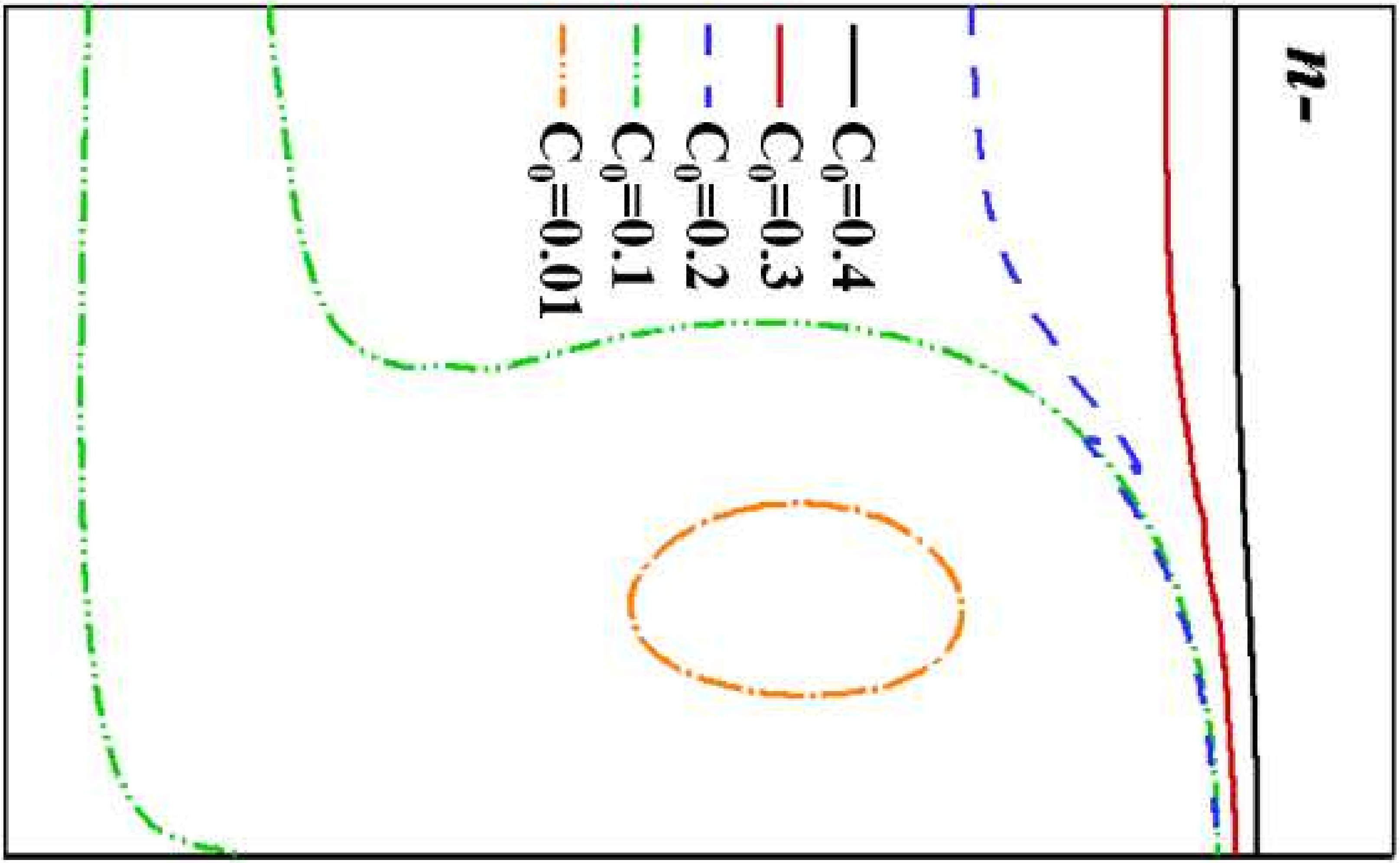

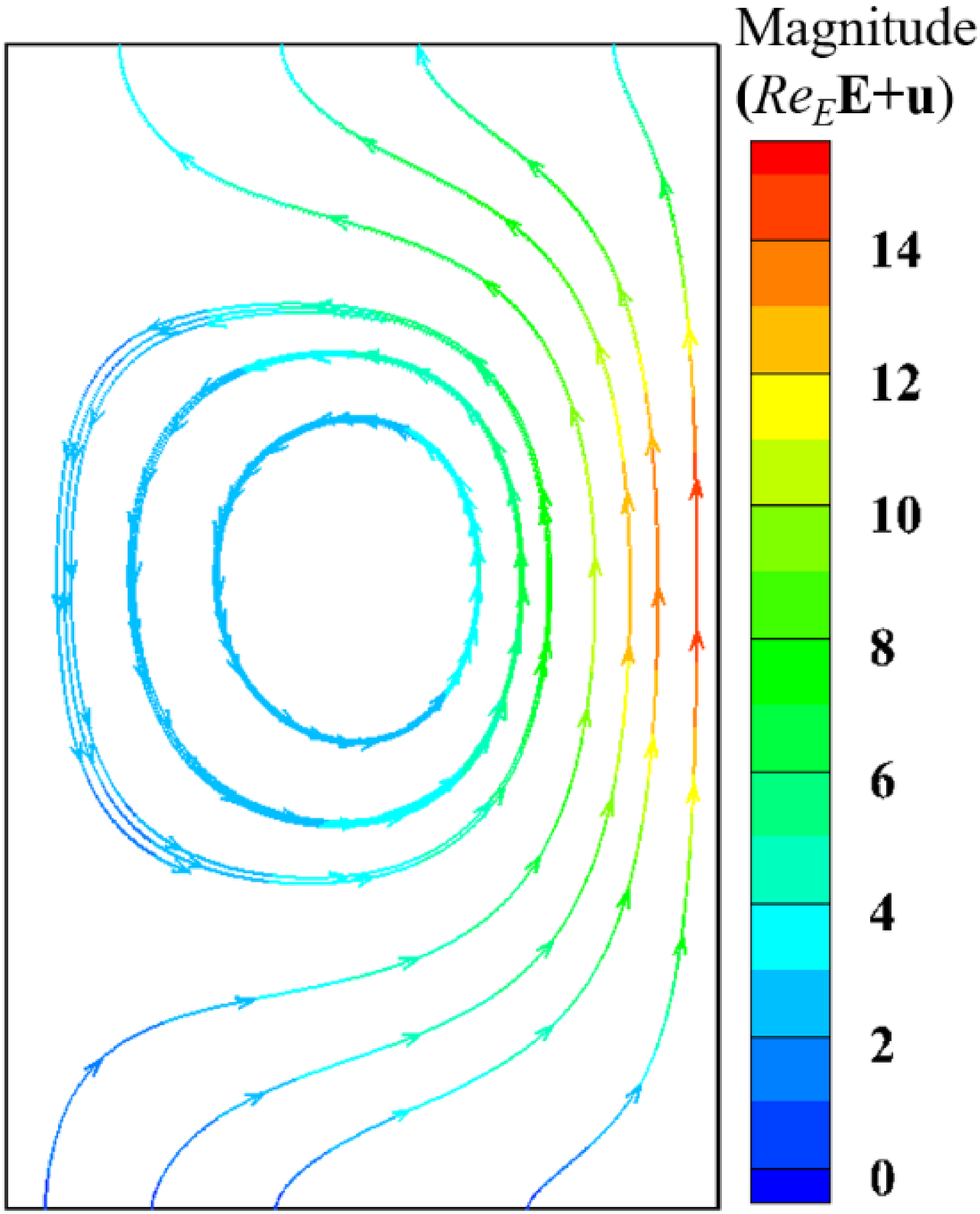
Magnitude
(Re_E**E**+**u**)
14
12
10
8
6
4
2
0

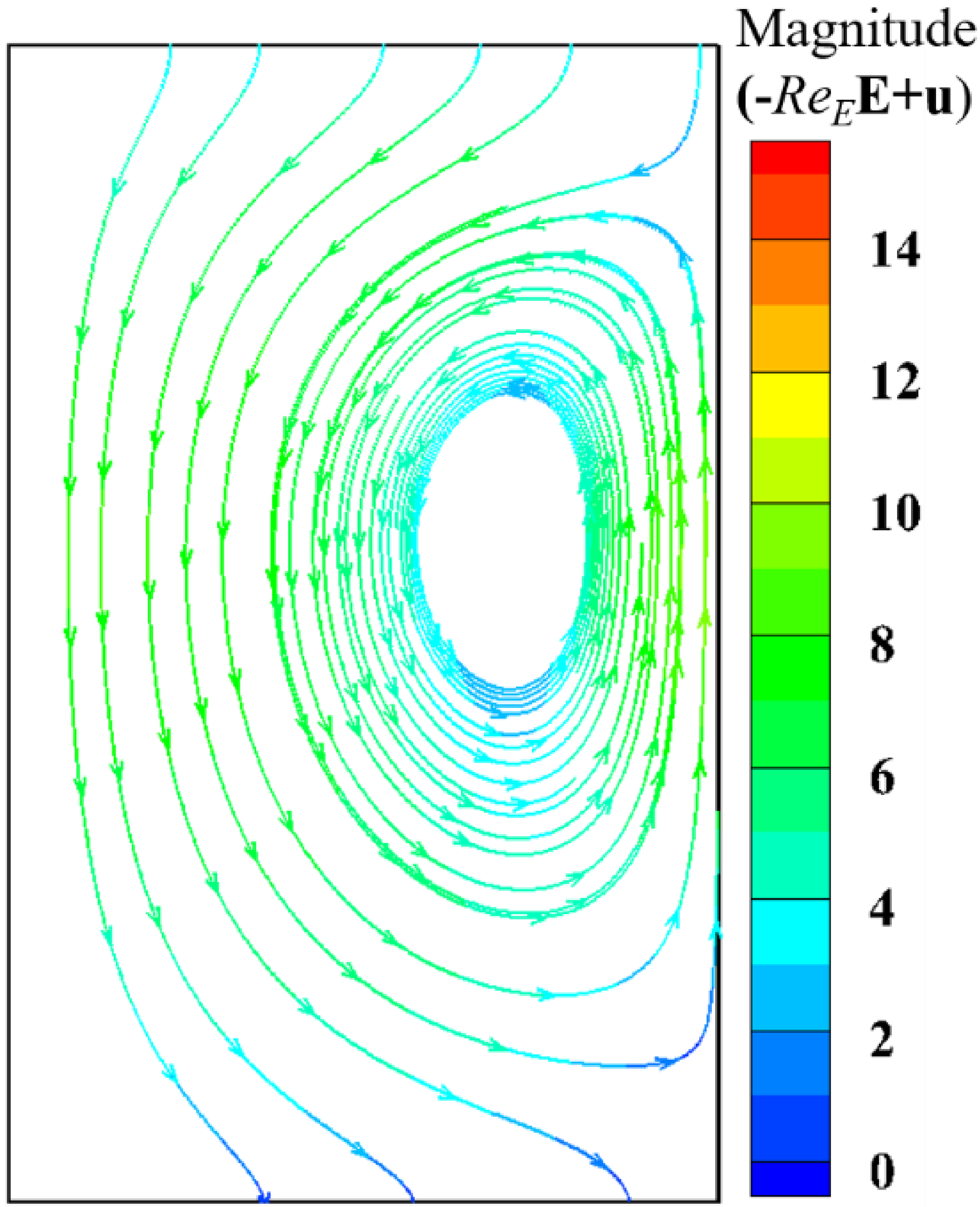
Magnitude
(-Re_E**E**+**u**)
14
12
10
8
6
4
2
0

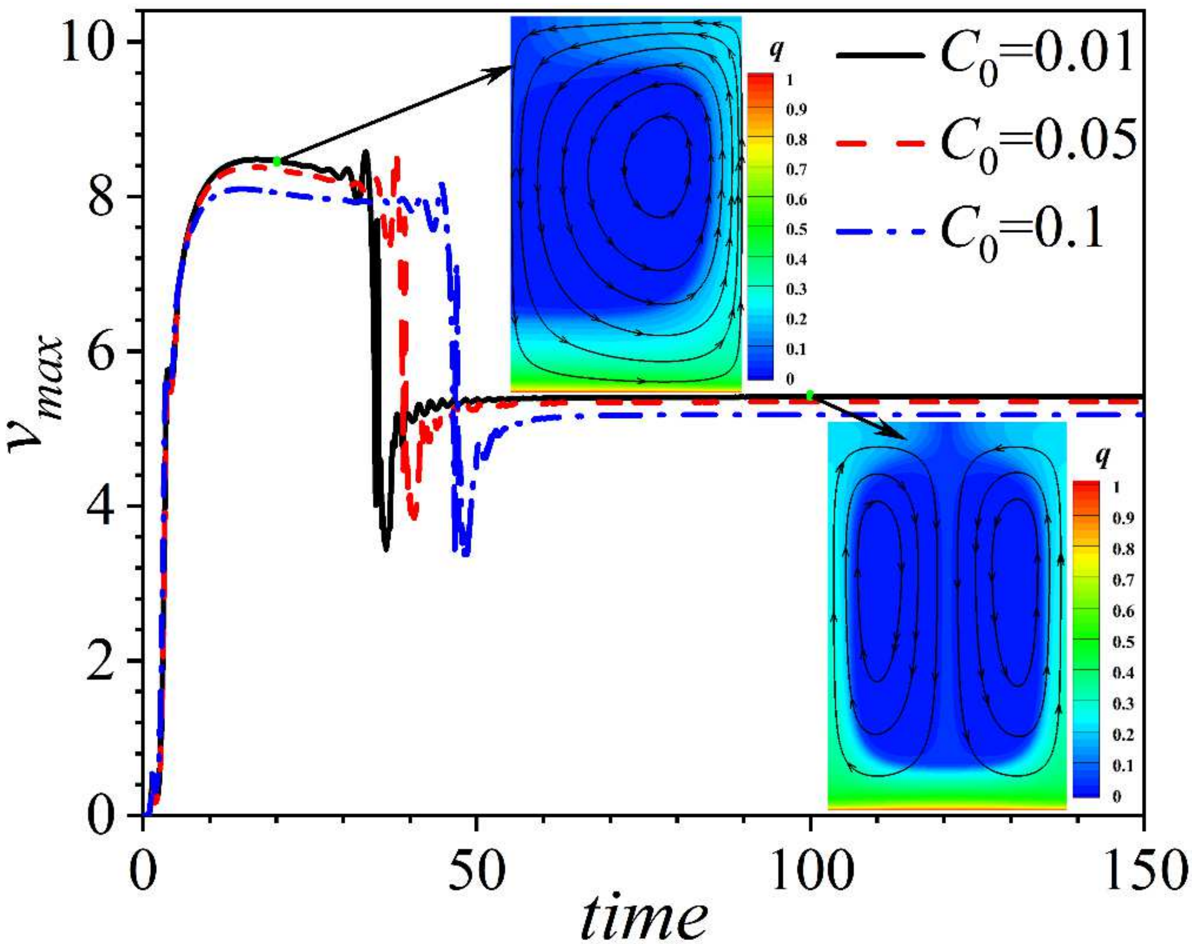
C_0=0.01
C_0=0.05
C_0=0.1
v_{max}
time
q
q
0
50
100
150
0
2
4
6
8
10

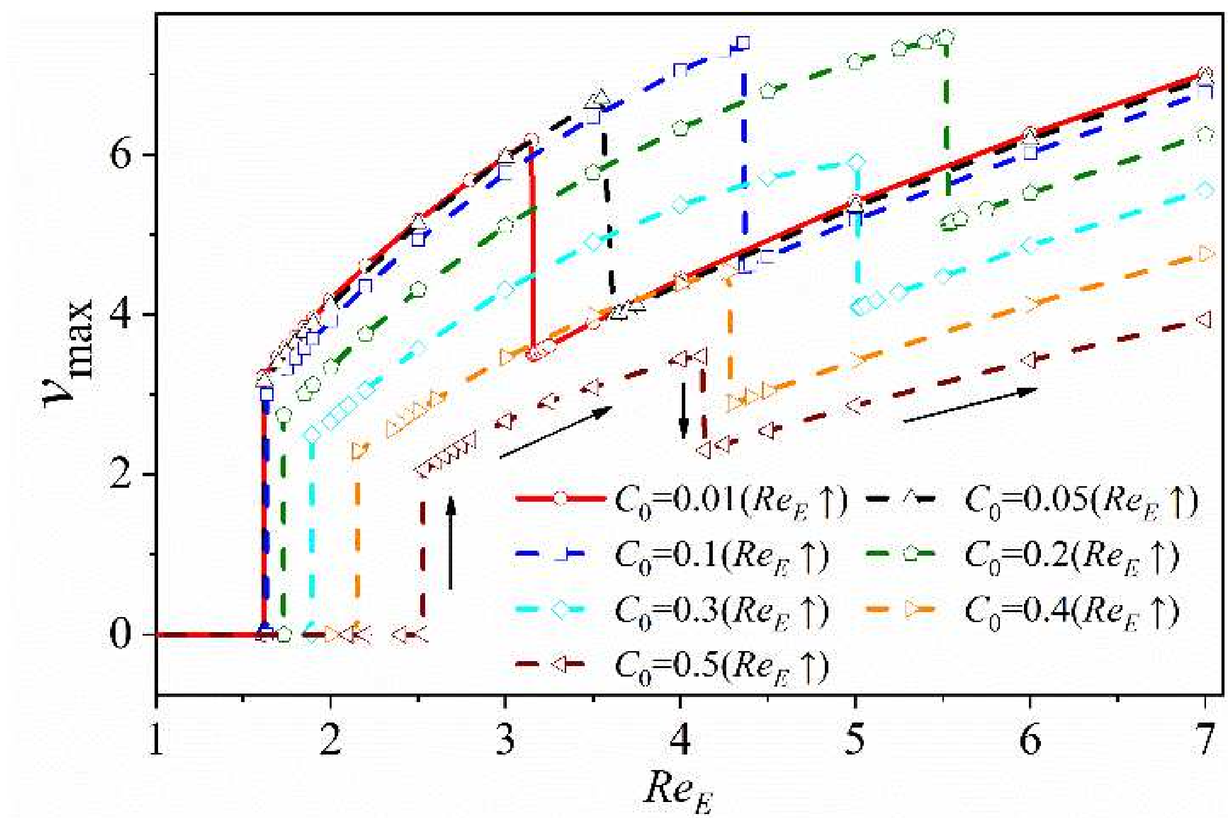
v_{max}
Re_E
C_0=0.01(Re_E↑)
C_0=0.05(Re_E↑)
C_0=0.1(Re_E↑)
C_0=0.2(Re_E↑)
C_0=0.3(Re_E↑)
C_0=0.4(Re_E↑)
C_0=0.5(Re_E↑)

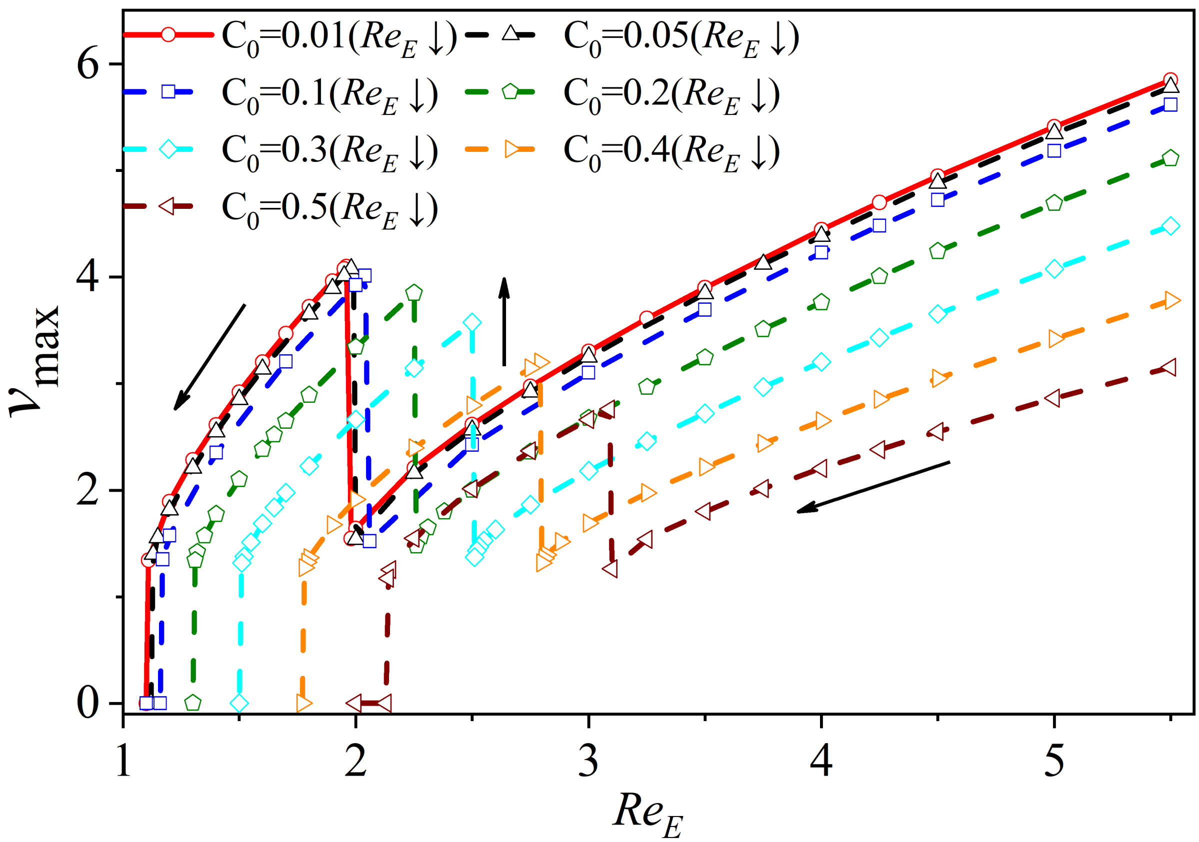
C0=0.01(ReE ↓)
C0=0.05(ReE ↓)
C0=0.1(ReE ↓)
C0=0.2(ReE ↓)
C0=0.3(ReE ↓)
C0=0.4(ReE ↓)
C0=0.5(ReE ↓)
vmax
ReE
0
2
4
6
1
2
3
4
5

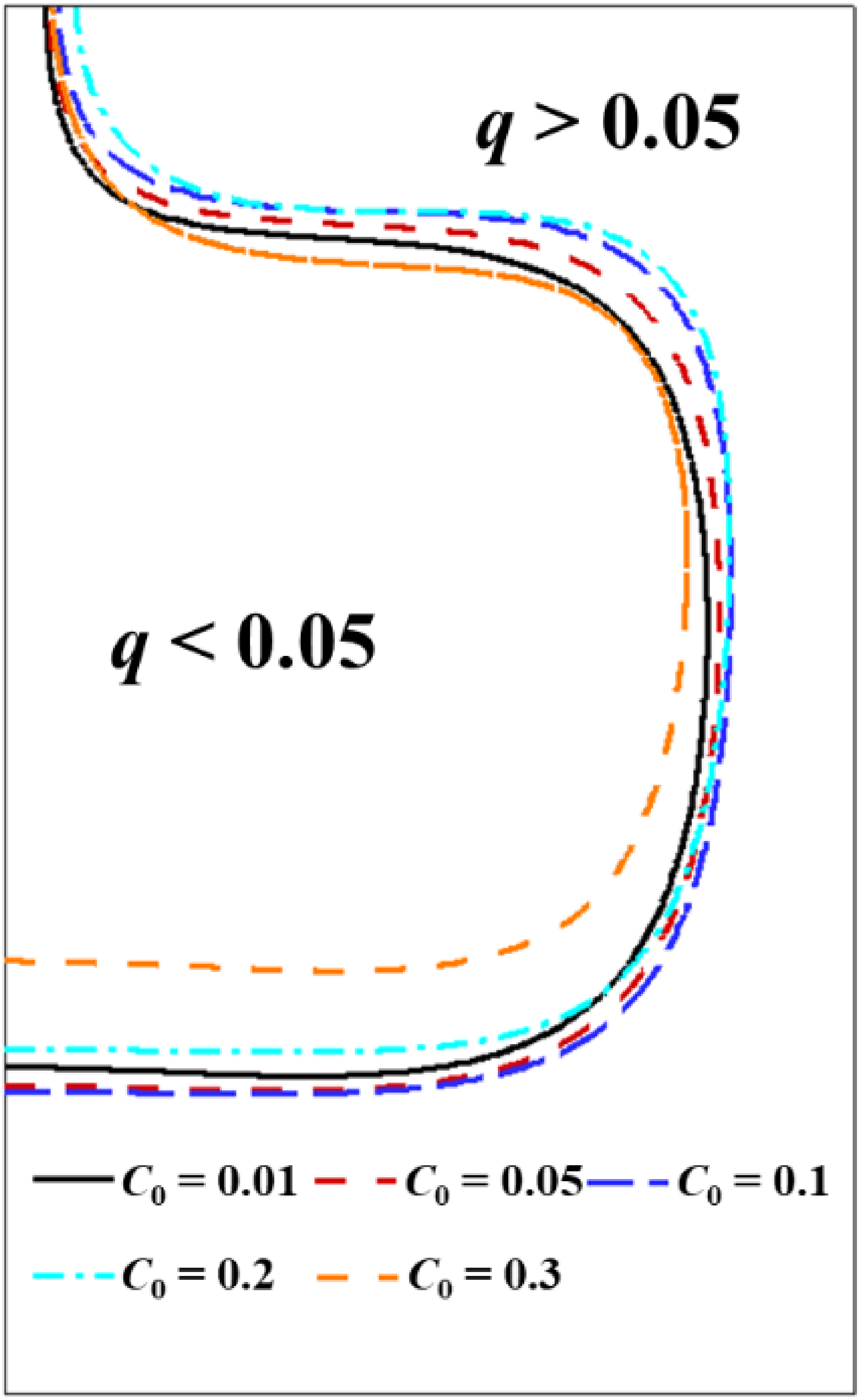
$q > 0.05$
$q < 0.05$
$C_0 = 0.01$
$C_0 = 0.05$
$C_0 = 0.1$
$C_0 = 0.2$
$C_0 = 0.3$

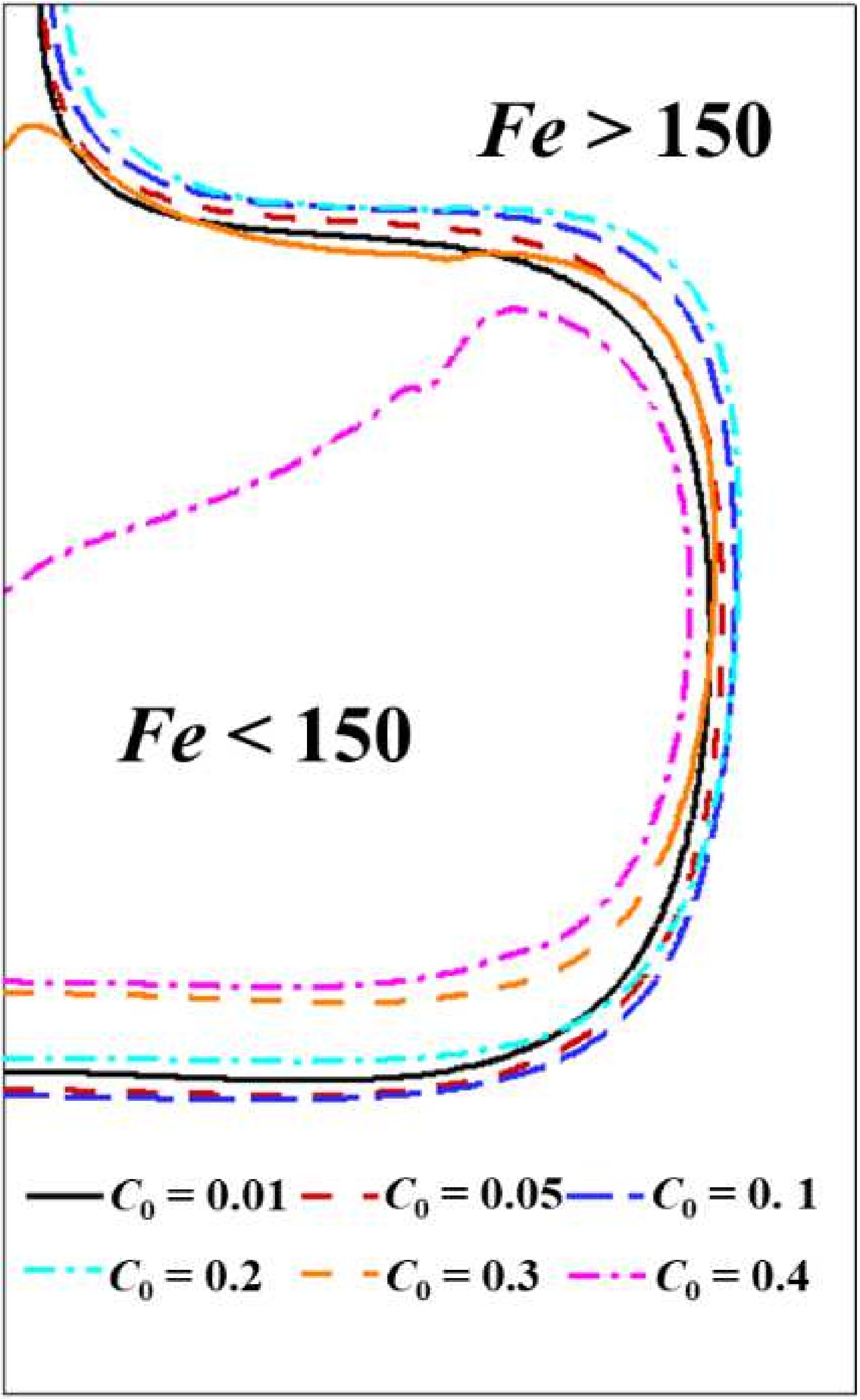
Fe > 150
Fe < 150
C0 = 0.01
C0 = 0.05
C0 = 0. 1
C0 = 0.2
C0 = 0.3
C0 = 0.4

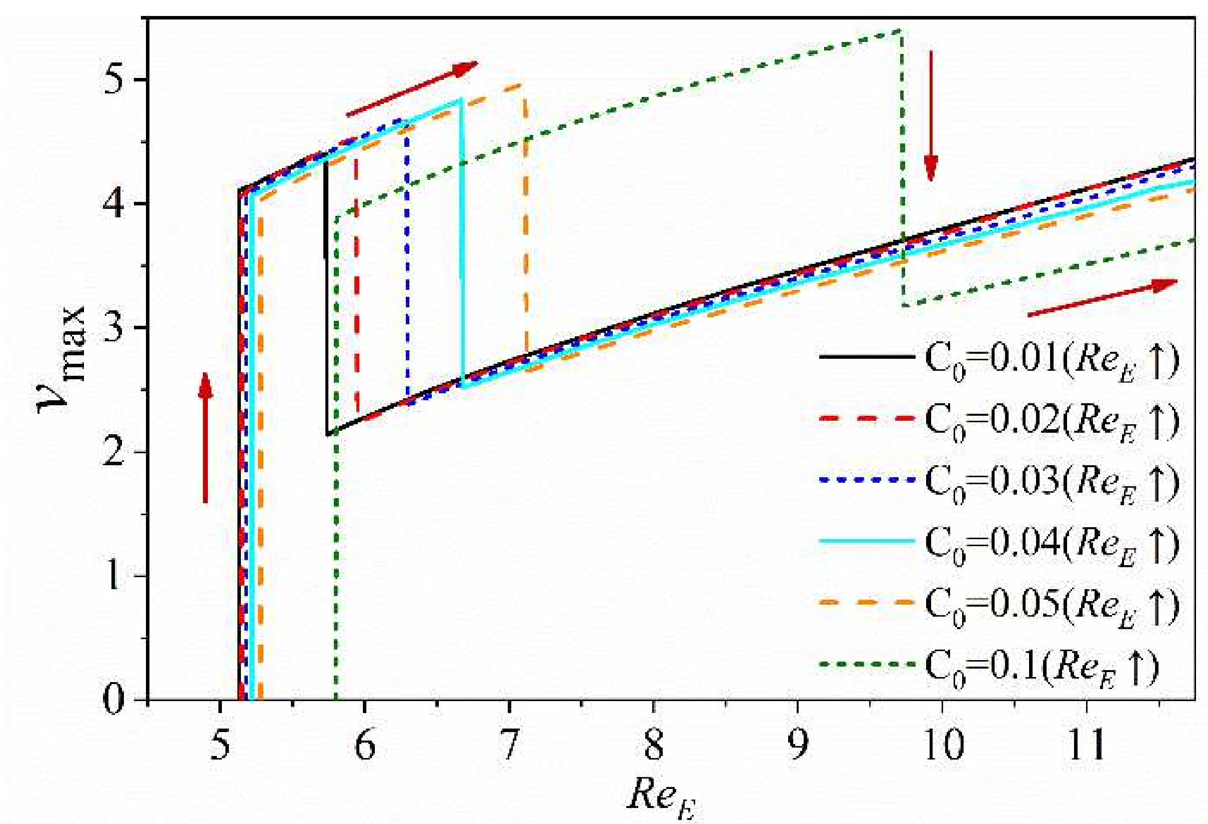
v_{max}
Re_E
0
1
2
3
4
5
5
6
7
8
9
10
11
C_0=0.01(Re_E ↑)
C_0=0.02(Re_E ↑)
C_0=0.03(Re_E ↑)
C_0=0.04(Re_E ↑)
C_0=0.05(Re_E ↑)
C_0=0.1(Re_E ↑)

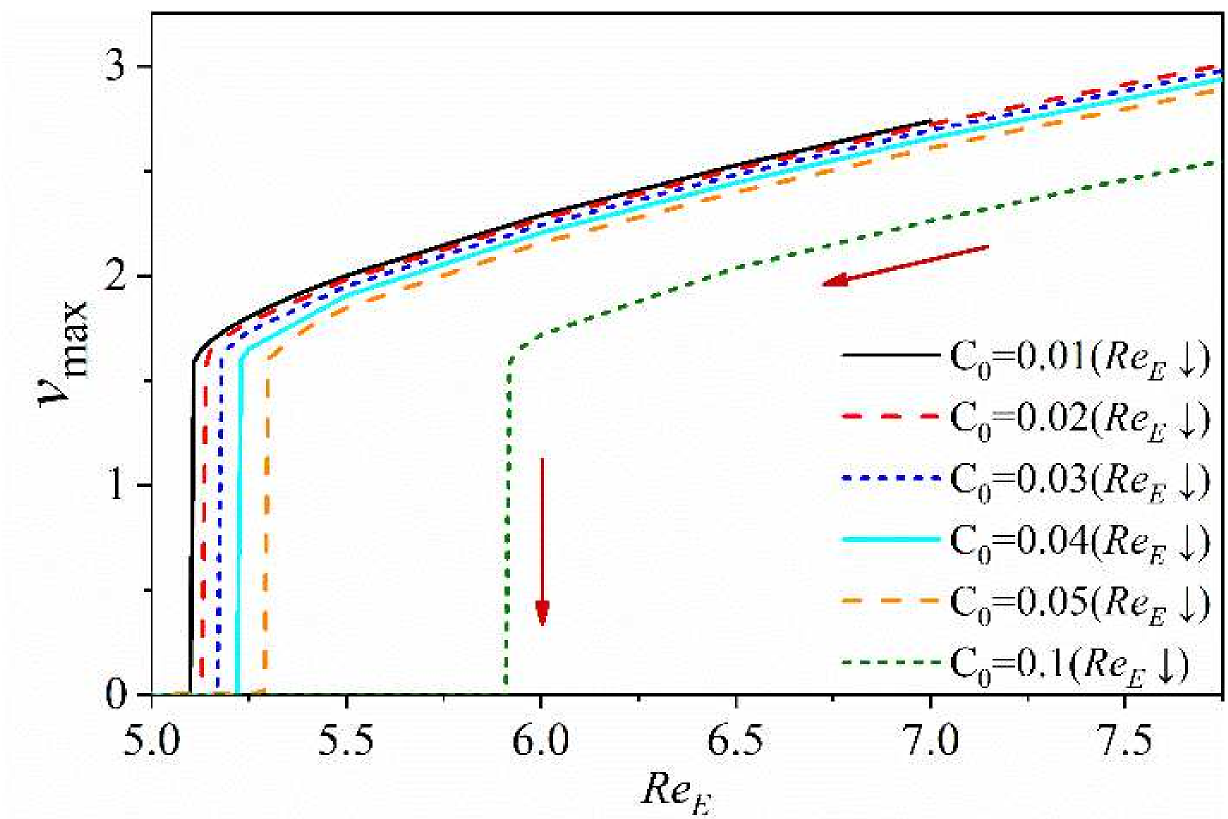
v_{max}
Re_E
0
1
2
3
5.0
5.5
6.0
6.5
7.0
7.5
C_0=0.01(Re_E ↓)
C_0=0.02(Re_E ↓)
C_0=0.03(Re_E ↓)
C_0=0.04(Re_E ↓)
C_0=0.05(Re_E ↓)
C_0=0.1(Re_E ↓)

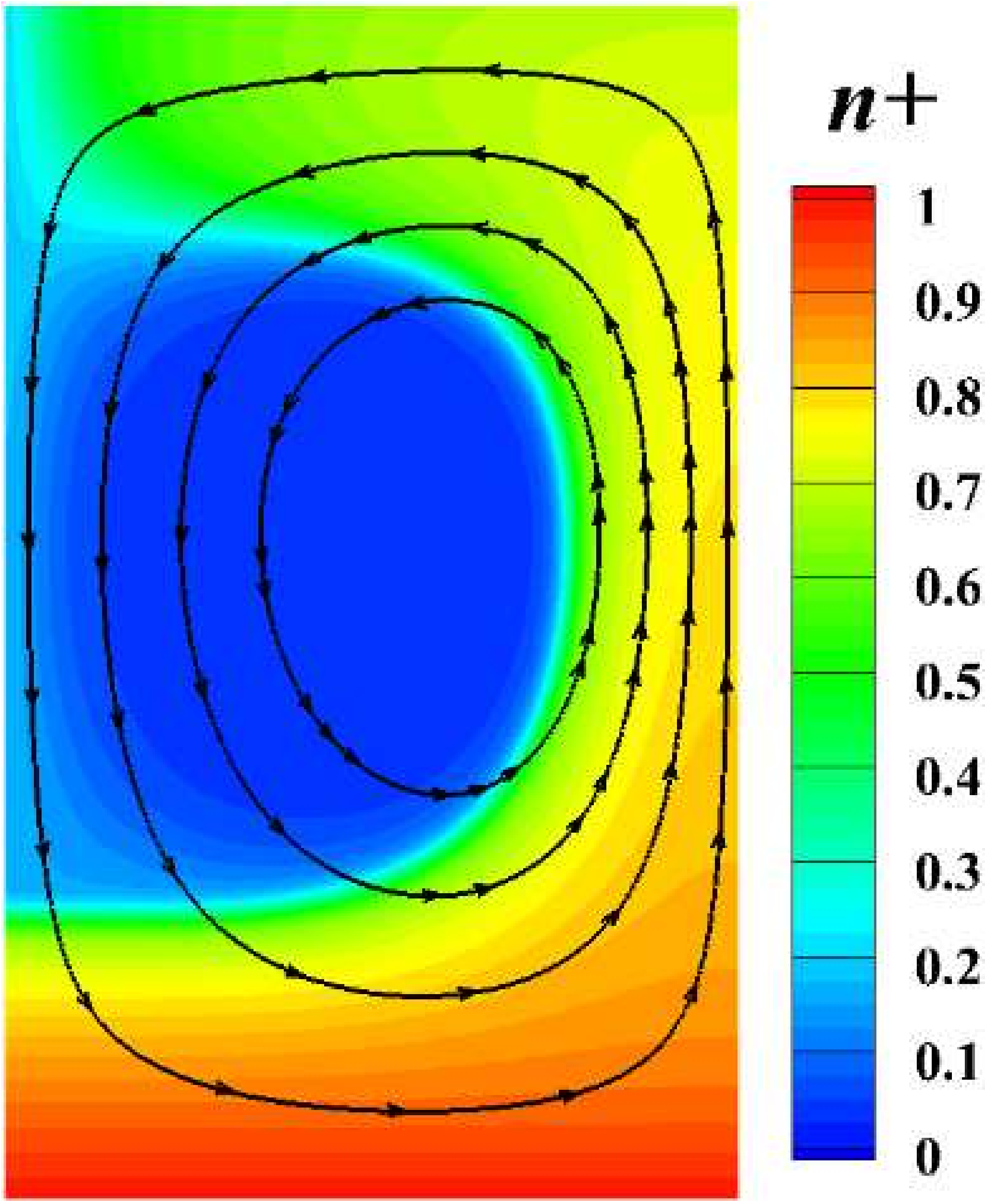
$n+$
1
0.9
0.8
0.7
0.6
0.5
0.4
0.3
0.2
0.1
0

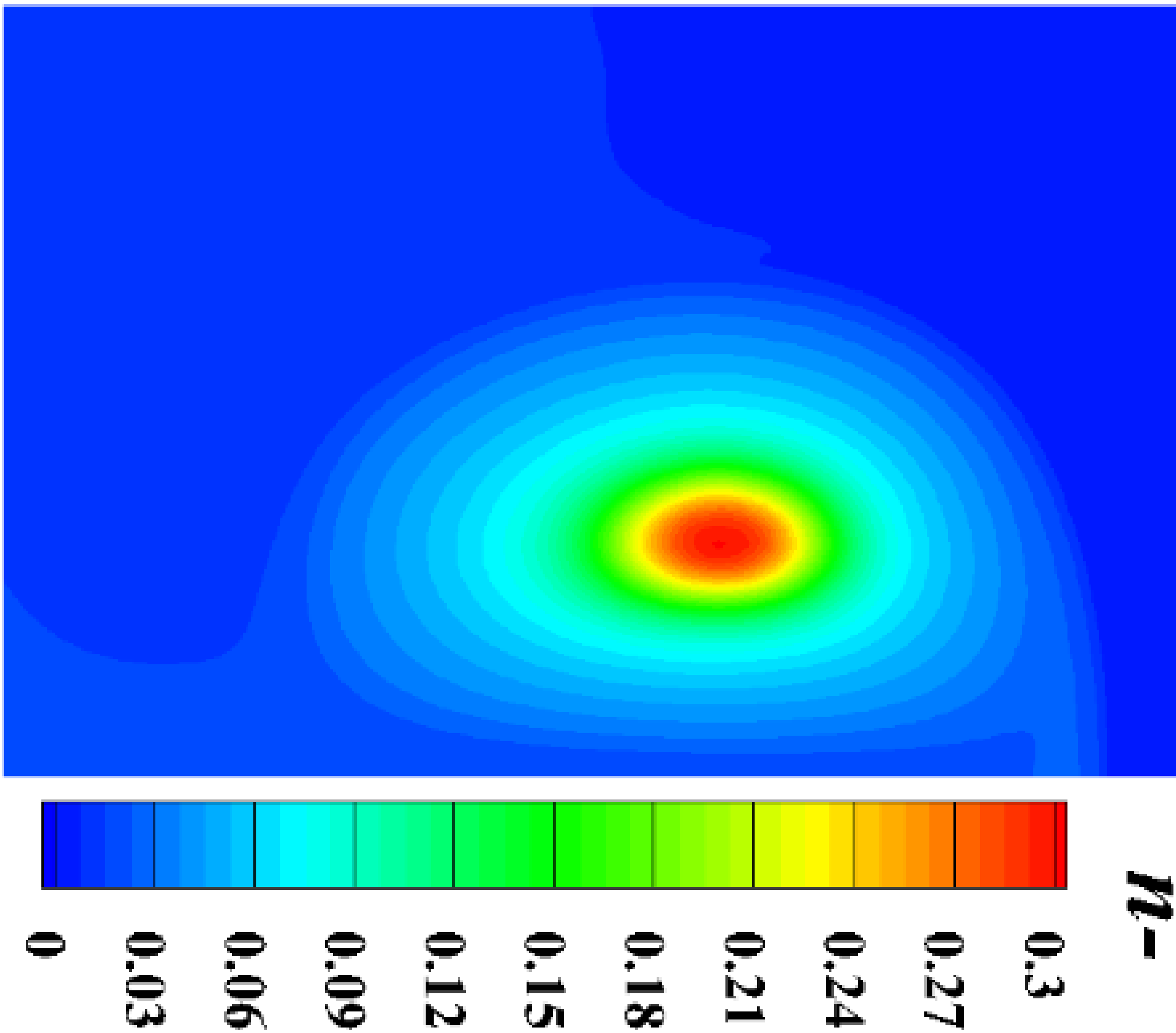
n-
0
0.03
0.06
0.09
0.12
0.15
0.18
0.21
0.24
0.27
0.3

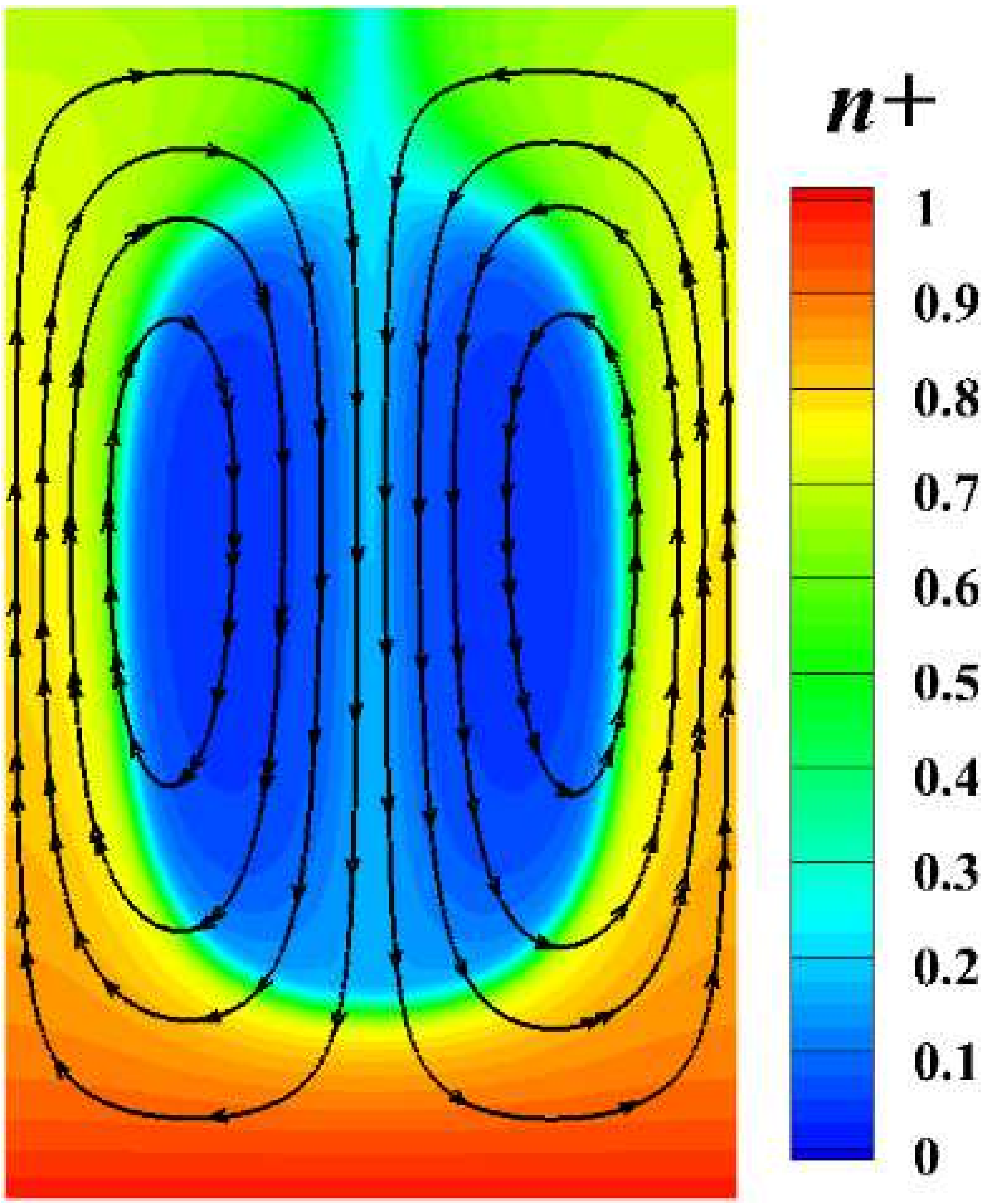
n+
1
0.9
0.8
0.7
0.6
0.5
0.4
0.3
0.2
0.1
0

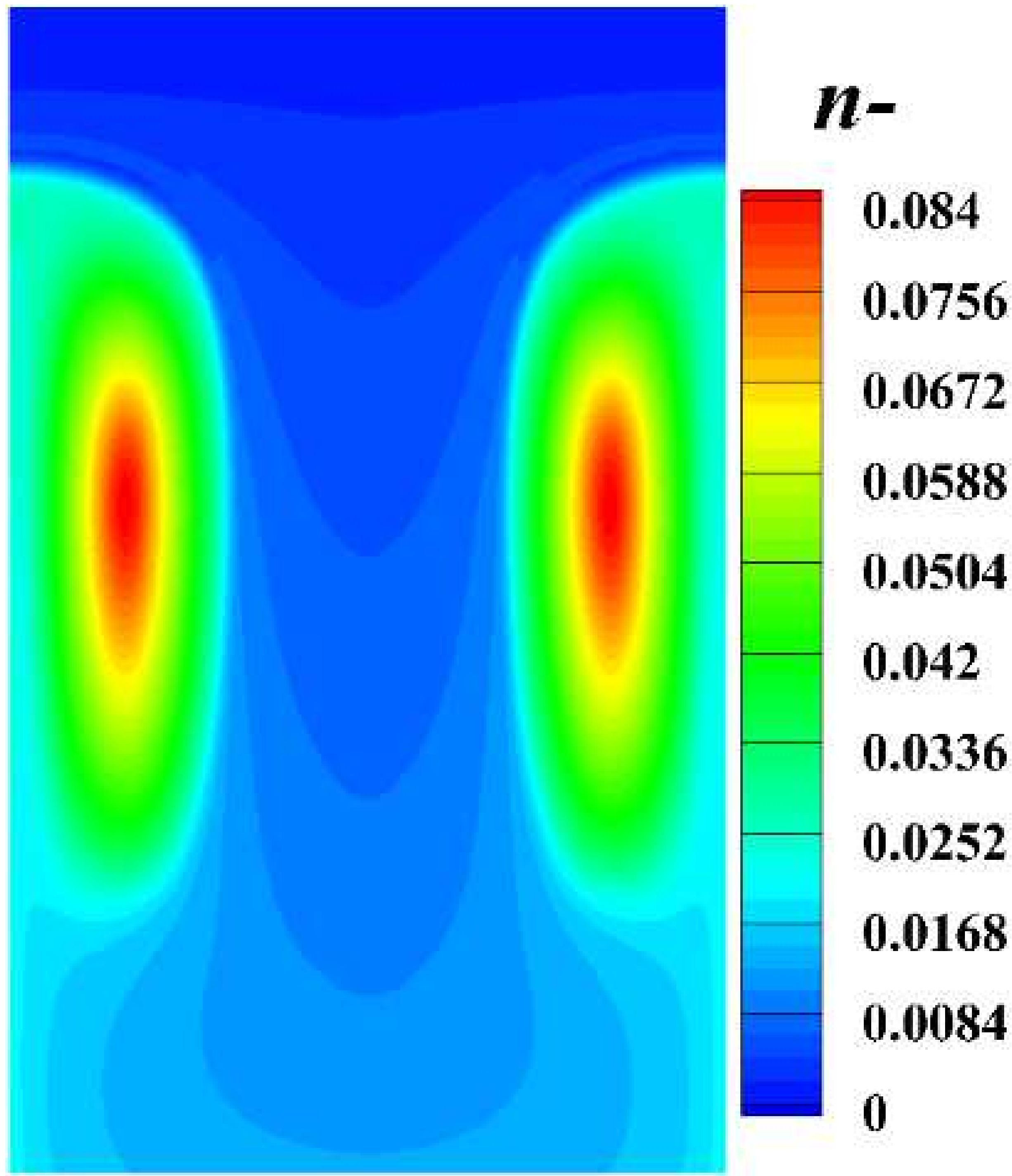
n-
0.084
0.0756
0.0672
0.0588
0.0504
0.042
0.0336
0.0252
0.0168
0.0084
0

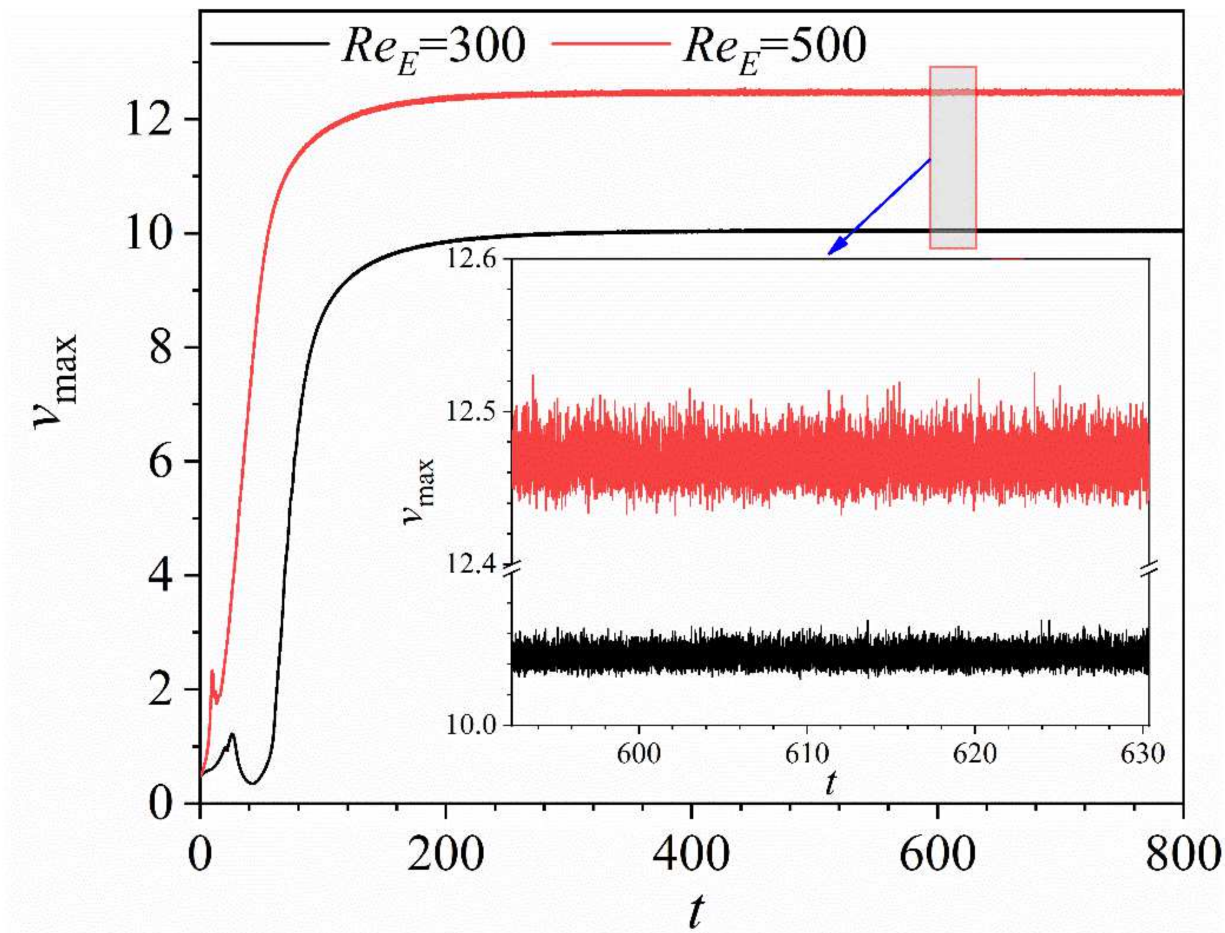
Re_E=300
Re_E=500
v_{max}
t
0
2
4
6
8
10
12
0
200
400
600
800
12.6
12.5
12.4
10.0
600
610
620
630

PLEASE CITE THIS ARTICLE AS DOI: 10.1063/5.0086189

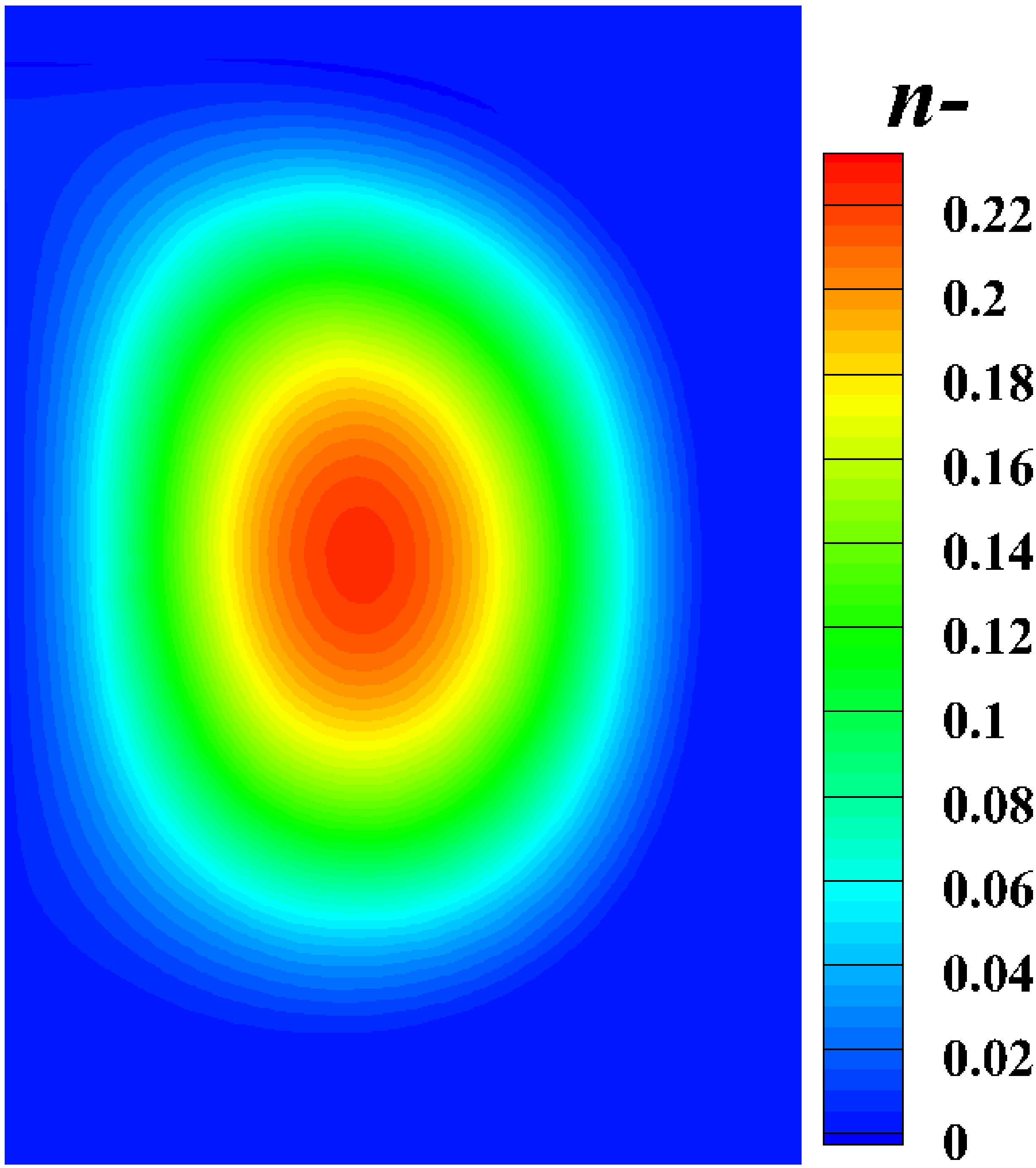

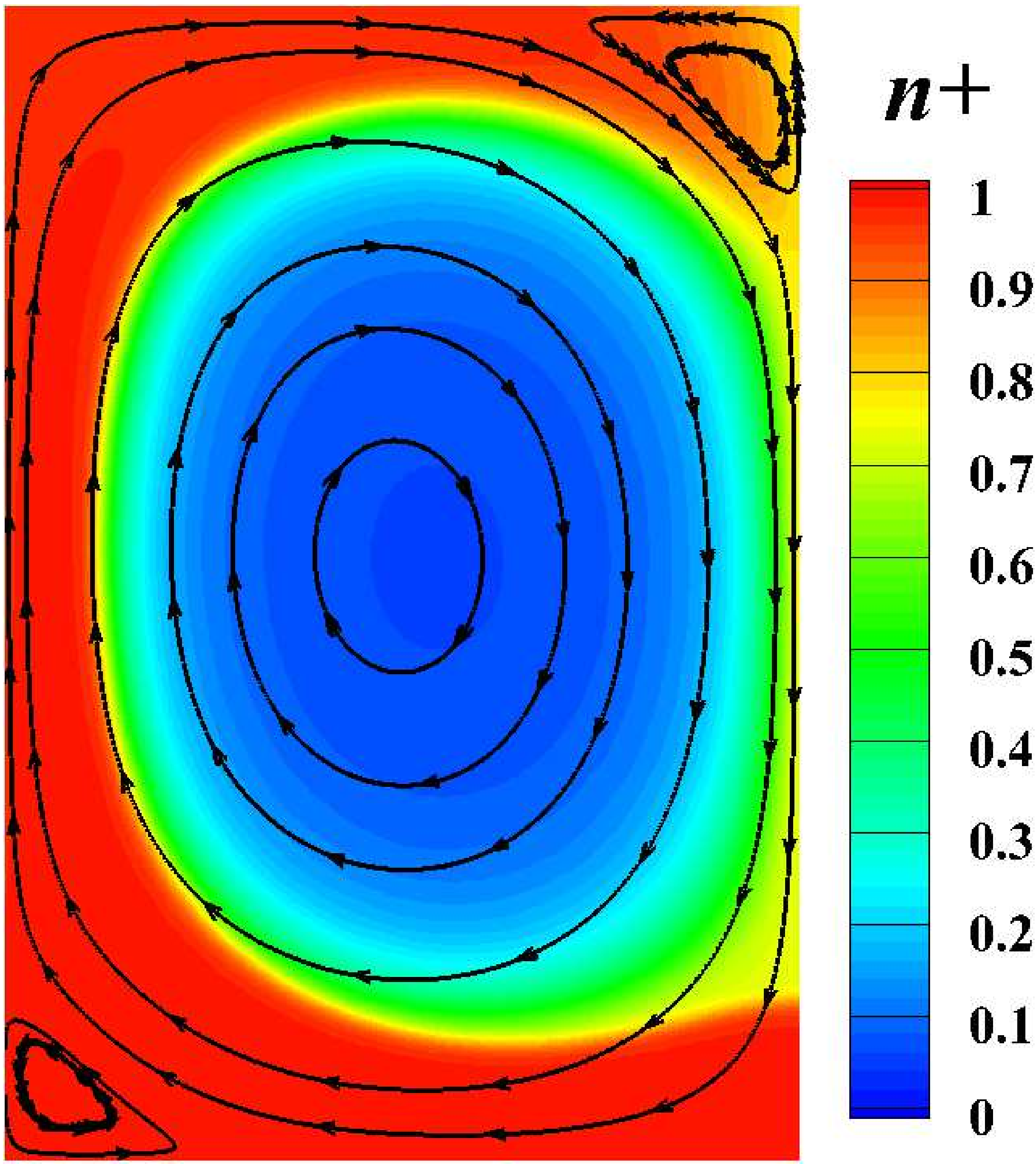
n+
1
0.9
0.8
0.7
0.6
0.5
0.4
0.3
0.2
0.1
0

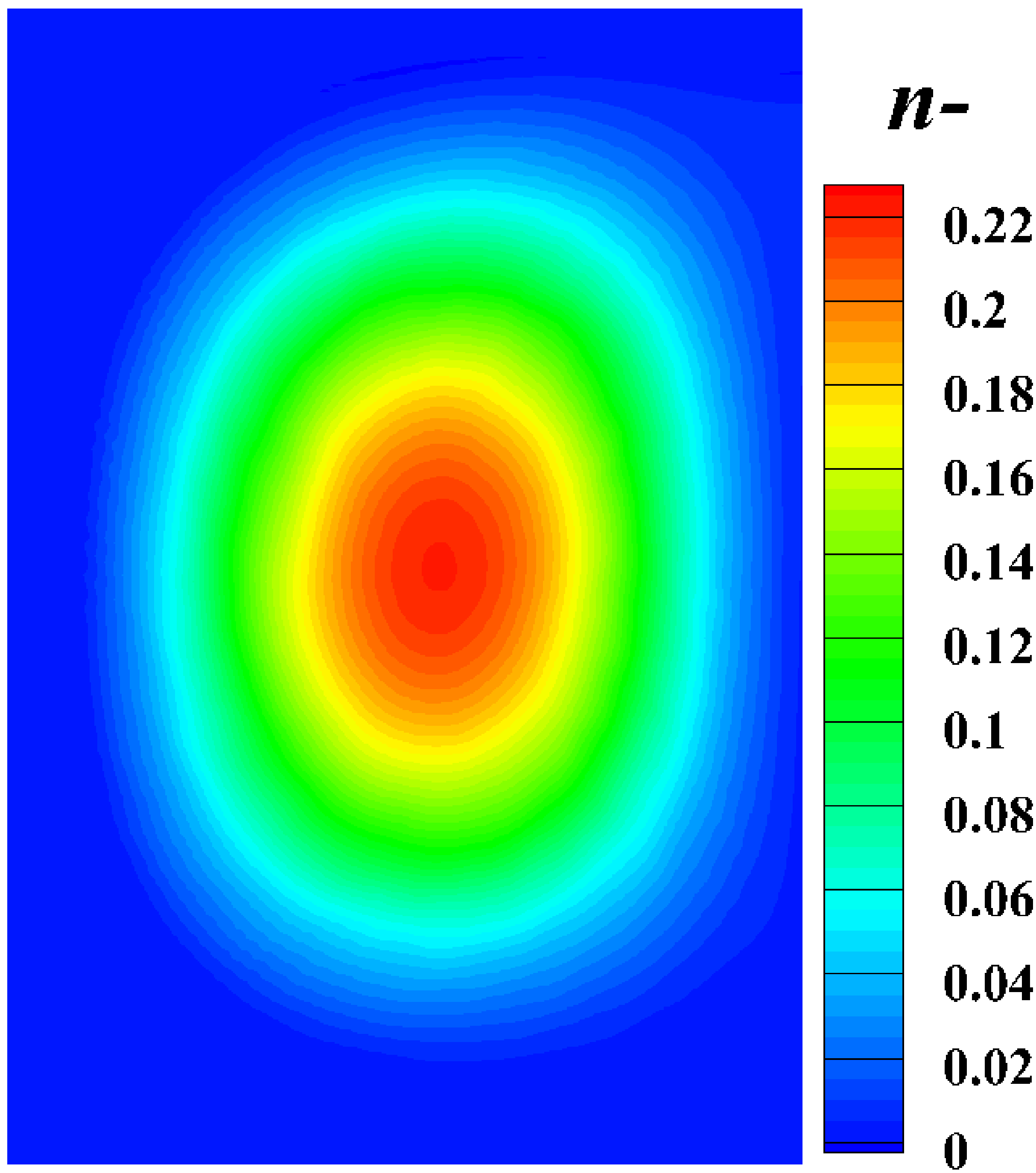
n-
0.22
0.2
0.18
0.16
0.14
0.12
0.1
0.08
0.06
0.04
0.02
0

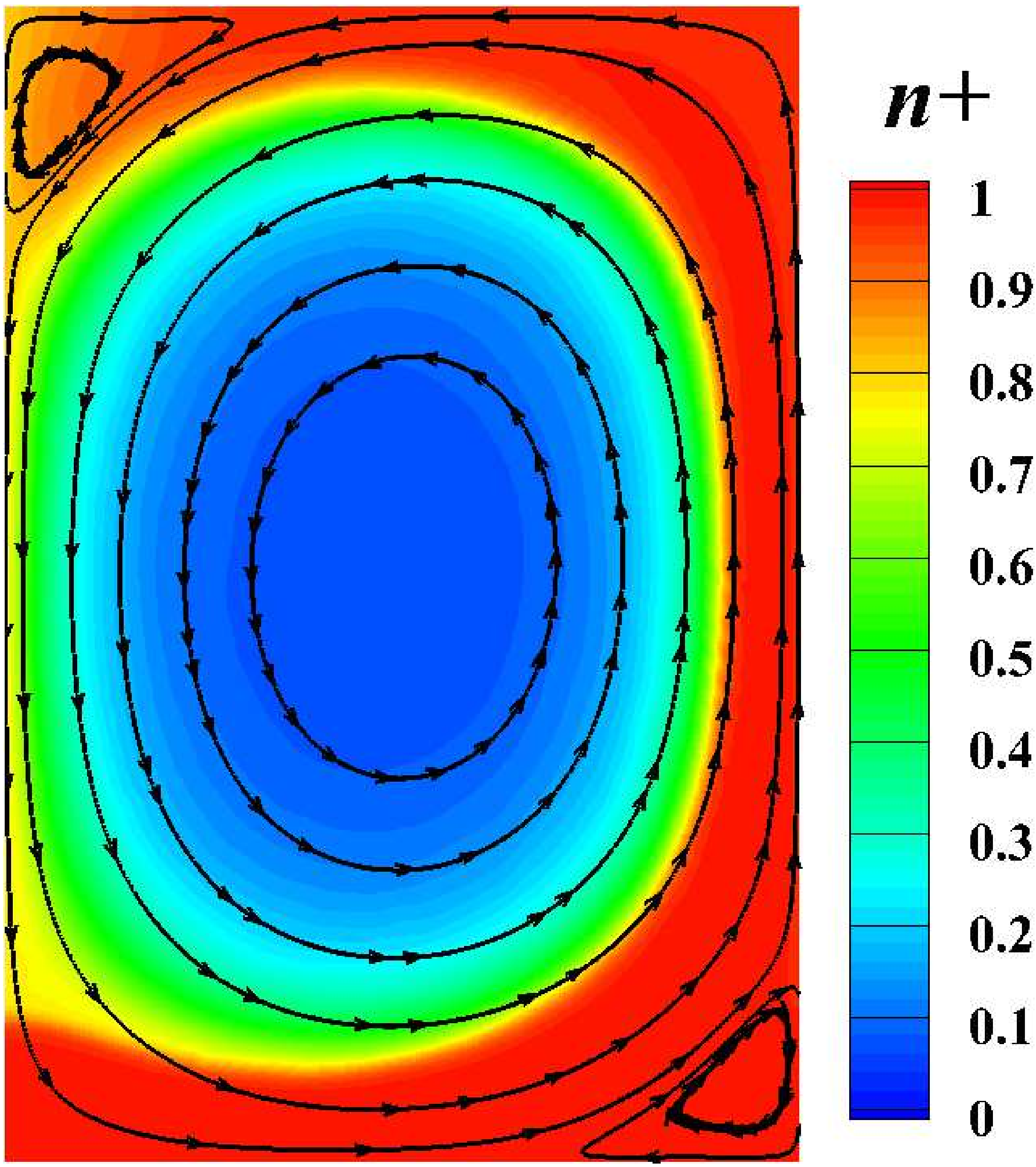
$n+$
1
0.9
0.8
0.7
0.6
0.5
0.4
0.3
0.2
0.1
0

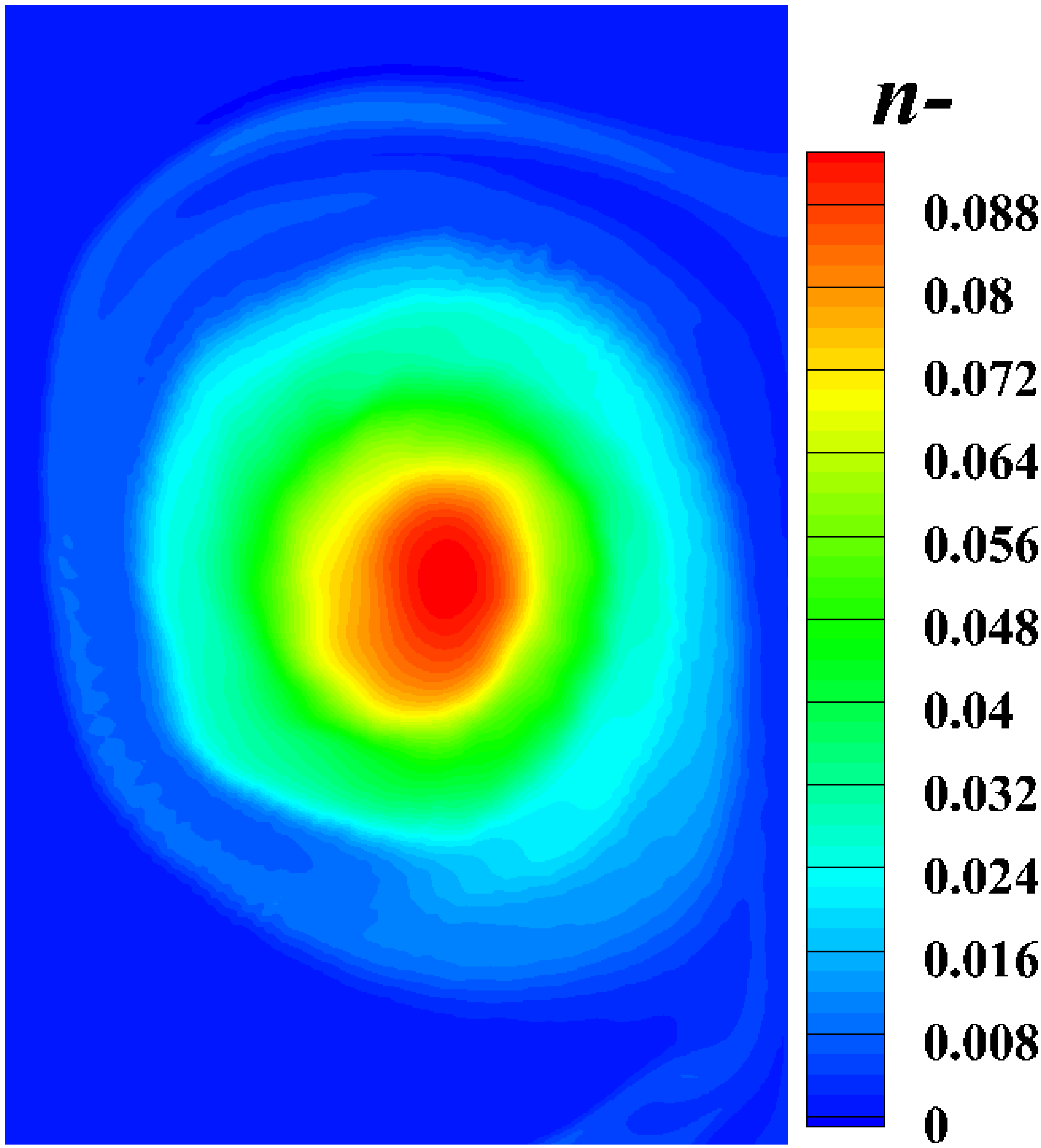
n-
0.088
0.08
0.072
0.064
0.056
0.048
0.04
0.032
0.024
0.016
0.008
0

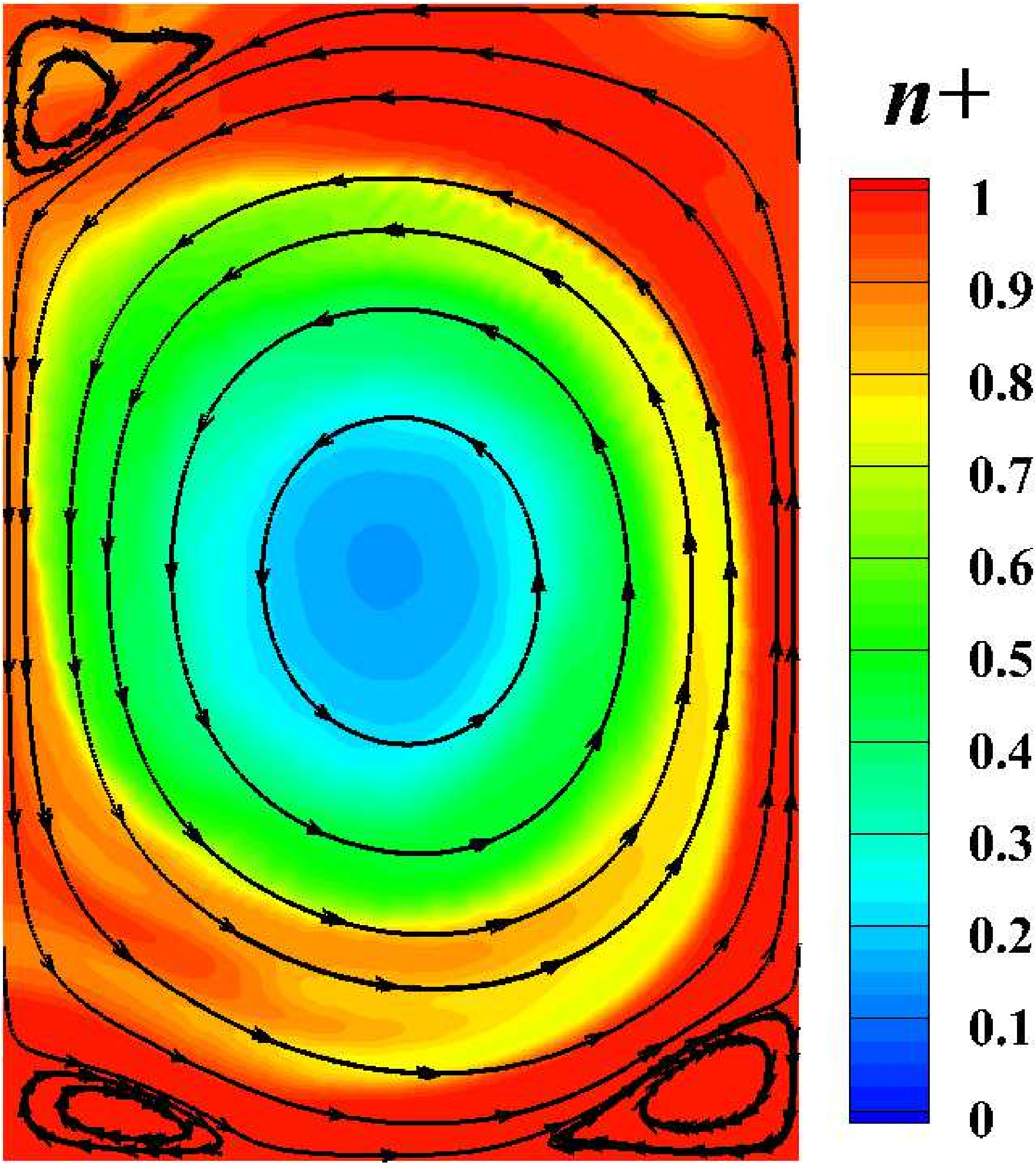
n+
1
0.9
0.8
0.7
0.6
0.5
0.4
0.3
0.2
0.1
0

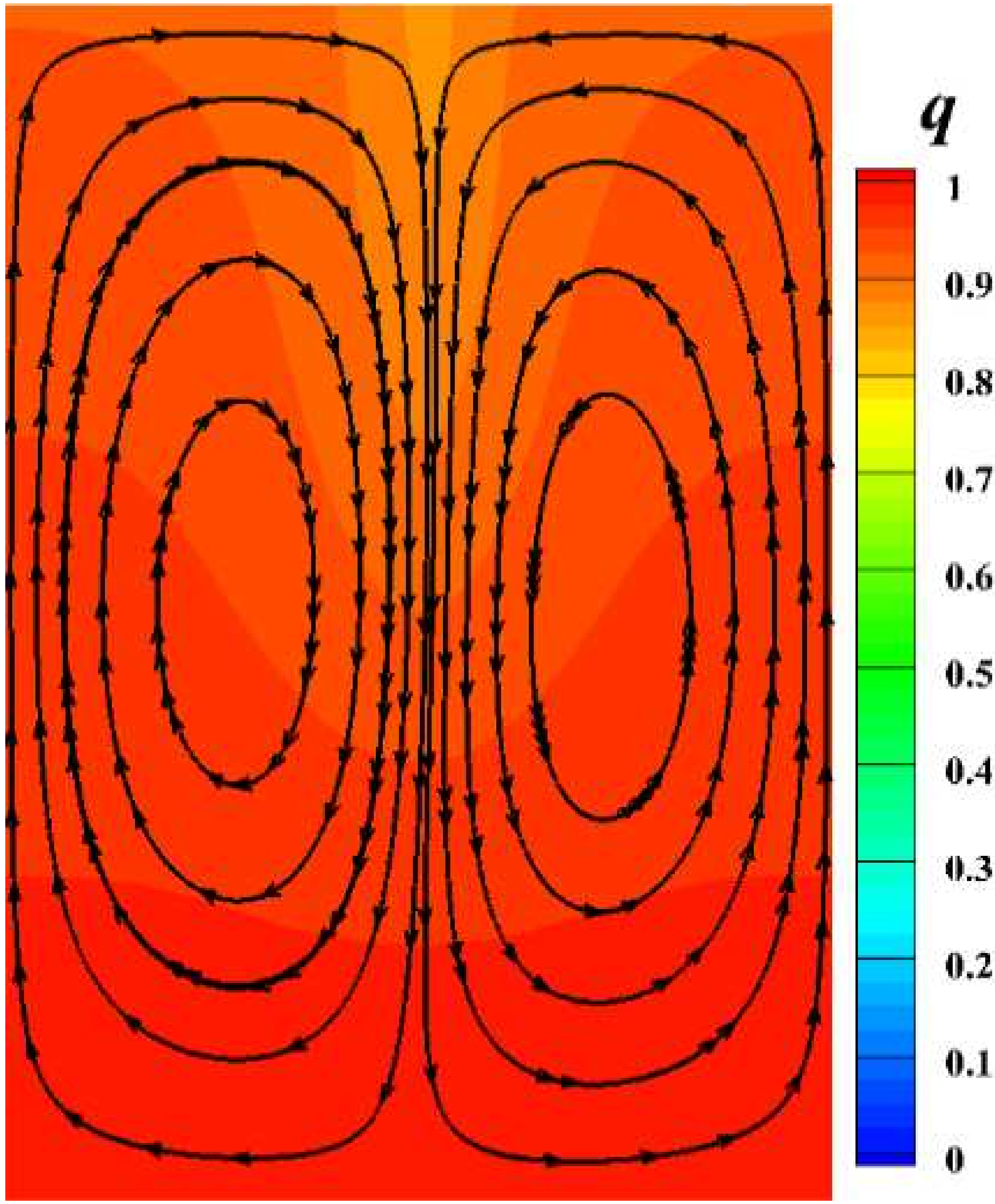
q
1
0.9
0.8
0.7
0.6
0.5
0.4
0.3
0.2
0.1
0

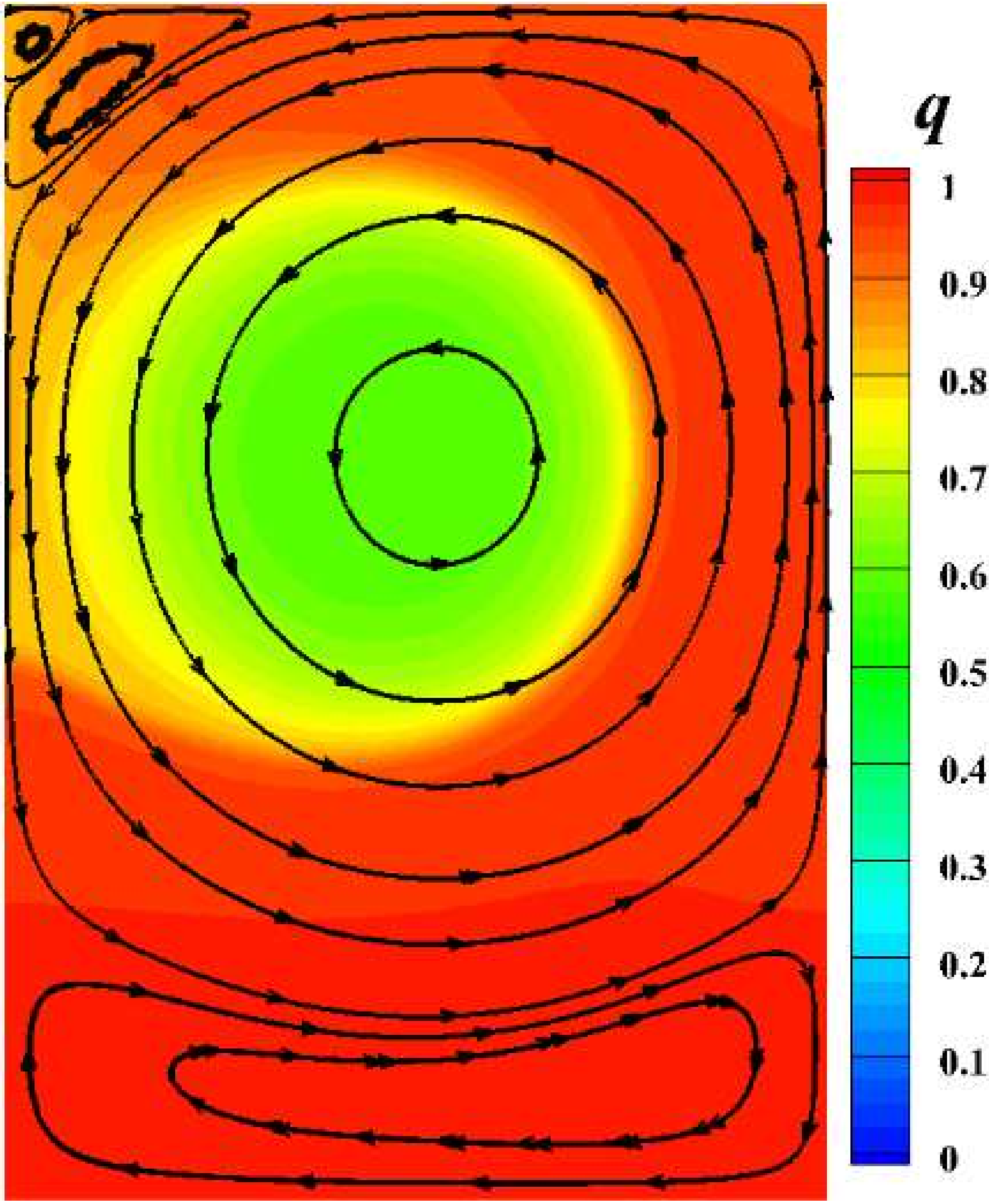
q
1
0.9
0.8
0.7
0.6
0.5
0.4
0.3
0.2
0.1
0

PLEASE CITE THIS ARTICLE AS DOI: 10.1063/5.0086189

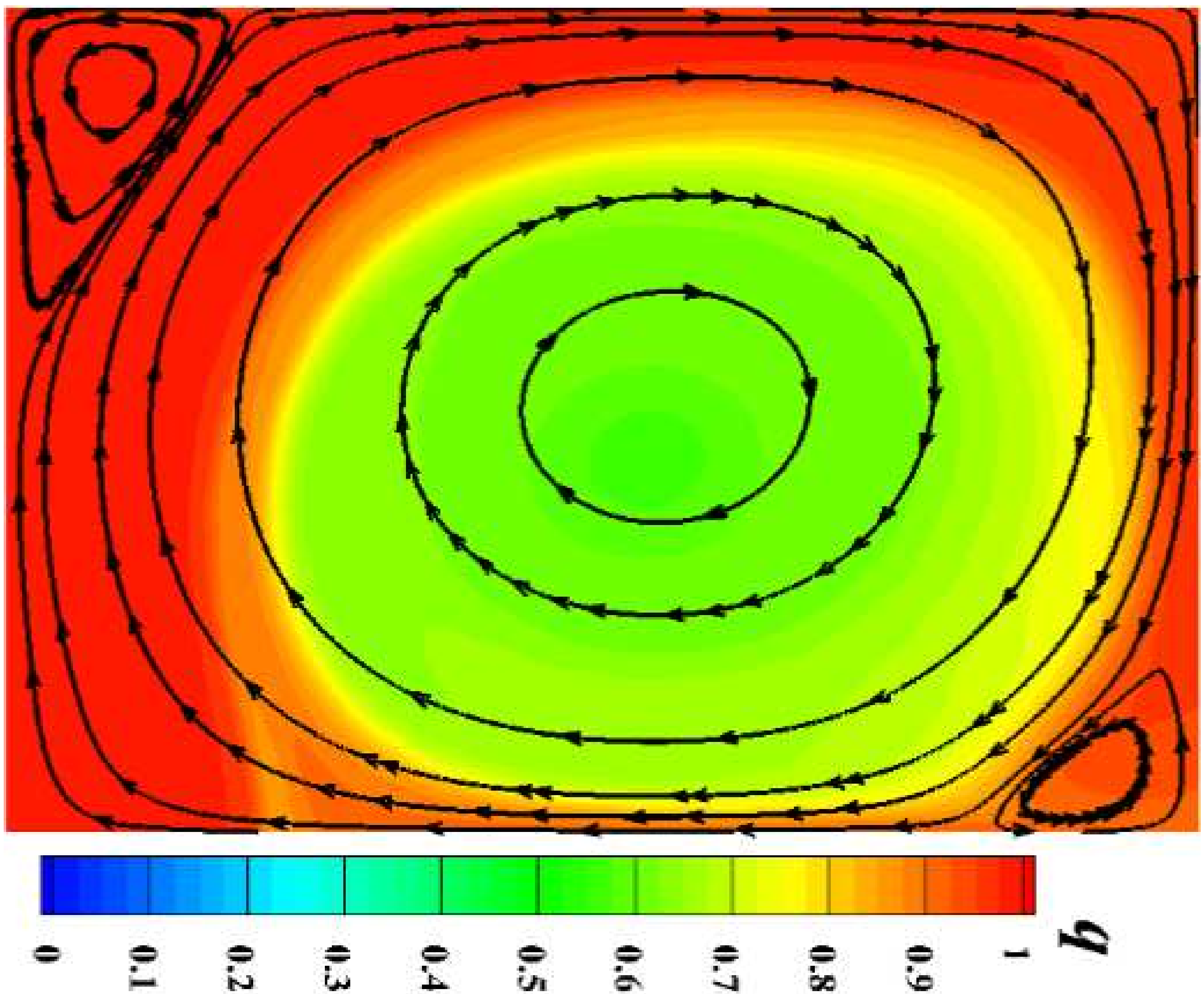

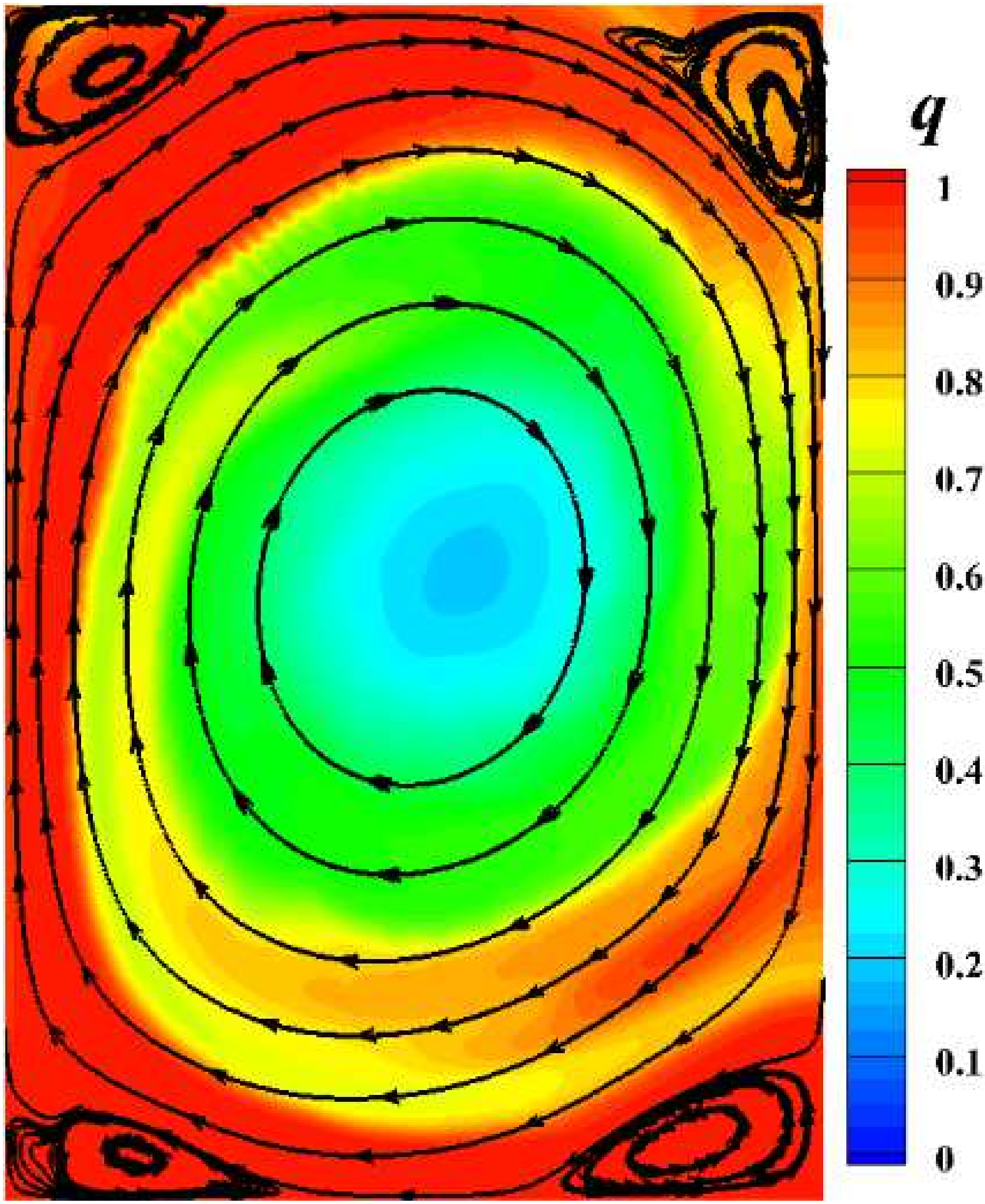
q
1
0.9
0.8
0.7
0.6
0.5
0.4
0.3
0.2
0.1
0